Charge Transport and Contact Effects in Nanoscopic Conjugated Molecular Junctions Characterized by Conducting Probe Atomic Force Microscopy

A THESIS

SUBMITTED TO THE FACULTY OF THE GRADUATE SCHOOL OF THE

UNIVERSITY OF MINNESOTA

BY

Bong Soo Kim

IN PARTIAL FULFILLMENT OF THE REQUIREMENTS FOR
THE DEGREE OF DOCTOR OF PHILOSOPHY

C. Daniel Frisbie, Adviser

October, 2008

Acknowledgements

First of all, I would like to thank my advisor, Dr. C. Daniel Frisbie for giving me the opportunity to do research in his laboratory. During difficult times in my research, his continuous encouragement and advice helped me accomplish my thesis. His attitude in discussing data is always keen and enthusiastic, and meeting with him is always an enjoyable moment. He gave me invaluable help on how to write paper drafts, answer questions, and present my data in an impressive way, and recommendations on pursuing my future career.

I would also like to thank Dr. X.-Y. Zhu, Dr. J. G. Kushmerick, Dr. S. Rigaut, Dr. J. M. Beebe, Dr. V. B. Engelkes, Dr. Y. Jun, and S.-H. Choi. Collaboration with them has provided me with valuable experience in scientific exchange and in the analysis of data. Dr. Beebe, Dr. Engelkes, and Dr. Y. Jun trained my experimental skills and knowledge. Choi was always a good friend to work with. I would especially like to thank Dr. Zhu who coached and supported my research countless times.

I also owe a debt of gratitude to our current and past group members: Dr. Cho, Dr. Lee, Dr. Kim, Salil, two Bryans, Dave, Mingjing, Vivek, Moonsung, Keunhyung, Derek, Xia, Sipei, Yan, Paul, Jeff, Kanan, Lei, Sandy, Xiuyu, Chris, and Matt. I would like to thank all of them for taking pains in building and maintaining our lab facilities. Without their assistance this project certainly would not have been possible.

I must also thank my family, especially my wife, for giving me ardent support. I also owe many thanks to my friends at school and outside of school. Sharing enjoyable moments with them have kept me cheerful for many years.

Lastly, I am indebted to the National Science Foundation for financial assistance. I must also thank the staff at the University of Minnesota Characterization Facility for equipment assistance including Dr. John Nelson (Ellipsometry and SEM) and Dr. Jinping Dong (FTIR).

Abstract

This thesis describes electrical characterization of nanoscale molecular junctions based on a small assembly of molecules. Gaining rigorous knowledge about nanoscopic molecular junctions is essential to the field of molecular electronics, a field that is driven by the potential of utilizing molecules as active elements in electronic circuits. Further advancement requires detailed understanding of factors that influence charge transport through molecules. Critical aspects include molecular length, molecular structure, contact effects, and energy level alignment. For example, the precise dependence of resistance (or conductance) on molecular length is subject to the electronic structure of the molecule and to the charge transport mechanisms. In addition, contact effects can be dominant in current-voltage characteristics due to the inherently small dimensions of these junctions.

To address these issues, my research focused on understanding how currents flow through molecular assemblies in metal-molecule-metal junctions using conducting probe atomic force microscopy (CP-AFM). The CP-AFM technique allows us to form a molecular junction conveniently by contacting metal-coated AFM tips with self-assembled monolayers (SAMs) on metal substrates, and the current-voltage characteristics can then be recorded. Electrical measurements on several series of conjugated molecules revealed the length dependent tunneling efficiency of each molecular structure. In addition, spectroscopic measurements on the metal/molecule interfaces revealed a direct correlation between contact resistance and energy level alignment. In terms of transport mechanisms, a mechanistic transition from nonresonant tunneling to field emission was observed under high bias.

Table of Contents

List of Figures and Tables

1 Measuring Electrical Resistance of Molecular Wires

How to scale down conventional electronic devices into the nano-regime is of critical importance for future high density electronic applications since Si-based device technology is rapidly approaching a technical limit. Many researchers believe that molecular electronics is a promising alternative because (i) molecules are inherently nanoscale, (ii) they can be self-assembled on noble metals, and (iii) their electrical functions can be tailored by modifying chemical structures.[1] Recent inspiring discoveries including Coulomb blockade,[2,3] Kondo resonance,[4] current rectification,[5] switching, [6] and negative differential resistance[7,8] attracted great attention. However, fundamental understanding of charge transport in molecular junctions where molecules are sandwiched by two metal electrodes via surface linkers (Figure 1.1(top)) is highly limited. For instance, there remain many open questions, e.g. (i) what is the precise dependence of molecular wire resistance (or conductance) on molecular length, (ii) what are the roles of metal-molecule contacts, and (iii) how do applied biases and metal work function affect charge transport?

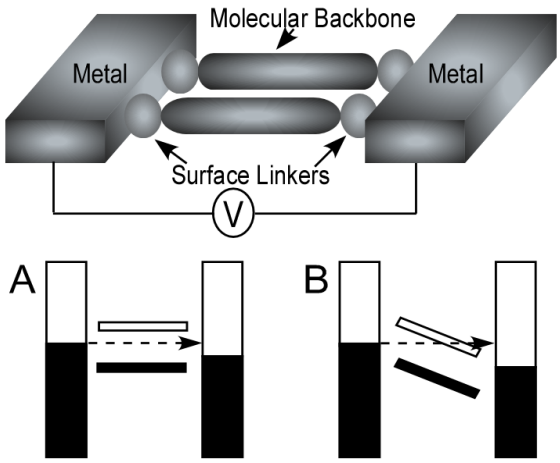

Figure 1.1. Schematic representation of a metal-molecule-metal junction (top) and transport mechanisms: (A) direct tunneling and (B) field emission. In metal-molecule-metal junction, molecules are bridged between two metal electrodes. Direct tunneling transitions to field emission at high biases due to high electrical field.

To address these issues, I have focused my thesis research on understanding how currents flow through molecular wires in metal-molecule-metal junctions. Electrical measurements on several series of molecules revealed the length dependent tunneling efficiency of each molecular structure. In addition, spectroscopic measurements on the metal/molecule interfaces have showed the direct correlation between contact resistance and energy level alignment. Furthermore, a significant portion of my thesis has been devoted to establishing a mechanistic transition from direct tunneling to field emission under high bias.

I and my coworkers have examined the electrical properties of molecules using conducting probe-atomic force microscopy (CP-AFM). Nanoscopic molecular junctions were formed by contacting metal-coated AFM tips with self-assembled monolayers (SAMs) on metal substrates, and the current-voltage characteristics were recorded. The tips contact ~100 molecules at a load of 1-2 nN. The SAMs were formed by immersing metal substrates into a molecular solution. The SAM formation was monitored by various techniques including infrared spectroscopy, x-ray photoelectron spectroscopy, and ellipsometry. Energy level alignments were elucidated by ultraviolet photoelectron spectroscopy (UPS), ultraviolet-visible spectroscopy, and cyclic voltammetry.

We have determined the length dependence of charge transport in molecular wires of oligoacene thiols, oligoacene isocyanides, oligoacene dithiols, and oligo(ruthenium (II) σ-arylacetylide) complexes. At low biases, all of these molecules have shown the exponential scaling of resistance with length: $R = R_0 \exp(\beta \bullet s)$ where R_0 is contact resistance, β is length dependent tunneling attenuation factor, and s is molecular length. This is consistent with direct tunneling mechanism. The β values of the above series are found to be 0.5/Å, 0.5/Å, 0.2/Å, and 0.1/Å, respectively. The β values of 0.2-0.5/Å are within the range of common conjugated molecules. On the other hand, the 0.1/Å observed in the ruthenium complexes is exceptionally low due to a high electronic coupling between ruthenium centers.

We also examined contact effects of surface linkers (thiols, isocyanides, and dithiols) on various kinds of metals. Electrical measurement of Au-molecule-Au junctions based on oligoacene thiols and isocyanides have revealed that contact resistances of thiols are smaller than those of isocyanides. The difference is attributed to the smaller energy offset (E_{Fermi}–E_{HOMO}) of oligoacene thiols. In parallel, electrical measurements of oligoacene thiols and dithiols utilizing a variety of different tip/substrate metal combinations (e.g., Ag/Ag, Ag/Au, Au/Au, Au/Pt, and Pt/Pt) have shown that dithiols have much smaller contact resistance than monothiols and also that the contact resistance is reduced with increasing metal work function. Collectively, we have found not only the crucial role of surface linkers and metal types but also the good correlation between contact resistance and the energy offset at the metal/organic interfaces.

Further, we have investigated charge transport mechanisms. A transition from direct tunneling to field emission upon increasing the applied bias was universally observed (Figure 1.1(bottom)) and the voltage at which this transition occurs (V_{trans}) is linearly correlated with the energy offset ($E_{Fermi} - E_{HOMO}$). This observation allows us to probe the effective tunneling barrier of molecules and to find the dependence of barrier height on molecular structure and its energy level alignment.

1.1 Thesis Overview

This thesis covers not only general aspects in the field of molecular electronics but also detailed experimental results of my research described above. Chapter 2 is intended to provide general information about self-assembled monolayers including molecular structure, preparation and characterization. Chapter 3 is devoted to explaining the theoretical background of molecular electronics and representative junction fabrication techniques that have been developed.

Chapter 4 through Chapter 7 presents my publications and details. Chapter 4 has been published as B.-S Kim, J. M. Beebe, Y. Jun, X.-Y. Zhu, and C. D. Frisbie

"Correlation between HOMO Alignment and Contact Resistance in Molecular Junctions: Aromatic Thiols versus Aromatic Isocyanides," *Jounral of the American Chemical Society* **2006**, 128, 4970. This chapter discusses the relationship between electrical property and energy level alignment. Conducting probe atomic force microscopy (CP-AFM) and ultraviolet photoelectron spectroscopy (UPS) on rigid, conjugated oligoacenes of increasing length with either thiol (-S) or isocyanide (-CN) linkers have revealed that the lower energy offset (E_{Fermi}–E_{HOMO}) is responsible for the lower contact resistance with no significant difference in the length dependent tunneling attenuation factor (β).

Chapter 5 has been prepared for submission to *Jounral of the American Chemical Society* as B.-S. Kim, S.-H. Choi, M.-S. Kang, X.-Y. Zhu, and C. D. Frisbie, "Length-Dependent Transport in Molecular Junctions based on SAMs of Aromatic Thiols and Dithiols: Effect of Contact Type and Metal Work Function." This chapter deals with importance junction parameters, i.e. molecular length, energy level alignment, surface linkers, and metal work function with increasing length of oligoacene thiols and dithiols. We have found that dithiol junctions has much lower contact resistance than thiol junctions. Also, contact resistance decreases with increasing metal work function. Moreover, the transition voltage (V_{trans}) is strongly dependent on metal/molecule contacts and energy level alignment.

Chapters 6 and 7 have been published respectively as J. M. Beebe, B.-S. Kim, J. W. Gadzuk, C. D. Frisbie, and J. G. Kushmerick, "Transition from Direct Tunneling to Field Emission in Metal-Molecule-Metal Junctions," *Physical Review Letters* **2006**, 97, 026801 and as J. M. Beebe, B.-S. Kim, J. W. Gadzuk, C. D. Frisbie, and J. G. Kushmerick, "Measuring Relative Barrier Heights in Molecular Electronic Junctions with Transition Voltage Spectroscopy," *ACS Nano* **2008**, 2, 827. Both chapters address the transition from direct tunneling to field emission upon increasing the applied bias. We have observed that the transition voltage (V_{trans}) is dependent on molecular structures and metal work function and correlates linearly with the energy offset ($E_{Fermi} - E_{HOMO}$).

Chapter 8 has been published as B.-S. Kim, J. M. Beebe, C. Olivier, S. Rigaut, D. Touchard, J. G. Kushmerick, X.-Y. Zhu, and C. D. Frisbie, "Temperature and Length Dependence of Charge Transport in Redox-Active Molecular Wires Incorporating Ruthenium (II) Bis(σ-arylacetylide) Complexes." *Journal of Physical Chemistry C* **2007**, 111, 7521. This chapter describes unique properties of organometallic molecular wires. Electrochemistry and infrared spectroscopic data suggest a strong electronic coupling between ruthenium cores in molecules, resulting in a very low length dependent tunneling attenuation factor (β = 0.1/Å). In addition, we have observed Coulomb blockade-like behavior in the longest molecule (~50 Å) at 5 K because direct carrier tunneling between metal electrodes is not possible in such long molecular length.

1.2 References

(1) Heath, J. R.; Ratner, M. A. *Physics Today* **2003**, *56*, 43.

(2) Kubatkin, S.; Danilov, A.; Hjort, M.; Cornil, J.; Bredas, J. L.; Stuhr-Hansen, N.; Hedegard, P.; Bjornholm, T. *Nature* **2003**, *425*, 698.

(3) Park, H.; Park, J.; Lim, A. K. L.; Anderson, E. H.; Alivisatos, A. P.; McEuen, P. L. *Nature* **2000**, *407*, 57.

(4) Park, J.; Pasupathy, A. N.; Goldsmith, J. I.; Chang, C.; Yaish, Y.; Petta, J. R.; Rinkoski, M.; Sethna, J. P.; Abruna, H. D.; McEuen, P. L.; Ralph, D. C. *Nature* **2002**, *417*, 722.

(5) Metzger, R. M. *Chem. Rev.* **2003**, *103*, 3803.

(6) Blum, A. S.; Kushmerick, J. G.; Long, D. P.; Patterson, C. H.; Yang, J. C.; Henderson, J. C.; Yao, Y. X.; Tour, J. M.; Shashidhar, R.; Ratna, B. R. *Nat. Mater.* **2005**, *4*, 167.

(7) Chen, J.; Reed, M. A.; Rawlett, A. M.; Tour, J. M. *Science* **1999**, *286*, 1550.

(8) Rawlett, A. M.; Hopson, T. J.; Nagahara, L. A.; Tsui, R. K.; Ramachandran, G. K.; Lindsay, S. M. *Appl. Phys. Lett.* **2002**, *81*, 3043.

2 Molecular Self-Assembly

In the field of molecular electronics, understanding charge transport through organic molecules is of critical importance for real nanodevices. Organothiols have the potential of being used in charge transport systems due to their ability to make strong bonds to the coinage metals. Thus, the self-assembly of organothiols is a significant tool to unravel charge transport mechanisms at the molecular scale. Before discussing detailed electrical properties through molecular wires based on organothiols, I review in this chapter various aspects of self-assembled monolayers (SAMs) of organothiols, particularly on gold.

2.1 Self-Assembled Monolayers of Organothiols

The field of self-assembled monolayers (SAMs) has undergone tremendous growth and advances in the past twenty years. In 1983, Nuzzo and Allara[1] showed that di-n-alkyl disulfides formed SAMs on gold from dilute solutions. Self-assembled monolayer systems with organothiols have since been investigated by chemists and physicists, because SAMs are excellent systems for studies of structure-property relationships, self-organization, and interfacial phenomena.[2]

SAMs are well-ordered, dense molecular assemblies of chainlike or rodlike molecules that are chemically anchored to a solid surface. The SAM-forming molecules generally consist of two groups: head and tail. The head group binds strongly to suitable substrates. Thiol, disulfide, thioacetate, isocyanide, and pyridine groups offer chemical bonds to the surfaces of gold, silver, palladium, and copper.[3-5] The tail group constitutes of the outer surface of the film. The tail-tail interactions aid the formation of the monolayer structure. The intermolecular interaction among neighboring molecules induces them to align, maximizing the van der Waals interactions and electrostatic forces.[6] Figure 2.1 represents three idealized structures for SAMs. Mismatch between the van der Waals radii of the tail groups and the head groups, and also between these radii

and the substrate lattice parameters causes a deviation from well-ordered structures as depicted in Figure 2.1a and 2.1b and formation of structural disorder and defects. Figure 2.1c, for example, represents an assembly of lower density packing arrangement.[7]

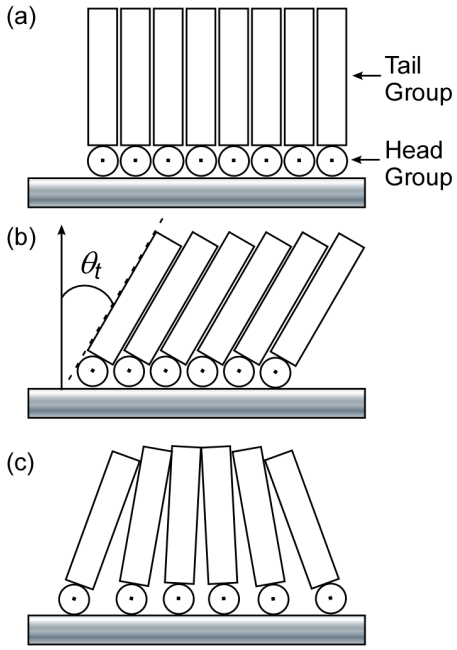

Figure 2.1. Structural models of a self-assembled monolayer: (a) closest packed arrangement of tail groups oriented normal to the substrate surface, (b) closest packed arrangement of tail groups uniformly oriented at an angle θ_t from the surface, and (c) closest packed arrangement of head groups with a distribution of tilted tail groups. (Reproduced with permission from reference 7. Copyright 1987 American Chemical Society)

2.2 Preparation and Characterization of SAMs

2.2.1 Preparation of Monolayers and Gold Substrates

In general, self-assembled monolayers of thiols are spontaneously formed by immersing freshly metal-coated substrates, such as a gold-coated silicon wafer, into dilute (0.1-1.0 mM) thiol solutions of an organic solvent such as absolute ethanol.[7] After an approximately 24 h deposition to obtain well-ordered SAMs, the films are rinsed with copious amounts of various organic solvents to remove residual solvent and adsorbates,

and then blown dry with a stream of N_2 gas. A schematic outline of the SAM preparation procedure on such gold substrates is given in Figure 2.2.

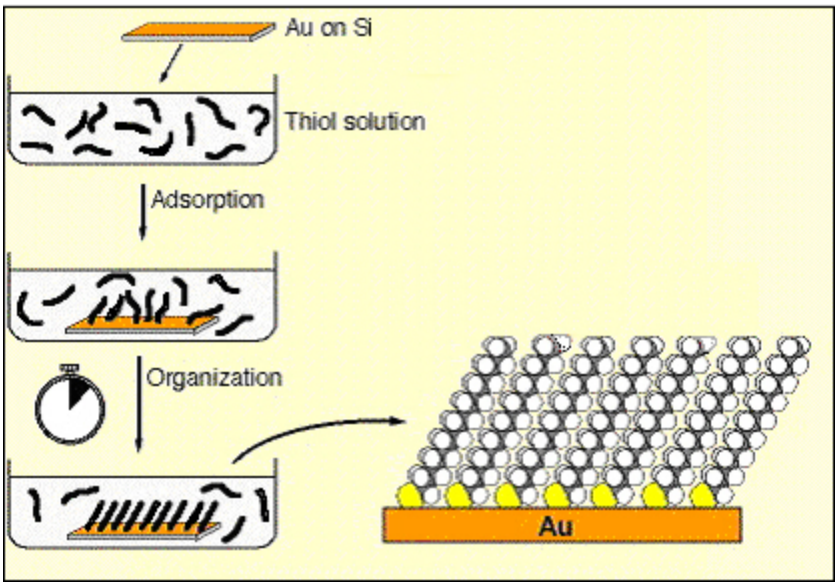

Figure 2.2. Preparation of SAMs. The substrate, Au on silicon wafer, is immersed into an ethanol solution of the desired thiol(s). Initial fast adsorption is followed by an organization phase, which is allowed to continue for approximately 24 h. A scheme of a fully assembled SAM is shown to the right.

Polycrystalline gold substrates are typically prepared by deposition of a 5-20 nm adhesion layer of Cr and 100-200 nm of active gold layer onto silicon wafers at about 1×10^{-6} Torr in a thermal evaporator. In addition, our group prepares atomically flat substrates via the template stripping method.[8,9] 300-500 nm of metal are deposited on a Si wafer with no adhesion layer. Square pieces of Si (1 cm × 1 cm) are attached to the exposed side of gold surface using an epoxy (EPO-TEK 377). After curing the wafers in an oven for 1 h at 125 ºC, substrates are stripped from the parent wafer.

2.2.2 Characterization of SAMs

Self-assembled monolayers have been characterized by a wide variety of techniques. In this section, several representative techniques to characterize self-assembled monolayers are described.

Optical Ellipsometry. One of the most widely used techniques for the study of SAMs is optical ellipsometry. This technique is applied as a convenient and quatitative means of determining the average thicknesses of the monolayer films and estimating the progress of film growth. In ellipsometry, the polarization of circularly polarized light is altered by reflection from a surface. In general, both the phase and the relative amplitude of the parallel and perpendicular components of light are changed. These changes are reflected in the ellipsometric quantities Δ (a relative phase parameter) and Ψ (a relative amplitude parameter) which can be used to determine the refractive index and thickness of the film. In theory, both the film thickness and the refractive index can be determined independently, but in practice this is only applicable to films thicker than approximately 50 Å.[10] For most monolayers, therefore, a refractive index must be assumed to calculate a film thickness. For studies of alkanethiols monolayers, a refractive index value of 1.45 or 1.50 is used almost exclusively.[7,11,12]

Contact Angle Measurement. This technique is a simple but sensitive probe for surface analysis related to surface energy and tension. Contact angle measurements can be used to estimate the degree of order and the polarity of the monolayer surface functional groups. In addition, the surface free energy of the monolayers can be determined by measuring contact angles as a function of surface tension of a series of liquids. The contact angle is defined by the shape of a liquid droplet resting on a solid surface. When drawing a tangent line to the droplet at the solid surface interface, the contact angle is the angle between the tangent line and the solid surface. The shape of this interface is governed by the interactions of the monolayer, the liquid, and the surrounding medium. When a liquid drop is on a solid surface in equilibrium, the relationship between the surface free energies from Young's equation is given by:[13]

$$\gamma_{lv} \cos\theta = \gamma_{sv} - \gamma_{sl} \quad (2.1)$$

where γ_{lv}, γ_{sv}, and γ_{sl} represent the surface tensions of the liquid-vapor, solid-vapor and solid-liquid interfaces, respectively, and θ is the contact angle. For a liquid which wets the surface, the solid-liquid surface tension is very small, and thus $\cos\theta$ approaches 1, and θ goes to zero. On the contrary, if the liquid does not wet the monolayer, then γ_{sl} becomes large relative to the other terms. In this case, $\cos\theta$ can be zero, or even negative, corresponding to contact angles of 90° or greater. Although any suitable pure liquid can be used for contact angle measurements, the water contact angle, θ_{H2O}, is most commonly used for alkanethiols SAMs. For a close-packed long-chain n-alkanethiol monolayer terminated with $-CH_3$, θ_{H2O} is reported to be 112^o. In contrast, a similar monolayer terminated with –OH or –COOH showed θ_{H2O} is 0^o.[11]

Another useful quantity is the hysteresis of the contact angle, defined as the difference between advancing contact angle and receding contact angle ($\theta_{ADV} - \theta_{REC}$). The advancing angle ($\theta_{ADV}$) is the largest possible angle and the receding (θ_{REC}) is the smallest possible contact angle. Qualities of SAMs such as surface roughness and uniformity can be estimated by the hysteresis.[13]

Fourier Transform Infrared Spectroscopy. Fourier Transform Infrared spectroscopy (FTIR) is an extremely attractive method for the analysis of molecular orientation and packing in monolayer structures. The excitation of a normal vibrational mode by infrared radiation is active if a change of the dipole moment (**p**) occurs and thus the dynamic dipole moment ($\boldsymbol{\rho} = \partial p/\partial q_i$) is nonzero, and the projection of this change onto the direction of the electric field is also nonzero. The integral intensity (**A**) of the absorption band of the normal mode is proportional to the probability per unit time of a transition between an initial state i and a final state j. This probability is proportional to the square of the matrix element of the Hamiltonian $\mathbf{H} = -\mathbf{E}\cdot\mathbf{p}$, resulting in the absorption: [14]

$$A \sim E^2 |\langle j|\boldsymbol{\rho}|i\rangle|^2 \cos^2\theta \quad (2.2)$$

where **E** is the electric field, $|\langle j|\boldsymbol{\rho}|i\rangle|$ is transitional dipole moment and θ is the angle between vectors **E** and **ρ**. If the transition dipole moment is distributed anisotropically in the films, the absorption of linearly polarized radiation depends on the orientation of the transition dipole moment. This is known as selective absorption. For dipoles aligned parallel to the surface, this results in the cancellation of the dipole, and thus a decrease in intensity of the absorption. In contrast, dipoles aligned normal to the surface exhibit an enhancement of the resonance. Infrared reflection absorption spectroscopy (IRRAS) revealed that long *n*-alkanethiol SAMs on gold adopt about a 30^{o} tilt,[2] and *p*-terphenylthiols on gold yield a tilt angle of $24^{o} \pm 12^{o}$.[15]

The peak shape and position of IR spectra provide insight into the intermolecular environment of the alkyl chains in monolayer assembly. The characteristic C-H stretching (ν_a-CH_2-) modes observed for *n*-alkanethiol SAMs are shifted to lower energy as molecular length increases, indicating that shorter chain n-alkanethiol SAMs are more liquid-like than long-chain monolayers.[7] Recently, in attenuated total internal reflection Fourier transform infrared spectroscopy (ATR-FTIR) experiment, Jun *et al.* built sandwich structures of SAMs between metals, and studied the dependence of conformational change upon metal deposition, as well as the interaction of alkyl chains with the deposited metal.[16]

Cyclic Voltammetry. In cyclic voltammetry, the current is measured as a function of electrode potential. In order to measure current and potential simultaneously, three electrodes are required. The reference electrode is typically a Ag/AgCl. A platinum wire or gauze is used as a counter electrode, and a monolayer-coated metal surface is incorporated as a working electrode. This working electrode may be a portion of a bare or monolayer-coated gold electrode. To obtain a cyclic voltammogram, the current flow between the working electrode and counter electrode is recorded as a sawtooth potential is applied to the working electrode. At the same time, the magnitude of the resulting potential is measured between the working and reference electrodes.

While ellipsometry and IR spectroscopy provide average molecular properties of adsorbed molecules, cyclic voltammetry provides means to probe the nature and extent of structural defects and coverage, as well as to determine the dynamics of electron transfer reactions occurring in the monolayer. Porter *et al.*[7] examined the SAMs of alkanethiols by cyclic voltammetry using $Fe(CN)_6^{3-}$ and $Fe(H_2O)_6^{3+}$ as an electroactive species, and found that the shape of the current behavior may suggest an assembly of pinholes in the monolayer. Sikes *et al.*[17] measured rapid electron tunneling transfer through oligophenylenevinylene bridges between a gold electrode and a tethered redox species, Ferrocene. They revealed that electronic coupling for oligophenylenevinylene bridges up to 28 Å long does not limit the rate constants, suggesting that oligophenylenevinylene bridges could be useful wires for molecular electronic applications.

X-ray Photoelectron Spectroscopy. X-ray Photoelectron Spectroscopy (XPS) provides a way to examine the chemical composition in the monolayer. X-ray photoelectron spectroscopy involves irradiation of a sample under vacuum by x-rays of known energy, which causes the ejection of photoelectrons from the atoms near the surface. The emitted electrons have a kinetic energy E_k, given by:

$$E_k = h\nu - E_b - \Phi \qquad (2.3)$$

where $h\nu$, E_b, and Φ represent the photon energy, the binding energy, and the work function, respectively. The dispersion of kinetic energy of the ejected electrons provides a spectrum of binding energies. The locations of peaks in this spectrum indicate both the presence of specific elements and their respective oxidation states.

In addition, the intensity of a photoelectron peak varies linearly with the surface concentration of the corresponding element. Within the shallow region, the signal from atoms buried within the monolayer will be attenuated according to their depth. By varying the take-off angle, the effective escape depth for photoelectrons from low-lying species can be increased or decreased. Thus, spectra taken at a series of different take-off angles can be used to construct a crude depth profile of a monolayer. Nuzzo and Allara[18] were the first to use XPS to characterize self-assembled monolayers of thiols on gold.

Bain *et al.*[19] studied the formation of terminally functionalized alkanethiol monolayers by observing the presence of heteroatoms in the monolayer with XPS.

Many researchers have also used this technique to determine the film-thickness. There are two main approaches to obtaining thickness. In one technique, attenuation of photoelectron peaks from metal substrate is used. The intensity of x-ray photoelectrons from the metal is defined by:

$$I = I_0 \exp\left(-\frac{d}{\lambda \sin\theta}\right) \tag{2.4}$$

where I = the intensity of the metal photoelectrons attenuated by a monolayer, I_0 = the intensity from a clean metal substrate, d = the thickness of the monolayer, λ = the attenuation length, and θ = the angle between the surface parallel and the analyzer axis (take-off angle). Measurement of the thickness of the monolayer (d) is accomplished experimentally by measuring intensities of x-ray photoelectrons with a known attenuation length (λ) at a fixed photoelectron kinetic energy.[20] The second method involves using the relative x-ray photoelectron intensities. For instance, in the case of organothiol monolayer on gold, the sample thickness can be calculated using the relative intensities of the Au 4f and the C 1s peaks and by using decanethiol on Au as a reference system. (Assuming the same attenuation length of the gold (λ_{Au}) and carbon (λ_C) photoelectrons for the alkane or aromatic films.) The calculation is based on: [21]

$$\frac{\frac{I_c}{I_{Au}}(sample)}{\frac{I_c}{I_{Au}}(reference)} = \frac{\left\{1-\exp(-\frac{d_{sample}}{\lambda_c})\right\}\exp(-\frac{d_{reference}}{\lambda_{Au}})}{\exp(-\frac{d_{sample}}{\lambda_{Au}})\left\{1-\exp(-\frac{d_{reference}}{\lambda_c})\right\}} \tag{2.5}$$

where I_C = the intensity of C 1s photoelectons and I_{Au} = the intensity of Au 4f photoelectrons.

2.2.3 Structure of Monolayer Films

Structure of *n*-alkanethiol monolayers on Au have been studied in detail. Electron diffraction studies of *n*-alkanethiol monolayers on Au[22] showed that sulfur atoms bond in hexagonal overlayers with a interchain spacing of 4.97 Å indicating freely rotating methylene chains. Helium diffraction[23] and atomic force microscopy (AFM)[24] studies revealed that the structure formed by *n*-alkanethiols on Au (111) is commensurate with the underlying gold lattice and is a simple $\sqrt{3}\times\sqrt{3}R30^{o}$ overlayer. Additionally, ultrahigh vacuum scanning tunneling microscopy (STM) studies[25-27] found further information. Short-chain butanethiol and hexanethiol films showed a coexistence of a two-dimensional (2-D) liquid phase at room temperature. The nucleation and growth of ordered domains having a unit cell of $p\times\sqrt{3}$ ($8\leq p\leq 10$) are induced by slow desorption of surface alkanethiols. On the other hand, no 2-D liquid phase was observed for longer chain alkanethiols (octanethiol and decanethiol). Both form densely packed SAMs with a $c(4\times2)$ superlattice of a $\sqrt{3}\times\sqrt{3}R30^{o}$. (see Figure 2.3)

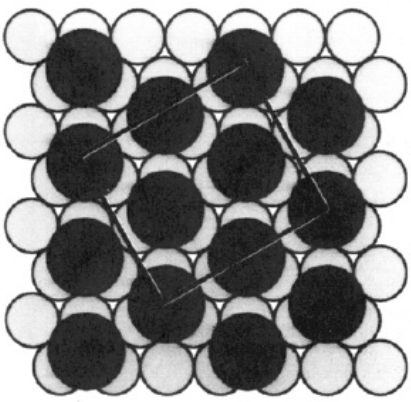

Figure 2.3. Schematic drawing of a model explaining the $c(4\times2)$ superlattice. Light gray circles represent Au atoms, dark gray circles represent *n*-alkanethiol molecules. Diagonal lines indicate the projection of the plane the all-trans hydrocarbon backbone. (Reproduced with permission from reference 27. Copyright 1994 American Chemical Society)

Compared to aliphatic thiols, aromatic thiols have been investigated less because of the difficulty to achieve well-ordered films. Sabatani *et al.*[28] first assembled

phenylthiol, 4-biphenylthiol, and 4-terphenylthiol on gold. They found that phenylthiol forms poorly defined layers, while 4-biphenylthiol and 4-terphenylthiol created stable reproducible monolayers. They also reported, using molecular mechanics calculations, that 4-biphenylthiol and 4-terphenylthiol might form $\sqrt{3}\times\sqrt{3}R30^{o}$ overlayers on Au (111) with the molecules nearly perpendicular to the gold surface. Such overlayers would have favorable intermolecular interactions and retain the same structure as alkanethiols on Au (111). In a study with a biphenyl backbone by Leung and co-workers,[29] a $\sqrt{3}\times\sqrt{3}R30^{o}$ structure for 4-methyl-4'mercaptobiphenyl was seen with grazing-incidence X-ray diffraction and He-atom scattering. Ishida *et al.* [30] observed a $\sqrt{3}\times\sqrt{3}R30^{o}$ structure for *p*-terphenylmethanethiol on Au (111) in their STM measurements. Fuxen *et al.* [21] also found a dominant $\sqrt{3}\times\sqrt{3}R30^{o}$ structure for aromatic thiols on Au (111) and, instead of the $c(4\times2R30^{o})$ found in *n*-alkanethols, a $2\sqrt{3}\times\sqrt{3}R30^{o}$ superstructure. (see Figure 2.4)

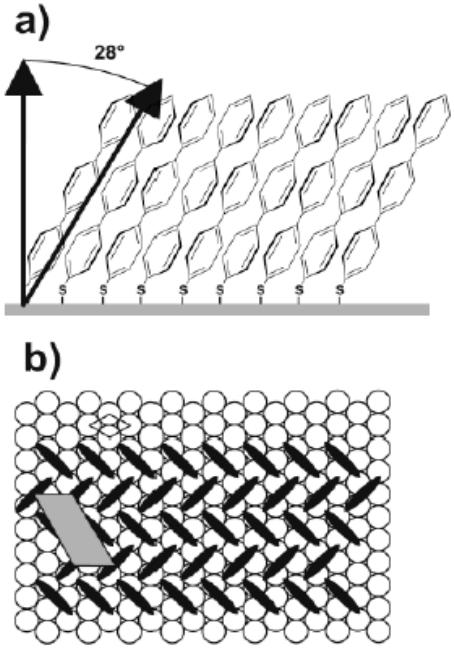

Figure 2.4. Structural model for adsorbed p-terphenylthiol on Au (111). (a) The side view of the molecules shows the molecular tilt angle. (b) The top view of the molecules displays the herringbone arrangement, where the unit cell of the adsorbate ($2\sqrt{3}\times\sqrt{3}R30^{o}$ superstructure) is indicated. (Reproduced with permission from reference 21. Copyright 1987 American Chemical Society)

2.2.4 Kinetics of Monolayer Film Growth

Kinetic studies of alkanethiol adsorption onto Au (111) surfaces have shown that the formation of an alkanethiol SAM involves a sequence of several structural phase transitions. Contact angle and ellipsometry measurements of SAMs on gold by Bain *et al.*[11] revealed at least two time scales in the growth process. At moderate concentrations (*ca.* 1 mM) initial formation of monolayer was rapid. The contact angles and film thicknesses were observed to reach 80-90 % of their final values within a few minutes. This initial rapid formation was governed by the surface (Au)-head group (thiol) reaction, and the activation energy may depend on the electron density of the adsorbing sulfur.[2] The second step was a slower period lasting several hours, at the end of which, the contact angles and thicknesses reached their maximum value. The kinetics of the second step can be rationalized by a slower process of additional adsorption, and lateral diffusion on the surface to reduce defects and enhance ordered packing. On the other hand, Poirier[31] observed the formation of a decanethiol SAM on Au (111) involving a series of structural phase transitions in STM experiments. In the lower coverage regimes, an unstacked "lying-down" phase dominates. This initial phase undergoes a transition into a stacked lying-down with modest coverage, and finally achieves a "standing-up" phase.

The effects of solvents, concentrations, and temperatures on the rate of formation of SAMs have been investigated. Ethanol is frequently used to assemble *n*-alkanethiol monolayers, but due to reactivity, solubility, or other considerations, alternative solvents, such as dichloromethane, tetrahydrofran, and toluene, may be required. Schneider and Butty[32] observed significantly different behavior of SAM formation using dimethylformamide (DMF) and acetonitrile (CH_3CN) as a solvent. In DMF solution, adsorption of alkanethiols was rapid, but no initial multilayer formation was observed. In CH_3CN solution, on the other hand, adsorption was slower, but physisorbed multilayers slowly evolved to a stable monolayer after long exposure. Thus, they suggested that poorer solvents for *n*-alkanethiols may create better SAMs assuming DMF is better solvent than CH_3CN. In STM experiments, Ishida *et al.*[33] found that ethanol facilitated

the formation of the more densely packed 4-terphenylthiol SAMs than dichloromethane. Dannenberger *et al.*[34] found that the *n*-alkanethiol SAM growth kinetics are affected by solvents in the following order: hexane>ethanol>dodecane>hexadecane, and thus proposed that the displacement of solvent molecules adsorbed at the surface might be a rate-limiting step in SAM growth. The effect of concentration of solution was studied by Bain *et al.*[11] Both ellipsometry and contact angle measurements showed that at 1 mM, a suitable concentration for most experimental work, film growth was much faster than at very dilute solutions. Yamada *et al.*[35] found that alkanethiol solutions of elevated temperature generate the larger size of the well-ordered domains with $\sqrt{3}\times\sqrt{3}R30^{o}$ structure.

2.3 References

(1) Nuzzo, R.G.; Allara, D. L. *J. Am. Chem. Soc.* **1983**, *105*, 4481.

(2) Ulman, A. *Chem. Rev.* **1996**, *96*, 1533.

(3) Andres, R. P.; Bielefeld, J. D.; Henderson, J. I.; Janes, D. B.; Kolagunta, V. R.; Kubiak, C. P.; Mohoney, W. J. Osifchin, R. G. *Science* **1996**, *273*, 1690.

(4) Castner, D. G.; Hinds, K.; Grainager, D. W. *Langmuir* **1996**, *12*, 5083.

(5) Nelles, G.; Schonherr, H.; Jaschke, M.; Wolf, H.; Schaub, M.; Kuther, J.; Tremel, W.; Bamberg, E.; Ringsdorf, H.; Butt, H.-J. *Langmuir* **1998**, *14*, 808.

(6) Lii, J.-H.; Allinger, N. L. *J. Am. Chem. Soc.* **1989**, *111*, 8576.

(7) Porter, M. D.; Bright, T. B.; Allara, D. L.; Chidsey, D. E. D. *J. Am. Chem. Soc.* **1987**, *109*, 3559.

(8) Blackstock, J. J.; Li, Z.; Freeman, M. R.; Stewart, D. R. Surface *Science* **2003**, *546*, 87.

(9) Wagner, P.; Hegner, M.; Guntherodt, H.-J., Semenza, G. *Langmuir* **1995**, *11*, 3867.

(10) Wasserman, S. R.; Whitesides, G. M.; Tidswell, I. M.; Ocko, B. M.; Pershan, P. S.; Axe, J. D. *J. Am. Chem. Soc.* **1989**, *111*, 5852.

(11) Bain, C.D.; Troughton, E. B.; Tao, Y.-T.; Evall, J.; Whitesides, G. M.; Nuzzo, R. G. *J. Am. Chem. Soc.* **1989**, *111*, 321.

(12) Engelkes, V. B.; Beebe, J. M.; Frisbie, C. D. *J. Am. Chem. Soc.* **2004,** *126*, 14287.

(13) Ulman, A. *An introduction to ultrathin organic films: from Langmuir-Blodgett to self-assembly*, First ed, (Academic Press, San Diego, **1991**).

(14) Tolstoy, V. P.; Chernyshova, I.V.; Skryshevsky, V. *A Handbook of infrared spectroscopy of ultrathin films* (John Wiley & Sons, Inc., New Jersey, **2003**).

(15) Arnold, R.; Terfort, A.; Woll, C. *Langmuir* **2001**, *17*, 4980.

(16) Jun, Y.; Zhu, X.-Y. *J. Am. Chem. Soc.* **2004**, *126*, 13224.

(17) Sikes, H. D.; Smalley, J. F.; Dudek, S. P.; Cook, A. R.; Newton, M. D.; Chidsey, C. E. D.; Feldberg, S. W. *Science* **2001**, *291*, 1519.

(18) Nuzzo, R. G.; Fusco, F. A.; Allara, D. L. *J. Am. Chem. Soc.* **1987**, *109*, 2358.

(19) Bain, C. D.; Evall, J.; Whitesides, G. M. *J. Am. Chem. Soc.* **1989**, *111*, 7155.

(20) Liu, D.; Szulczewski, G. J.; Kispert, L. D.; Primak, A.; Moore, T. A.; Moore, A. L.; Gust, D. *J. Phys. Chem. B.* **2002**; *106*, 2933.

(21) Fuxen, C.; Azzam, W.; Arnold, R.; Witte, G.; Terfort, A.; Woll, C. *Langmuir* **2001**, *17*, 3689-3695.

(22) Strong, L.; Whitesides, G. M. *Langmuir* **1988**, *4*, 546.

(23) Chidsey, C. E. D.; Liu, G.-Y.; Rowntree, Y. P.; Scoles, G. *J. Chem. Phys.* **1989**, *91*, 4421.

(24) Alves, C. A.; Smith, E. L.; Porter, M. D. *J. Am. Chem. Soc.* **1992**, *114*, 1222.

(25) Poirier, G. E.; Tarlov, M. J.; Rushneier, H. E. *Langmuir* **1994**, *10*, 3383.

(26) Poirier, G. E. *Chem. Rev.* **1997,** *97*, 1117.

(27) Poirier, G. E.; Tarlov, M. J. *Langmuir* **1994**, *10*, 2853.

(28) Sabatani, E.; Cohne-Boulakia, J.; Bruening, M.; Rubinstein, I. *Langmuir* **1993,** *9*, 2914.

(29) Leung, T.; Schwartz, P.; Scoles, G.; Schreiber, F.; Ulman, A. *Surf. Sci.* **2000**, *458*, 34.

(30) Ishida, T.; Mizutani, W.; Akiba, U.; Umemura, K.; Inoue, A.; Choi, N.; Rujihira, M.; Tokumoto, H. *J. Phys. Chem. B* **1999**, *103*, 1686.

(31) Poirier, G. E. *Langmuir* **1999,** *15*, 1167.

(32) Schneider, T. W.; Butty, D. A. *J. Am. Chem. Soc.* **1993**, *115*, 12391.

(33) Ishida, T.; Mizutani, W.; Azehara, H.; Sato, F.; Choi, N.; Akiba, U.; Fujihira, M.; Tokumoto, H. *Langmuir* **2001**, *17*, 7459.

(34) Dannenberger, O.; Buck, M.; Grunze, M. *J. Phys. Chem. B* **1999**, *103*, 2202.

(35) Yamada, R.; Wano, H.; Uosaki, K. *Langmuir* **2000,** *16*, 5523.

3 Molecular Electronics

Thanks to Aviram and Ratner's pioneering paper[1] suggesting that molecules could perform the functions of semiconductor electronics, there have been a multitude of useful electronic, optical, sensory applications developed.[2] A critical issue in the field of molecular electronics is the understanding of electron tunneling in molecular junctions and fabrication of reliable metal-molecule-metal devices. This chapter is intended to present basic theoretical approaches and molecular junction experiments.

3.1 Theoretical Background in Molecular Electronics

3.1.1 Simmons Theory

In 1963, Simmons[3] derived a general formula for electric tunneling current through a rectangular potential barrier. In the Simmons model, for a metal-insulator-metal junction, the current-voltage relationship is described by the following equation:

$$J = \frac{e}{4\pi^2 \eta \cdot s^2}\left\{\phi \exp\left(-A\phi^{1/2}\right) - \left(\phi + eV\right)\exp\left[-A\left(\phi + eV\right)^{1/2}\right]\right\} \tag{3.1}$$

where $A = (2\alpha s/\hbar)(2m_e)^{1/2}$, ϕ is the average barrier height across the junction, s is the width of the barrier, m_e is the electron mass, and α is the correction factor (usually α~1). In the very low voltage range, since $eV \sim 0$ and $\phi \gg eV$, equation (3.1) reduces to:

$$J = J_L \phi^{1/2} V \exp(-A\phi^{1/2}) \tag{3.2}$$

where $J_L = [(2m_e)^{1/2}/s](e/2\pi\hbar)^2$. This expression implies that J is a linear function of V; that is, the junction is Ohmic for very low voltages.

In terms of the resistance (R), equation (3.2) can be rewritten into:

$$R = \frac{4\pi^2 \eta^2 s}{e^2\left\{(2m\phi)^{1/2} B\right\}} \exp\left\{\frac{2(2m\phi)^{1/2}}{\eta} s\right\} \tag{3.3}$$

where B is the junction area. Considering that the current depends exponentially on the thickness (s),[4,5] equation (3.3) can be simplified as follows:

$$R = R_0 \exp(\beta \bullet s) \tag{3.4}$$

where R_0 is an effective contact resistance, and β is a structure-dependent attenuation factor. Equation (3.4) works well for coherent non-resonant tunneling at the low bias regime,[5] and has also been derived from the Landauer formula and Green's function formulation, discussed below.

Even though the Simmons model explains the behavior of metal-metal oxide-metal junctions well,[6] it did not take into account a very important factor, the molecule-metal interaction, carefully. When a molecule is coupled to metal electrodes, the molecular orbitals mix with the metal electron states at the interface. This coupling of molecular levels to metal electron states leads to the broadening of the molecular states, which improves the electronic tunneling efficiency.[4] Another simplication is that the model ignores electron-nuclear coupling. This issue can be resolved by a quatum mechanical consideration, i.e. the Landauer and Green's function formalism.

3.1.2 Molecular Conduction

The Landauer approach is a simple and powerful way of addressing the problem of the conduction across molecular wires.[7] Landauer argued that electrons are "elastically" scattered between two electrodes (electron reservoirs) via a tunneling barrier, characterized by a transmission function *T(E)*. Considering a unidirectional current at zero temperature, the conductance (g) is given by: [7,8]

$$g = g_0 T(E_{Fermi}) \tag{3.5}$$

where $g_0 = e^2/\pi\hbar = (12.9\ \mathrm{k\Omega})^{-1}$ is the quantum unit of conductance and E_{Fermi} is the Fermi energy. More generally, if the two electrodes have finite size in the direction normal to the propagation, equation (3.5) becomes:

$$g = g_0 \sum T_{ij}(E) \tag{3.6}$$

where T_{ij} is the scattering probability from transversal mode i of the left electrode into transversal mode j of the right electrode. It should be noted that, in essence, the Landauer formula represents a clear connection between the transmission probability and the conductance, and shows that the maximum conductance allowed is finite. The Landauer

approach has been applied to several very successful computational studies of wire conductance.[9,10]

More careful quantum mechanical consideration, on the basis of the Green's function, yields:[11,12]

$$g = \frac{e^2}{\pi\eta}\Gamma^L\Gamma^R\left|G\right|^2 \qquad (3.7)$$

where Γ^L and Γ^R represent the strength of the coupling between molecule and electrode at the left and right ends, respectively, and G describe the Green's function matrix element between the first and last site state of the molecular wire, which contains all the molecular information. The importance of this expression is that the transmission probability is explicitly factorized into the molecule-metal contact effect (Γ^L and Γ^R) and the molecular structure dependence.

Despite the fact that equation (3.7) may be powerful and versatile for discussing atomic wires or small molecules, the exact description of electron transfer via a molecular bridge is still difficult. In actual conductance measurement, vibronic interactions between electrons and nuclear motion considerably modify the elastic picture. Such a problem, called inelastic scattering, may occur when the transport time becomes comparable to the time scale of any motions in the environment surrounding the molecular electrons. This is currently of great interest, and has been addressed in pervious studies.[8,13-17]

3.2 Molecular Junction Fabrication Techniques

With the rapid advance of technology, a variety of methods have been exploited to investigate electric properties of molecules. Representative techniques used include scanning tunneling microscopy,[19,20] break junctions,[21-24] mercury drop junctions,[25-27] cross-wire junctions,[28] nanopores,[29,30] and conducting probe atomic force microscopy.[4, 31-36] In this section, the principle of each method is briefly explained, along with experimental results.

3.2.1 Scanning Tunneling Microscope Measurement

The basic principle of scanning tunneling microscopy (STM) is based on the tunneling current between a sharpened metallic tip and a conducting material. When the tip is brought very close without physical contact, a tunneling current (pA to nA) flows across the intervening space between the tip and the sample in the presence of a small bias voltage. Owing to the electron-wave function overlapping between the tip and surface, electrons can tunnel across the vacuum barrier separating the tip and sample. Since the tunneling current is exponentially dependent upon the width of the tunneling barrier, the magnitude of tunneling current is extremely sensitive to the gap distance between the tip and sample and the local density of electronic states of the sample. As we measure the current with the tip moving across the surface, atomic information of the surface can be mapped out. In electron transfer measurements, scanning tunneling microscopy allows localized electron transfer through molecular wires via tunneling with high spatial resolution. However, the disadvantage of this method is susceptible to temperature drift and vibrations (especially in ambient conditions).[18]

Bumm *et al.*[19] measured the decay tunneling constant (β) value, 1.2 $Å^{-1}$or 1.5 per methylene unit for n-alkanethiols value with STM. Recently Xu and Tao[20] studied the conductance of a single molecule and found that the resistances near zero bias were 10.5, 51, 630, and 1.3 MΩs for hexanedithiol, octanedithiol, decanedithiol, and 4,4-bipyridine, respectively, and also the tunneling decay constant (β) for n-alkanedithiols was 1.0 per carbon atom.

3.2.2 Break Junction Measurement

Molecular conductance can be examined by a mechanically controllable break junction (MCB).[21,22] In this technique, a notched metal wire is glued onto a bending beam and stretched until breakage by bending the beam. Then the two open ends form an electrode gap which can be adjusted mechanically with subangstrom precision. (see Figure 3.1) A large reduction factor between the piezo elongation and the electrode

separation results in two electrodes which are inherently stable with respect to each other. To achieve molecular junction, the breakage occurs in a solution of molecules, followed by the evaporation of solvent. The atomically sharp wire contacts demonstrated conductance quantization, implying that the conductance is quantized in the fundamental unit of $2e^2/h$.[23] Reed *et al.* [21] assembled molecules of benzene-1,4-dithiol onto the two facing gold electrodes of a MCB junction, forming a gold-sulfur-benzene-sulfur-gold system. Current-voltage measurements at room temperature demonstrated a highly reproducible apparent gap at about 0.7 volt, and the conductance voltage curve showed two steps in both bias directions. (see Figure 3.2)

The advantage of break junctions is that they are less susceptible to temperature drift and vibrations due to such a large reduction factor, and the evaporation of a metal onto an organic layer is not required.[24] On the other hand, the MCB junctions are difficult to characterize and they often fail due to electrical shortening.[25]

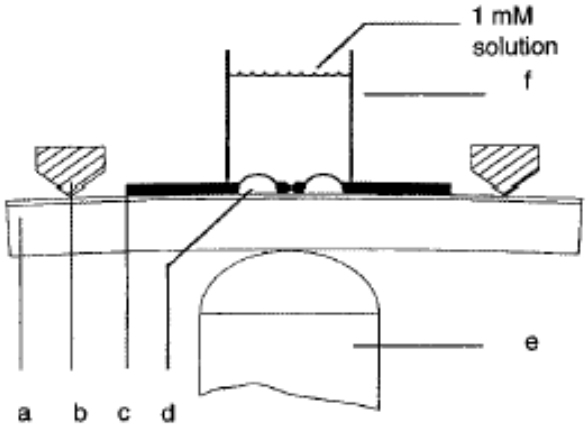

Figure 3.1. A schematic of the mechanically controllable break junction with (a) the bending beam, (b) the counter supports, (c) the notched gold wire, (d) the glue contacts, (e) the pizeo element, and (f) the glass tube containing the solution. (Reproduced with permission from reference 21. Copyright 1997 AAAS)

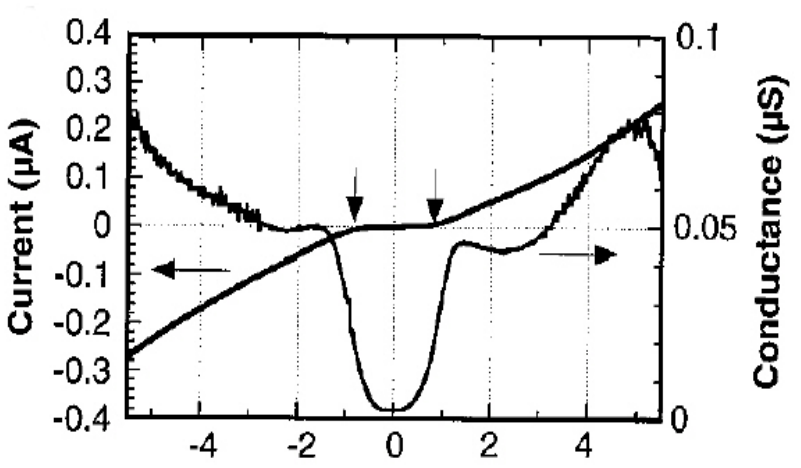

Figure 3.2. Current-voltage characteristics and conductance behavior of a gold-benzene-1,4,-dithiol-gold MCB junction. (Reproduced with permission from reference 21. Copyright 1997 AAAS)

3.2.3 Mercury-Drop Junctions

A significant number of molecular junction studies have used mercury-drop junctions. The mercury drop junction takes advantage of mercury, offering atomically smooth surfaces. Slowinski *et al.*[26,27] have assembled mercury-mercury junctions using two micrometrically driven hanging mercury drop electrodes (HMDE). (see Figure 3.3a) They used silanized 250 μm diameter capillaries to generate mercury drops. Two mercury electrodes were positioned vertically and coaxially, with the top electrode mounted on a vertically movable stage. A small glass cell was mounted coaxially with the glass capillary of the bottom HMDE, allowing for immersion of a junction in a desired alkanethiol solution or pure solvent. A 20 % (v/v) hexadecane solution of alkanethiols was usually used. They found that the tunneling decay constant (β) is 0.89 per CH_2 in the alkanethiol monolayers, which is comparable to the value by other methods, and also proposed a through-bond tunneling mechanism from the dependence of the decay constant on the voltage bias. Holmlin *et al.*[25] modified the experimental setup. One electrode, a drop of SAM-coated Hg, is in contact with the surface of another SAM supported by a second metal (Ag, Au, Cu, or Hg). (see Figure 3.3b) The SAM-coated Hg electrode generated compliant contact with the surface of the other. Merits of the

modified method are that the second electrode is easier to assemble than the mercury electrode, and that junctions are less susceptible to electrical and mechanical breakdown. Hg-molecule-Ag junction studies revealed that tunneling decay parameters (β) are 0.87 $Å^{-1}$ for alkanethiols, 0.61 $Å^{-1}$ for oligophenylene thiols, and 0.67 $Å^{-1}$ for benzylic derivatives of oligophenylene thiols.

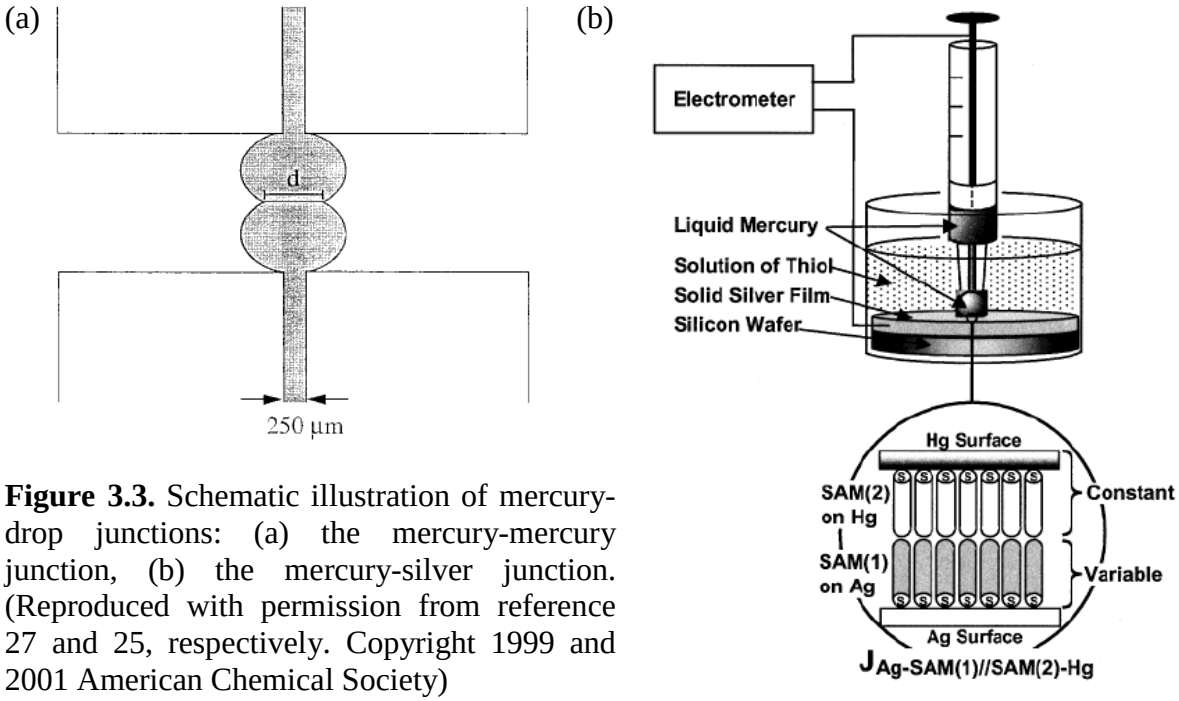

Figure 3.3. Schematic illustration of mercury-drop junctions: (a) the mercury-mercury junction, (b) the mercury-silver junction. (Reproduced with permission from reference 27 and 25, respectively. Copyright 1999 and 2001 American Chemical Society)

3.2.4 Crossed Wire Junctions

The current-voltage (*I-V*) characteristics of self-assembled monolayers (SAMs) can be measured by a cross-wire tunnel junction. A schematic of this device structure is shown in Figure 3.4. The crossed-wire tunnel junction consists of two 10 μm Au wires, one containing a SAM of the molecule of interest. The wires are mounted to a custom built test stage in such a manner that the wires are in a crossed geometry with one wire perpendicular to the applied magnetic field (**B**). The junction separation is controlled by deflecting this wire with the Lorentz force generated from a small dc current (<5 mA). The deflection current is slowly increased so that the wires can make a junction at the

contact point. This approach allows formation of molecular junctions with a high degree of control and the choice of the metal used. Using this method, Kushmerick *et al.*[28] observed that π-conjugated systems facilitate charge transport. Moreover, they found that the smaller bond-length alternation in a π-conjugated molecular wire leads to greater conductivity because of the resulting smaller HOMO-LUMO gap.

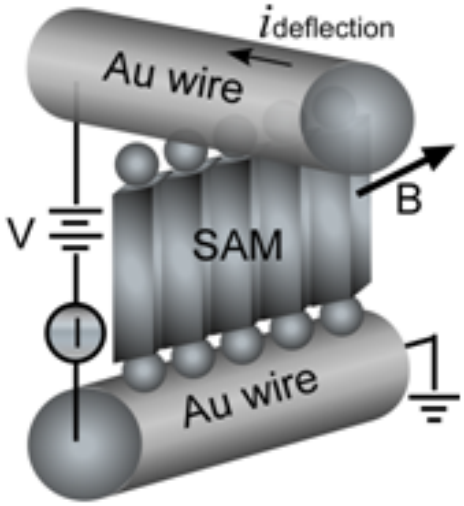

Figure 3.4. Schematic representation of the cross-wire tunnel junction. (Reproduced with permission from reference 28. Copyright 2002 American Chemical Society)

3.2.5 Nanopore Junctions

Nanopore junction fabrication was developed by Zhou *et al.*[29] to directly measure the conductance through a small number of organic molecules. The device consists of a metal top contact, a self-assembled monolayer of molecular wires, and a metal bottom contact. A schematic diagram of the device is shown in Figure 3.5. The process of fabrication begins with a 250-mm-thick double-side polished silicon (100) wafer. The silicon wafer is first coated with a 50 nm layer of low stress Si_3N_4 by low-pressure chemical vapor deposition. The nitride on the back surface is then removed in a (400 μm × 400 μm) square by optical lithography and reactive ion etching (RIE). Etching the exposed silicon with an anisotropic etchant (at 85 °C in a 35 % KOH solution) removes the Si beneath this opening to the top surface, leaving a suspended silicon nitride

membrane (40 μm × 40 μm). 100 nm of SiO_2 is then thermally grown on the Si sidewalls to obtain high electrical insulation. A single bowl-shaped nanopore (30 to 50 nm in diameter) is then made through the membrane by electron beam lithography and reactive ion etching. 200 nm of Au is then evaporated onto the top side of the membrane, forming the top contact. The sample is then immediately immersed into a solution of organothiols for 48 h, and followed by another 200 nm of Au evaporation for the bottom electrode. Finally, the devices are cut into separate chips and loaded into a variable-temperature cryostat, where the electric properties are examined.

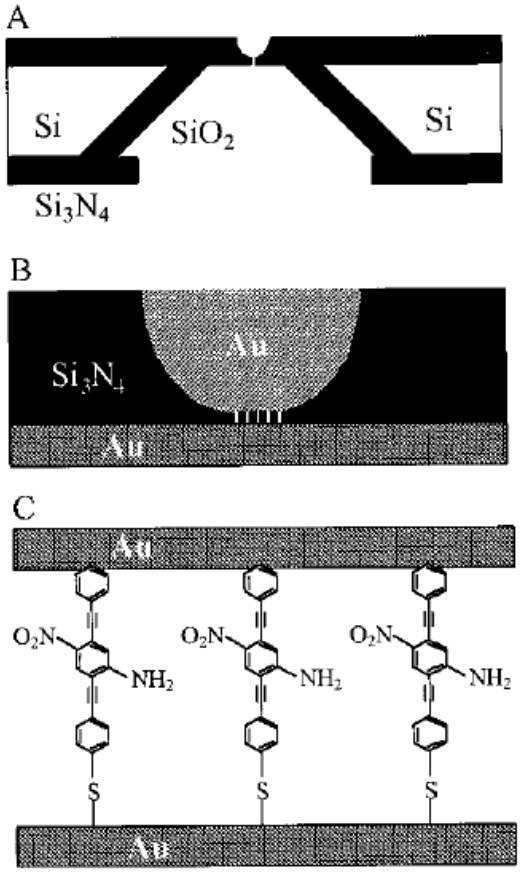

Figure 3.5. Schematics of a nanopore junction fabrication. (a) Cross section of a silicon wafer with a bowl-shaped nanopore etched in suspended silicon nitride membrane. (b) Au top electrode/self-assembled monolayer/Au bottom electrode sandwich junction structure in the nanopore. (c) Blow-up of (b) with molecular structure sandwiched with Au electrodes. (Reproduced with permission from reference 29. Copyright 1999 AAAS)

This nanopore junction technique can have good control over the small device area and intrinsic contact stability, like break junctions and produce a large number of devices with acceptable yield (80 %), so that statistical results can be extracted. Another attractive feature of this method is that we can study molecular junctions at various temperatures. Variable temperature conductance measurements with 1,4-phenylene diisocyanide-metal (Au or Pd) junctions have revealed the dominant charge transport mechanism changes from hopping conduction to thermionic emission depending on the temperature and applied bias.[30]

3.2.6 Conducting Probe Atomic Force Microscopy

Our group[4,31-34] and others[35,36] have developed conducting probe atomic force microscopy (CP-AFM) to characterize self-assembled monolayers. CP-AFM is an attractive technique complementary to other junction forming methods for exploring the current-voltage (*I*-*V*) characteristics of molecular wires. In CP-AFM, a metal-coated AFM tip is brought into contact with a self-assembled monolayer (SAM) under controlled load. (see Figure 3.6.) Metal-coated tips are prepared by thermal evaporation of a 5 nm chromium adhesion layer followed by a 100 nm metal (gold, silver, or palladium) layer. Probe position is adjusted through an optical feedback system using a laser that reflects off the back surface of the AFM tip. Deflections in the laser are registered on the photodiode mounted in the head of the instrument as a change in both frictional and lateral force. A desired contact load on the surface can be obtained by changing a set-point with the help of feedback electronics. In stationary contact AFM mode, *I*-*V* characteristics of the monolayer are measured by sweeping the tip voltage.

CP-AFM junctions have several attractive features. First, CP-AFM offers the ability to characterize the electrical properties in a simple and fast manner. It does not require micro- or nanofabrication processes. Second, CP-AFM junction assembly provides significant flexibility. That is, the tip and substrate can be coated with a variety of metals, which enables us to probe the contact resistance of the molecule-metal contact.

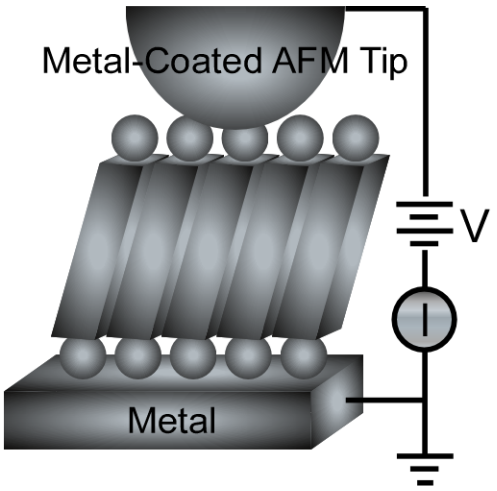

Figure 3.6. Schematic representation of a CP-AFM junction.

Our group has published two papers regarding the contact resistance dependence on metal work function[4,31] For alkanethiol or dithol SAMs, it was apparent that junction contact resistance decreases with increasing metal work function. Third, the delicate control of load in CP-AFM renders opportunities to examine conduction as a function of molecular deformation. Also, the current-contact area behavior can be established. Our group[33] and Cui *et al.*[35] have already investigated the resistance-load dependence. Finally, when compared to STM, CP-AFM allows the probe tip to be controllably positioned in direct contact with the monolayer. STM uses the current through both the molecules and the vacuum gap present between the molecules and the STM tip to control tip-positioning. Since the conductivity of the molecules is generally unknown, the position of the probe with respect to the molecules can be dubious. Moreover, the vacuum gap may affect junction transport, so that we cannot estimate the intrinsic molecular conductivity. However, CP-AFM can provide higher reliability than STM. The efficacy of this method is brought about because we examine the surface in stationary contact mode, and use an independent feedback signal, allowing the tip to touch the molecules at a desired position. Cui *et al.*[36] demonstrated that CP-AFM can be reliably utilized to measure the resistance of a single octanedithiol molecule (900 MΩ), and they pointed out that the intrinsic molecular conductance measurements required chemically bonded contacts.

3.3 References

(1) Aviram, A.; Ratner, M.A. *Chem. Phys. Lett.* **1974**, *29*, 277.

(2) Fendler, J. H. *Chem. Mater.* **2001**, *13*, 3196.

(3) Simmons, J. G. *J. Appl. Phys.* **1963**, *34*, 1793.

(4) Engelkes, V. B.; Beebe, J. M.; Frisbie, C. D. *J. Am. Chem. Soc.* **2004,** *126*, 14287.

(5) Wold, D. J.; Haag, R.; Rampi, M. A.; Frisbie, C. D. *J. Phys. Chem. B* **2002**, *106*, 2813.

(6) Dorneles, L. S.; Schaefer, D. M.; Carara, M.; Schelp, L. F. *Appl. Phys. Lett.* **2003**, *82*, 2832.

(7) Landauer, R. *Phys. Lett. A.* **1981**, *85*, 91.

(8) Nitzan, A. *Annu. Rev. Phys. Chem.* **2001**, *52*, 681.

(9) Samanta, M. P.; Tian, W.; Datta. S.; Henderson, J. I.; Kubiak, C. P. *Phys. Rev. B.* **1996**, *79*, 7626.

(10) Datta. S.; Tian, W.; Hong, S.; Reifenberger, R.; Henderson, J. I.; Kubiak, C. P. *Phys. Rev. Lett.* **1997**, *79*, 2530.

(11) Yaliraki, S. N.; Kemp, M.; Ratner, M. A. *J. Am. Chem. Soc.* **1999**, *121*, 3428.

(12) Zhu, X.-Y. *J. Phys. Chem. B* **2004**, *108*, 8778.

(13) Burin, A. L.; Berlin, Y. A.; Ratner, M. A. *J. Phys. Chem. A.* **2001**, *105*, 2652.

(14) Nitzan, A.; Jortner, J.; Wilkie, J.; Burin, A. L.; Ratner, M. A. *J. Phys. Chem. B* **2000**, *104*, 5661.

(15) Ness, H.; Shevlin, S. A.; Fisher, A. J. *Phys. Rev. B* **2001**, *63*, 125422.

(16) Nitzan, A.; Ratner, M. A. *Science* **2003**, *300*, 1384.

(17) Skourtis, S. S.; Waldeck, D. H.; Beratan, D. N. *J. Phys. Chem. B.* **2004**, *108*, 15511.

(18) Kummel, A. C. *Science* **2003**, *302*, 69.

(19) Bumm, L. A.; Arnold, J. J.; Dunbar, T. D.; Allara, D. L.; Weiss, P. S. *J. Phys. Chem. B* **1999**, *103*, 8122.

(20) Xu, B.; Tao, N. J. *Science* **2003**, *301*, 1221.

(21) Reed, M. A.; Zhou, C.; Muller, C. J.; Burgin, T. P.; Tour, J. M. *Science* **1997**, *278*, 252.

(22) Reichert, J.; Ochs, R.; D. Beckmann, D.; Weber, H. B.; Mayor, M.; Löhneysen H. V. *Phys. Rev. Lett.* **2002**, *88*, 176804.

(23) Muller, C. J.; Krans J. M.; Todorov, T. N.; Reed, M. A. *Phys. Rev. B* **1996**, *53*, 1022.

(24) Muller, C. J.; Vleeming, B. J.; Reed, M. A.; Lamba, J. J. S.; Hara, R.; Jones II, L.; Tour, J. M. *Nanotechnology* **1996**, *7*, 409.

(25) Holmlin, R.; Haag, R.; Chabinyc, M. L.; Ismagilov, R. F.; Cohen, A. E.; Terfort, A.; Rampi, M. A.; Whitesides, G. M. *J. Am. Chem. Soc.* **2001**, *123*, 5075.

(26) Slowinski, K.; Majda, M.; *J. Electroanal. Chem.* **2000**, *491*, 139.

(27) Slowinski, K.; Fong, H. K. Y.; Majda, M. *J. Am. Chem. Soc.* **1999**, *121*, 7257.

(28) Kushmerick, J. G.; Holt, D. B.; Pollack, S. K.; Ratner, M. A.; Yang, J. C.; Schull, T. L.; Naciri, J.; Moore, M. H.; Shashidhar, R. *J. Am. Chem. Soc.* **2002**, *124*, 10654.

(29) Chen, J.; Reed, M. A.; Rawlett, A. M.; Tour, J. M. *Science* **1999**, *286*, 1550.

(30) Chen, J.; Calvet, L. C.; Reed, M. A.; Carr, D. W.; Grubisha, D. S.; Bennett, D. W. *Chem. Phys. Lett.* **1999**, *313*, 741.

(31) Beebe, J. M.; Engelkes, V. B.; Miller, L. L.; Frisbie, C. D. *J. Am. Chem. Soc.* **2002**, *124*, 11268.

(32) Wold, D. J.; Haag, R.; Rampi, M. A.; Frisbie, C. D. *J. Phys. Chem. B* **2002**, *106*, 2813.

(33) Wold, D. J.; Frisbie, C. D. *J. Am. Chem. Soc.* **2001**, *123*, 5549.

(34) Wold, D. J.; Frisbie, C. D. *J. Am. Chem. Soc.* **2000**, *122*, 2970.

(35) Cui, X.D.; Zarate, X.; Tomfohr, J.; Sankey, O.F.; Primak, A.; Moore, A.L.; Moore, T.A.; Gust, D.; Harris, G.; Lindsay, S.M. *Nanotechnology* **2002,** *13*, 5.

(36) Cui, X.D.; Primak, A.; Zarate, X.; Tomfohr, J.; Sankey, O.F.; Moore, A.L.; Moore, T.A.; Gust, D.; Harris, G.; Lindsay, S.M. *Science* **2001,** *294*, 571.

4 Correlation between HOMO Alignment and Contact Resistance in Molecular Junctions: Aromatic Thiols versus Aromatic Isocyanides[†]

4.1 Abstract

Understanding electron transport in metal-molecule-metal (MMM) junctions is of great importance for the advancement of molecular electronics. Critical factors that determine conductivity in a MMM junction include the nature of metal-molecule contacts and the electronic structure of the molecular backbone. We have studied the electronic transport property and the valence electronic structure on rigid, conjugated oligoacenes of increasing length with either thiol (-S) or isocyanide (-CN) linkers using conducting probe atomic force microscopy (CP-AFM) and ultraviolet photoelectron spectroscopy (UPS). We find that for these conjugated systems the Au-CN contact is more resistive than Au-S. The difference in contact resistance correlates with UPS measurements that show the highest-occupied molecular orbital (HOMO) of the isocyanide series is lower in energy (relative to the Fermi level of Au) than the HOMO of the thiol series, indicating the presence of a higher tunneling barrier at the contact for the isocyanide-linked molecules. By contrast, the difference in the HOMO positions for the two series of molecules does not appear to affect the length dependence of the junction resistance (i.e., the β value = 0.5 $Å^{-1}$).

4.2 Introduction

Understanding electron transport in metal-molecule-metal (MMM) junctions is of great importance for the advancement of molecular electronics.[1] Critical factors that determine conductivity in a MMM junction include the nature of metal-molecule contacts and the electronic structure of the molecular backbone. While most junction experiments have utilized thiol (-S) metal contacts, theoretical studies of transport in conjugated

[†] Reproduced with permission from Kim, B.-S.; Beebe, J. M.; Jun, Y.; Zhu, X.-Y.; Frisbie, C. D. *J. Am. Chem. Soc.* **2006**, *128*, 4970-4971. Copyright 2006 American Chemical Society

molecules have addressed a number of surface linkers, including -O, -S, -CN (isocyanide), and -Se.[2] Here we report transport and electronic structure measurements on rigid, conjugated oligoacenes of increasing length with either thiol (-S) or isocyanide (-CN) linkers (Figure 4.1). We use conducting probe atomic force microscopy (CP-AFM) to measure transport and ultraviolet photoemission spectroscopy (UPS) to establish the valence electronic structure. We find that for these conjugated systems the Au-CN contact is more resistive than Au-S. The difference in contact resistance correlates with UPS measurements that show the highest-occupied molecular orbital (HOMO) of the isocyanide series is lower in energy (relative to the Fermi level of Au) than the HOMO of the thiol series, indicating the presence of a higher tunneling barrier at the contact for the isocyanide-linked molecules. By contrast, the difference in the HOMO positions for the two series of molecules does not appear to affect the length dependence of the junction resistance (i.e., the β value).

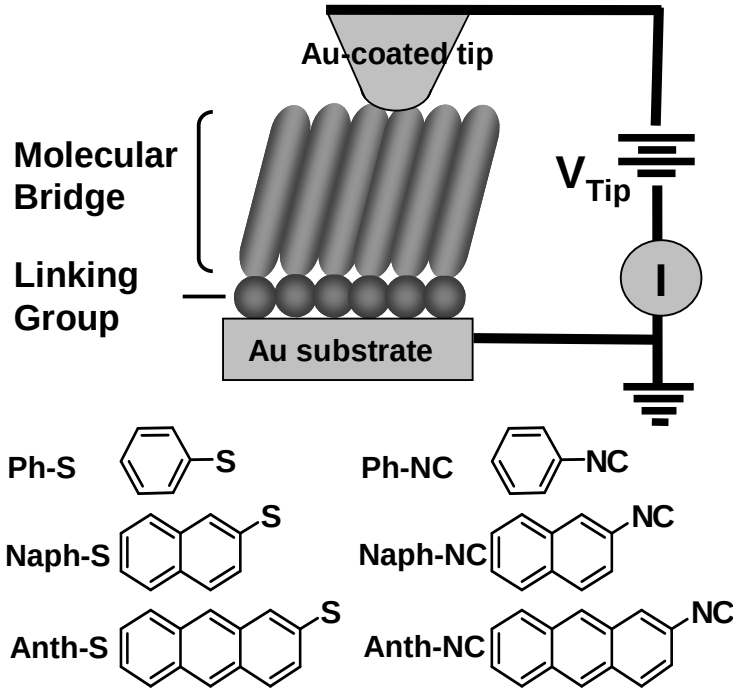

Figure 4.1. Illustration of a metal-molecule-metal junction formed using CP-AFM. An Au-coated tip is brought into contact with a SAM of aromatic molecules on an Au substrate. *I-V* traces are obtained over ±0.3 V at a load of 2 nN. The molecular structures are shown at the bottom.

4.3 Experimental

Synthesis. General Procedure. All solvents were spectrophotometric or reagent grade and were used without further purification. Thiophenol (Ph-SH), 2-naphthalenethiol (Naph-SH), aniline, 2-aminonaphthalene, and 2-aminoanthracene were purchased from Aldrich. ^{1}H NMR spectra were obtained on a Varian VI-300 spectrometer. Proton chemical shifts are referenced to tetramethylsilane (TMS). Infrared spectra were taken on a Nicolet Magna 550 FTIR. High-resolution mass spectra (HRMS) were recorded on a Finnigan FTMS 2001 mass spectrometer.

Benzeneisocyanide (Ph-NC). Ph-NC was prepared by slight modification of a literature procedure.[13] To a round-bottom flask was added aniline (2 ml, 22 mmol) which was diluted with 100 mL of CH_2Cl_2. Then 50 mL of 50 wt % aqueous NaOH and 1 mol % tetrabutylammonium bromide were added. To the CH_2Cl_2/NaOH solution was added 2.6 mL (1.5 equiv, 33 mmol) of $CHCl_3$. The reaction mixture was stirred for 6 h at room temperature, and diluted with 200 mL of H_2O. The mixture was transferred to a separatory flask. The organic layer was separated and washed twice with 100 mL of H_2O and then once with 100 mL of saturated aqueous NaCl. The organic layer was dried over $MgSO_4$, filtered, and the solvent was removed under reduced pressure at room temperature. The product was further purified by column chromatography (silica gel, dichloromethane-hexane (1:4 v/v), yielding 1.2 g (53%). IR: ν(CN), 2125 cm^{-1}. ^{1}HNMR (300 MHz, $CDCl_3$): δ 7.44-7.38 (m, 5H). HRMS Calc for C7H5N: 103.0422. Found: 103.0425.

2-Naphthaleneisocyanide (Naph-NC). Naph-NC was prepared by the same procedure as described for Ph-NC, with a 45 % yield. IR: ν(CN), 2124 cm^{-1}. ^{1}HNMR (300 MHz, $CDCl_3$): δ 7.89-7.82 (m, 4H), 7.62-7.56 (m, 2H), 7.42 (d, 1H). HRMS Calc. for C11H7N: 153.0578. Found: 153.0574.

2-Anthracenyl isocyanide (Anth-NC). Anth-NC was prepared by the same procedure as described for Ph-NC, with a 40 % yield. IR: ν(CN), 2125 cm^{-1}. ^{1}HNMR

(300 MHz, $CDCl_3$): δ 8.46 (s, 2H), 8.06-8.02 (m, 4H), 7.59-7.53 (m, 2H), 7.38 (d, 1H). HRMS Calc. for C15H9N: 203.0735. Found: 203.0734.

SAM Characterization. SAMs of aromatic molecules were characterized by ellipsometry, x-ray photoelectron spectroscopy (XPS), attenuated total reflectance-Fourier transform infrared spectroscopy (ATR-FTIR),[13-15] and ultraviolet photoemission spectroscopy (UPS). Ellipsometry was performed using a Sopra ES4G spectroscopic ellipsometer equipped with a xenon light source. Measurements of the polarization angles Ψ and Δ were taken as a function of wavelength (λ) between 400 and 700 nm at an incident angle of 75°. The indices of refraction (n) and extinction coefficient (k) of Au-coated substrates were determined by measurement of the polarization angles prior to monolayer deposition. The instrument software converted these values to n and k by assuming that the substrate was of infinite thickness. After SAM deposition, the polarization angles were again measured and film thicknesses determined by the instrument software. n and k values of the SAM were assumed to be 1.5 and 0, respectively. XPS spectra were taken on a Perkin-Elmer Phi 5400 spectrometer with the Mg K_α x-ray (1253.6 eV) from an anode source using a hemispherical analyzer in an ultrahigh vacuum system. The x-ray anode was operated at 200 W, and the analyzer at a pass energy of 89.45 eV for survey scans and 17.9 eV for high-resolution scans. The binding energy scales of all spectra were referenced to the Au $4f_{7/2}$ peak (84.0 eV). The SAM thickness was calculated using the relative intensities of the Au_{4f} and the C_{1s} peaks and by using hexadecanethiol SAM on Au as a reference (d = 18.6 Å). Assuming the same attenuation length of the gold (λ_{Au} = 34.6 Å) and carbon (λ_C = 30.2 Å) photoelectrons for the SAMs, the calculation based on equation (4.1) yielded the thickness.[14,16,17]

$$\frac{\frac{I_c}{I_{Au}}(sample)}{\frac{I_c}{I_{Au}}(reference)} = \frac{\left\{1-\exp(-\frac{d_{sample}}{\lambda_c})\right\}\exp(-\frac{d_{reference}}{\lambda_{Au}})}{\exp(-\frac{d_{sample}}{\lambda_{Au}})\left\{1-\exp(-\frac{d_{reference}}{\lambda_c})\right\}} \quad (4.1)$$

where I_C = the intensity of C 1s peaks, I_{Au} = the intensity of Au 4f peaks, and d is the thickness.

Table 4.1 represents the estimated thickness and measured thickness using XPS and ellipsometry. Both methods revealed that thickness increases with molecular length and the thickness of a thiol is comparable to a corresponding isocyanide. In addition, survey scan XPS spectra are displayed in Figure 4.2. All spectra were normalized by Au $4f_{7/2}$ peaks. Au and C 1s peaks were identified from survey XPS spectra while N 1s and S 2p peaks from high-resolution XPS spectra.

Table 4.1. Film thicknesses for aromatic SAMs on Au (unit: Å)

	Estimated Molecular Length[a]	Thickness[b]	
		XPS	Ellipsometry
Ph-S	8.00	5.5	4.1
Naph-S	10.2	7.9	6.5
Anth-S	12.5	11.7	9.1
Ph-NC	8.40	5.9	4.6
Naph-NC	10.6	8.1	6.5
Anth-NC	12.9	11.7	9.0

[a] Molecular length was estimated with the Cambridge Scientific Chem3D software. Molecular length is the terminal H to S or C (isocyanide) distance plus the Au-S or Au-C (isocyanide) bond length. It was assumed that Au-S bond length is 2.36 Å[18] and Au-C(isocyanide) bond length 1.90 Å.[19] [b] Standard deviations are < 2 Å.

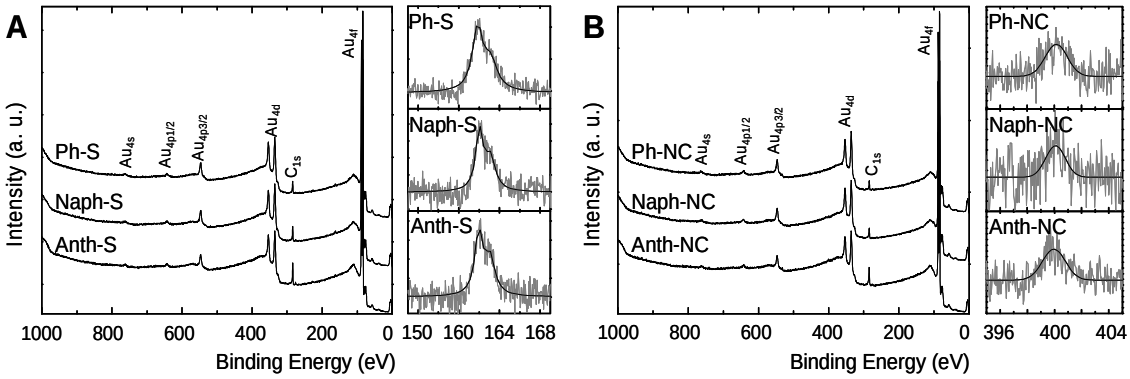

Figure 4.2. (A) Survey XPS spectra (left) and high-resolution spectra of S 2p region (right) of aromatic thiol SAMs and (B) Survey XPS spectra (left) and high-resolution spectra of N 1s region (right) of aromatic isocyanide SAMs.

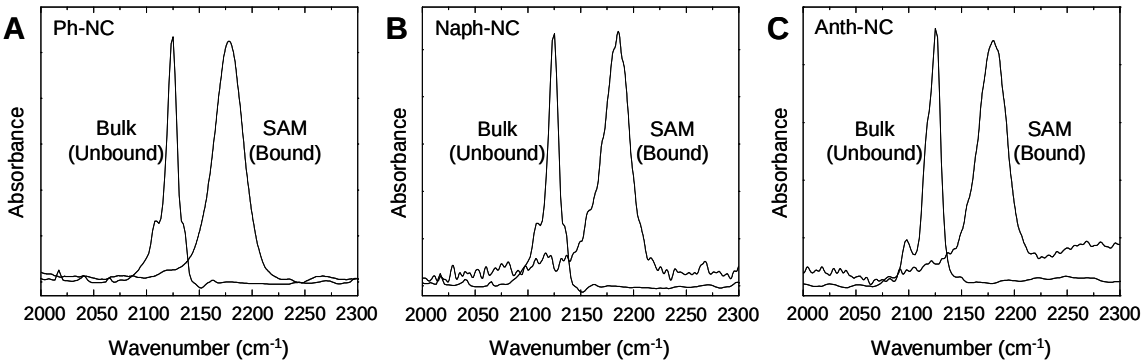

Figure 4.3. FTIR spectra of aromatic isocyanides in the region of 2000-2300 cm^{-1}: (A) Ph-NC, (B) Naph-NC, and (C) Anth-NC. Isocyanide stretching band in bulk (unbound) is displayed on the left and that in SAM (bound) on the right in each figure.

Table 4.2. Wavenumbers of isocyanide stretching mode for aromatic isocyanides

	Unbound NC (cm^{-1})	Bound NC (cm^{-1})
Ph-NC	2125	2186
Naph-NC	2124	2186
Anth-NC	2125	2184

Isocyanide stretching mode in bulk (unbound) and SAMs (bound) of aromatic isocyanides were monitored by FTIR spectroscopy. FTIR data of a bulk sample were collected using NaCl discs for Ph-NC or KBr pellets for Naph-NC and Anth-NC. For the aromatic isocyanide SAMs, ATR-FTIR experiments were carried out using a MIDAC spectrometer with a liquid N_2 cooled MCT detector at an instrument resolution of 1 cm^{-1}. The total scan time for each spectrum was ~20 min. A clean Si (111) sample (with native oxide) was used as reference. Single-pass parallelepiped 45^o Si crystals (50×10×1 mm^3) with 50 reflections were used. A thin (*ca.* 30 Å) Au film was deposited on the Si crystal in a vacuum evaporator at a deposition rate of 1 Å/s, which was then immersed into a 1 mM solution of molecules for 6 h. After thorough rinsing and drying under a stream of nitrogen, the SAM-coated Si crystal was examined. FTIR spectra are shown in Figure 4.3 and isocyanide peak wavenumbers are compiled in Table 4.2. The wavenumber of the isocyanide SAM (bound) is 50-60 cm^{-1} higher than that of bulk (unbound), as published.[19-24]

We optimized SAM preparation conditions (SAM growing period and rinsing method) by ATR-FTIR study, because it is easy to discern physisorbed unbound isocyanides in the SAMs due to strong isocyanide peak. In order to prepare isocyanide SAMs, the optimum condition was found to be growing SAMs for 6 h and rinsing with pure toluene for 20 min and pure acetonitrile for 20 min.

UPS Measurements. UPS spectra for SAMs of Ph-S, Ph-NC, Naph-S and Naph-NC along with bare gold are shown in Figure 4.4. Due to the weak intensity of the molecular energy level peaks obscured by the strong Au d band, the determination of molecular energy levels is guided by theoretical calculations and UPS spectra of corresponding aromatic derivatives.[25]

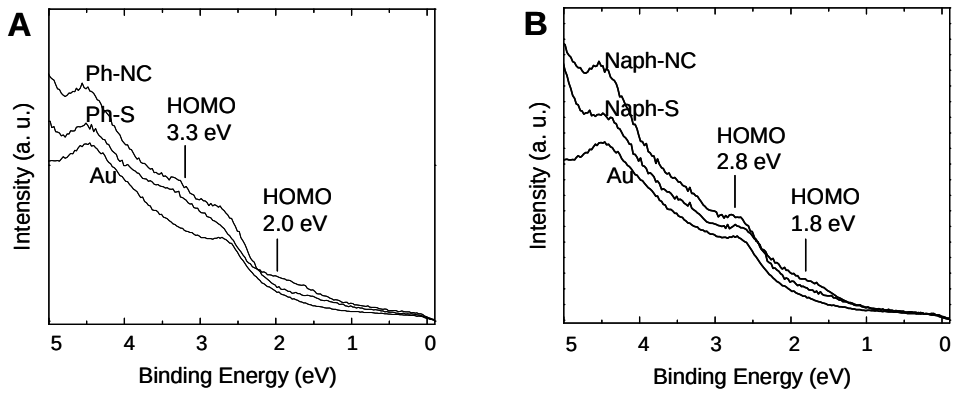

Figure 4.4. UPS spectra for SAMs: Ph-S and Ph-NC (A) and Naph-S and Naph-NC (B).

SAM surface coverage. We analyzed surface coverage of SAMs using XPS and ATR-FTIR. From high-resolution XPS spectra, it is found that the relative intensity ratio (C 1s/Au 4f) of a thiol is slightly lower than that of the corresponding isocyanide. The relative intensity ratios (S 2p/Au 4f) are comparable among aromatic thiols (Ph-S : Naph-S : Anth-S = 1 : 1.1 : 1.1), indicating similar surface coverage among thiols. In addition, peak intensities of isocyanide stretching band in the aromatic isocyanide SAMs are comparable to one another (Ph-NC : Naph-NC : Anth-NC = 1 : 0.9 : 1), implying that the surface coverage is almost the same in the aromatic isocyanide SAMs. Moreover, the thickness measurements by XPS and ellipsometry (in Table S.1) imply similar surface coverage between the aromatic thiols and isocyanides. Again, it should be noted that the surface coverage of isocyanides has been found to be comparable to that of thiols,[19-21,26,27] although aromatic isocyanides have weaker affinity on Au than aromatic thiols.[17] For example, the surface coverage of Ph-NC is 4.9×10^{-10} mol/cm^2 [21] and that of Ph-S is 4.4×10^{-10} mol/cm^2.[29] Therefore, the surface coverage is not a factor in the contact resistance difference between aromatic isocyanides and thiols.

Current-Voltage (*I*-*V*) Measurements. Au-coated AFM tips and flat Au substrates were prepared as described previously.[3] Self-assembled monolayers (SAMs) of

aromatic (benzene (Ph), 2-naphthalene (Naph), 2-anthracene (Anth)) thiols and isocyanides were grown on Au surfaces from 1 mM solutions in toluene for 24 and 6 h, respectively, rinsed thoroughly with toluene and acetonitrile, and dried under a stream of nitrogen. The SAMs have been extensively characterized, and the surface coverage of all of the molecules is comparable to within a factor of 10-20% (see above). We formed each junction by bringing a Au-coated tip into contact with a SAM, as illustrated in Figure 4.1. For each Au-SAM-Au junction, the resistance was determined from the linear current-voltage relationship in the bias voltage range of -0.3 to 0.3 V. A tip radius of ~50 nm was used in all experiments, and the number of molecules in each junction was estimated to be ~100.[4]

4.4 Results and Discussion

Figure 4.5 shows representative semilog plots of junction resistance versus molecular length for both the -S and -CN oligoacene series. The data shown in Figure 4.5 were acquired with a single Au-coated AFM tip. Each resistance value represents the average of approximately ten *I*-*V* traces. The linear fits in Figure 4.5 indicate that the data are well described by the typical non-resonant tunneling equation $R = R_0 \exp(\beta \bullet s)$,[3a] where R is the junction resistance, R_0 is the effective contact resistance (the y-axis intercept), β is the length-dependent tunneling attenuation factor (the slope), and s is the molecular length. Averages obtained from ten sets of measurements (10 different tips) on each series are compiled in Table 4.3. The β values for the two series of molecules are the same (0.5 ±0.1 $Å^{-1}$) within experimental error and are in the expected range[5] but the effective contact resistance R_0 of the isocyanide series is about three times (3×) higher than that of the thiol series. R_0 is an aggregate contact resistance that includes the resistance of both the top and bottom contacts; because the top (tip-molecule) contact is

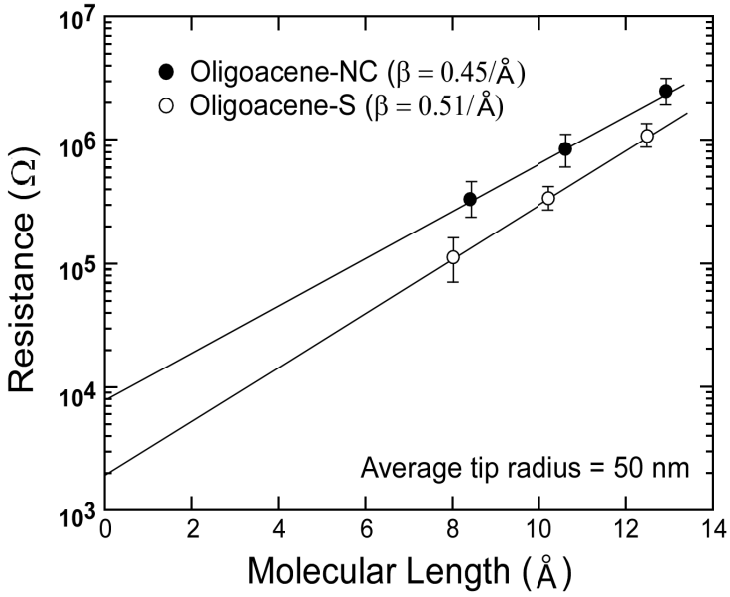

Figure 4.5. Semilog plot of resistance versus molecular length for Au/SAM/Au junctions. Each data point is the average of several I-V traces collected with a single AFM tip. The error bars represent one standard deviation. Straight lines show linear fits to the data.

Table 4.3. Length-dependent tunneling attenuation factors (β) and contact resistances (R_0) for each molecular series.

Molecular Series	β (Å^{-1})	R_0 (Ω)
Oligoacene-S	0.50 (± 0.09)	1.3 (± 1.2) × 10^3
Oligoacene-NC	0.49 (± 0.08)	3.6 (± 1.9) × 10^3

likely to be similar for the two series, we ascribe the difference in the R_0 values to the difference in resistance between the Au-CN-oligoacene and Au-S-oligoacene contacts.

It is not immediately obvious that the junction resistance for the oligoacenes should be well described by $R = R_0 \exp(\beta \bullet s)$, which also works well for aliphatic systems. The HOMO-LUMO gap of the oligoacene backbone decreases substantially with increasing number of rings and this changing electronic structure presumably should

change the β value. However, the influence of the changing molecular electronic structure on transport depends on where the Fermi level lies in the HOMO-LUMO gap, as has been pointed out theoretically.[2b,6] The linear dependence in Figure 4.2 may suggest that the Fermi level is too far from a molecular energy level to impact β substantially.[3a,7] The apparent linear dependence may also be simply a consequence of the small range of molecular lengths (8-13 Å) that we have probed. Interestingly, recent work on molecular junctions based on highly conjugated carotene molecules also demonstrated similar length dependent resistance and a well-defined β parameter.[8] Spectroscopic and electrochemical electron transfer studies have established that electron transfer rates through conjugated bridges of varying lengths can be well-characterized by a β value, typically less than 0.5 $Å^{-1}$.[7,9]

To probe the electronic structure of the SAMs on Au, UPS spectra were taken with He I ($h\nu$ = 21.2 eV) radiation incident at 50 ^{o} from the sample normal. Photoemitted electrons were collected at normal emission with a pass energy of 4.45 eV. All spectra were acquired at an applied bias of -7 V on the sample and the energy scale was referenced to the Fermi level of Au (E_{Fermi}). The intensities of the raw spectra were normalized at E_{Fermi}. Figure 4.6 shows UPS spectra of SAMs of Anth-S, Anth-NC and bare Au. The clean bare Au was prepared by dipping thermally evaporated polycrystalline Au in a piranha solution for 10 min, washing with deionized water and then immediately transferring to the UPS vacuum chamber. Its workfunction was 4.9 eV. Note that the HOMO level of Anth-S lies closer to E_{Fermi} than Anth-NC by 0.7 eV. We found a similar shift in the energy offset (E_{Fermi}- E_{HOMO}) for naphthalene and benzene derivatives, Table 4.4. That is, (E_{Fermi}-E_{HOMO}) was greater for the isocyanide species than for the corresponding thiol species of the same length. We also found that within each series (E_{Fermi}-E_{HOMO}) decreased with molecular length, consistent with expectation.

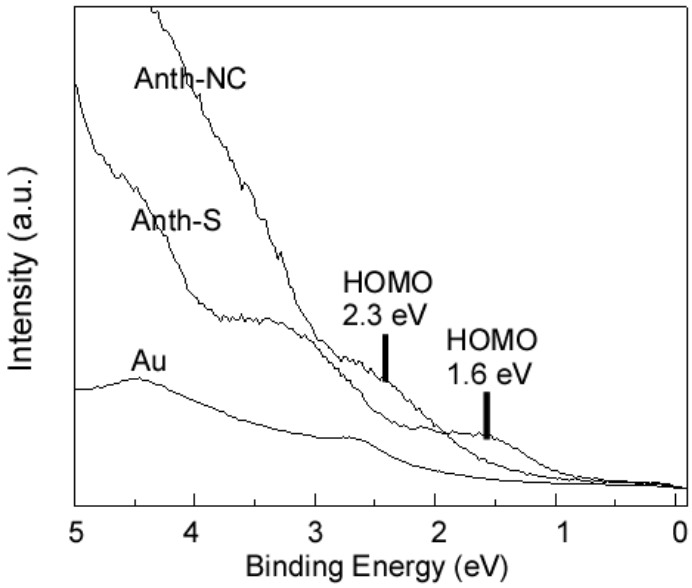

Figure 4.6. Ultraviolet photoelectron spectra for SAMs of Anth-S and -NC along with bare gold. Binding Energy is referenced to E_{Fermi} and the intensities of the raw spectra were normalized at E_{Fermi}.

Table 4.4. Energy offsets (E_{Fermi}-E_{HOMO}) of SAMs on Au (unit: eV).

	E_{Fermi}-E_{HOMO}		E_{Fermi}-E_{HOMO}
Ph-S	2.0	Ph-NC	3.3
Naph-S	1.8	Naph-NC	2.8
Anth-S	1.6	Anth-NC	2.3

We propose that the offset (E_{Fermi}-E_{HOMO}) for the -S and -NC series is the reason for the difference in contact resistance between aromatic thiols and isocyanides. The smaller offset observed for the aromatic thiols should produce more effective coupling between states in the metal and the HOMO level of the molecules, thereby reducing the effective barrier to tunneling at the contact.[10] However, one could have anticipated that a smaller offset would also affect β, particularly because the HOMO states for both the thiol and isocyanide compounds are delocalized across the linking group and the aromatic

system.[10] The dependence of β on Fermi level position has not been examined experimentally for conjugated systems beyond what is reported here, though theoretical work suggests a strong dependence may be expected.[10,11] Elucidating the precise dependence of R_0 and β on energy level alignment will require further experiments in which electronic structure and transport measurements are coupled with synthesis of homologous molecules having systematically varying electron affinities or ionizationpotentials. We note that preliminary UPS and CP-AFM measurements in our laboratory on oligophenylene thiols and isocyanides yield similar results to what we have reported here for the oligoacene systems.

4.5 Acknowledgment

We thank NSF (CHE-0315165) for financial support and Andreas Terfort, Universität Hamburg, for providing the 2-anthracenethiol (AnthSH).

4.6 References

(1) (a) Kushmerick, J. G. *Materials Today* **2005**, *8*, 26. (b) Nitzan, A.; Ratner, M. A. *Science* **2003**, *300*, 1384. (c) Heath, J. R.; Ratner, M. A. *Physics Today* **2003**, *56*, 43.

(2) (a) Patrone, L.; Palacin, S.; Charlier, J.; Armand, F.; Bourgoin, J. P.; Tang, H.; Gauthier, S. *Phys. Rev. Lett.* **2003**, *91*, 096802. (b) Yaliraki, S. N.; Kemp, M.; Ratner, M. A. *J. Am. Chem. Soc.* **1999**, *121*, 3428.

(3) (a) Engelkes, V. B.; Beebe, J. M.; Frisbie, C. D. *J. Am. Chem. Soc.* **2004**, *126*, 14287. (b) Engelkes, V. B.; Beebe, J. M.; Frisbie, C. D. *J. Phys. Chem. B* **2005**, *109*, 16801.

(4) (a) Beebe, J. M.; Engelkes, V. B.; Miller, L. L.; Frisbie, C. D. *J. Am. Chem. Soc.* **2002**, *124*, 11268. (b) Salomon, A.; Cahen, D.; Lindsay, S.; Tomfohr, J.; Engelkes, V. B.; Frisbie, C. D. *Adv. Mater*. **2003**, *15*, 1881.

(5) (a) Magoga, M.; Joachim, C. *Phys. Rev. B* **1997**, *56*, 4722. (b) Kaun, C. C.; Larade, B.; Guo, H. *Phys. Rev. B* **2003**, *67*, 121411. (c) Wold, D. J.; Haag, R.; Rampi, M. A.; Frisbie, C. D. *J. Phys. Chem. B* **2002**, *106*, 2813. (d) McCreery, R. *Electrochem. Soc. Interface* **2004**, 46.

(6) (a) Yaliraki, S. N.; Roitberg, A. E.; Gonzalez, C.; Mujica, V.; Ratner, M. A. *J. Chem. Phys.* **1999**, *111*, 6997. (b) Taylor, J.; Brandbyge, M.; Stokbro, K. *Phys. Rev. Lett.* **2002**, *89*, 138301. (c) Tomfohr, J. K.; Sankey, O. F. *Phys. Rev. B* **2002**, *65*, 245105

(7) Davis, W. B.; Svec, W. A.; Ratner, M. A.; Wasielewski, M. R. *Nature* **1998**, *396*, 60.

(8) He, J.; Chen, F.; Li, J.; Sankey, O. F.; Terazono, Y.; Herrero, C.; Gust, D.; Moore, T. A.; Moore, A. L.; Lindsay, S. M. *J. Am. Chem. Soc.* **2005**, *127*, 1384.

(9) (a) Sikes, H. D.; Smalley, J. F.; Dudek, S. P.; Cook, A. R.; Newton, M. D.; Chidsey, C. E. D.; Feldberg, S. W. *Science* **2001**, *291*, 1519. (b) Creager, S.; Yu, C. J.; Bamdad, C.; O'Connor, S.; MacLean, T.; Lam, E.; Chong, Y.; Olsen, G. T.; Luo, J. Y.; Gozin, M.; Kayyem, J. F. *J. Am. Chem. Soc.* **1999**, *121*, 1059. (c) Sachs, S. B.; Dudek, S. P.; Hsung, R. P.; Sita, L. R.; Smalley, J. F.; Newton, M. D.; Feldberg, S. W.; Chidsey, C. E. D. *J. Am. Chem. Soc.* **1997**, *119*, 10563. (d) Helms, A.; Heiler, D.; McLendon, G. *J. Am. Chem. Soc.* **1991**, *113*, 4325.

(10) (a) Xue, Y.; Ratner, M. A. *Phys. Rev. B* **2003**, *68*, 115406. (b) Xue, Y.; Datta, S.; Ratner, M. A. *J. Chem. Phys.* **2001**, *115*, 4292.

(11) Tada, T.; Nozaki, D.; Kondo, M.; Hamayama, S.; Yoshizawa, K. *J. Am. Chem. Soc.* **2004**, *126*, 14182.

(12) Weber, W. P.; Gokel, G. W.; Ugi, I. K. *Angew. Chem. Int. Ed.* **1972**, *11*, 530.

(13) Beebe, J. M.; Engelkes, V. B.; Liu, J. Q.; Gooding, J.; Eggers, P. K.; Jun, Y.; Zhu, X.-Y.; Paddon-Row, M. N.; Frisbie, C. D. *J. Phys. Chem. B* **2005**, *109*, 5207.

(14) Fuxen, C.; Azzam, W.; Arnold, R.; Witte, G.; Terfort, A.; Woll, C. *Langmuir* **2001**, *17*, 3689.

(15) Jun, Y. S.; Zhu, X.-Y. *J. Am. Chem. Soc.* **2004**, *126*, 13224.

(16) Bain, C. D.; Whitesides, G. M. *J. Phys. Chem.* **1989**, *93*, 1670.

(17) Laibinis, P. E.; Bain, C. D.; Whitesides, G. M. *J. Phys. Chem.* **1991**, *95*, 7017.

(18) Tour, J. M.; Jones, L.; Pearson, D. L.; Lamba, J. J. S.; Burgin, T. P.; Whitesides, G. M.; Allara, D. L.; Parikh, A. N.; Atre, S. V. *J. Am. Chem. Soc.* **1995**, *117*, 9529.

(19) Huc, V.; Bourgoin, J. P.; Bureau, C.; Valin, F.; Zalczer, G.; Palacin, S. *J. Phys. Chem. B* **1999**, *103*, 10489.
(20) Robertson, M. J.; Angelici, R. J. *Langmuir* **1994**, *10*, 1488.
(21) Shih, K. C.; Angelici, R. J. *Langmuir* **1995**, *11*, 2539.
(22) Swanson, S. A.; McClain, R.; Lovejoy, K. S.; Alamdari, N. B.; Hamilton, J. S.; Scott, J. C. *Langmuir* **2005**, *21*, 5034.
(23) Murphy, K. L.; Tysoe, W. T.; Bennett, D. W. *Langmuir* **2004**, *20*, 1732.
(24) Henderson, J. I.; Feng, S.; Bein, T.; Kubiak, C. P. *Langmuir* **2000**, *16*, 6183.
(25) Kim, B.-S.; Heimel, G.; da Silva Filho, D. A.; Bredas, J.-L.; Zhu, X.-Y.; Frisbie, C. D., unpublished results.
(26) Stapleton, J. J.; Daniel, T. A.; Uppili, S.; Cabarcos, O. M.; Naciri, J.; Shashidhar, R.; Allara, D. L. *Langmuir* **2005**, *21*, 11061.
(27) Hickman, J. J.; Laibinis, P. E.; Auerbach, D. I.; Zou, C.; Gardner, T. J.; Whitesides, G. M.; Wrighton, M. S. *Langmuir* **1992**, *8*, 357.
(28) Walker, B. R.; Wassel, R. A.; Stefanescu, D. M.; Gorman, C. B. *J. Am. Chem. Soc.* **2004**, *126*, 16330.
(29) Tao, Y. T.; Wu, C. C.; Eu, J. Y.; Lin, W. L.; Wu, K. C.; Chen, C. H. *Langmuir* **1997**, *13*, 4018.

5 Length-Dependent Transport in Molecular Junctions Based on SAMs of Aromatic Thiols and Dithiols: Effect of Contact Type and Metal Work Function

5.1 Abstract

We characterize the electronic properties of oligoacene (benzene, naphthalene, anthracene, tetracene) thiol and dithiol self-assembled monolayers (SAMs) using conducting probe atomic force microscopy (CP-AFM), in conjunction with ultraviolet photoelectron spectroscopy (UPS). Each nanoscopic tunnel junction consists of a metalized AFM tip (Ag, Au, or Pt) contacting a SAM on flat Ag, Au, or Pt substrates. At low biases (<0.3 V), junction resistance (R) increases exponentially with molecular length (s), i.e. $R = R_0 \exp(\beta \bullet s)$, where R_0 is the contact resistance and β the tunneling attenuation factor. The contact resistances of oligoacene dithiols are two orders of magnitude less than those of oligoacene thiols for a given electrode set, and both decrease with electrode metal work function. The β value is found to be 1.0 per ring or 0.5/Å for the monothiol series and 0.5 per ring or 0.2/Å for the dithiol series and is independent of metal work function. These measurements allow us to determine transmission values for each contact and each benzene ring as well as the characteristic voltage (V_{trans}) where a transition from nonresonant tunneling to field emission occurs. We find that the β values and contact resistance are well correlated with the energy offsets between the metal Fermi level and the highest occupied molecular orbital.

5.2 Introduction

Fundamental understanding of charge transport at metal/organic interfaces is essential to many molecule-based electronic and optoelectronic applications, including organic light-emitting diodes, organic thin film transistors (OTFTs), organic photovoltaics (OPVs), and nanoscopic junctions based on single molecules or a small assembly of molecules. For instance, self-assembled monolayers can modify the work function of the metal via interface dipole formation at the interface.[1-5] In this regard, it is of great importance to determine the energy alignment of molecular levels with respect to the metal Fermi level using spectroscopic techniques such as ultraviolet photoelectron spectroscopy (UPS). Information on energy level alignment is critical to the mechanistic understanding of nanoscopic molecular junctions where molecules are sandwiched between two metal electrodes (see Figure 5.1). In such junctions, tunneling is expected to be the dominant transport mechanism at low bias. In a zeroth order approximation, conduction is dictated by barrier height (ϕ) and width (i.e. molecular length – typically 20 Å).[6-8] The former is determined by the energy offset between the electrode Fermi level (E_{Fermi}) and the frontier molecular energy level, closest in energy to E_{Fermi}. In addition,

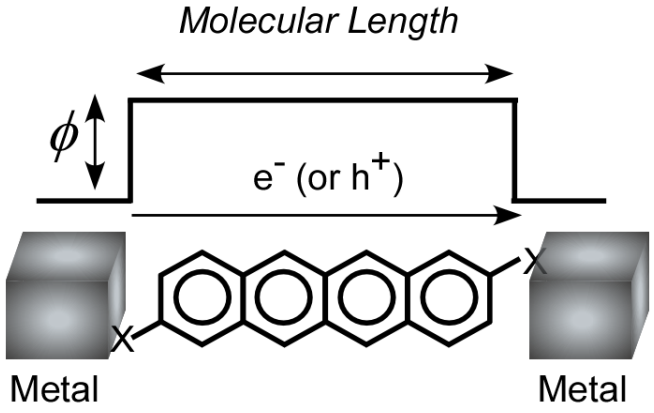

Figure 5.1. Schematic representation of charge transport in metal-molecule-metal junctions. Charge carriers (electrons or holes) across a tunneling barrier with width of molecular length.

surface linkers and metal types can also tune the energy level alignment, resulting in different current-voltage characteristics. To date, there have been a few publications aimed at energy level alignment at the interfaces of SAM/metal systems.[9-14]

To establish the structure-property relationship for molecular conductance, we and others investigated junction properties of various organic molecules. Due to difficulties in reliable junction fabrication and the lack of systematic studies on molecular structures, there is limited understanding of this structure-property relationship. For most organic thiols, the highest occupied molecular orbitals (HOMOs) lie closer to the E_F than the lowest unoccupied molecular orbitals (LUMOs) do and conductance behaviors are strongly influenced by the HOMOs.[3,9,15-21] Extensive research on the linking groups, e.g. thiols (-SH),[19] dithiols,[22-24] isocyanides (-NC),[19] amines (-NH_2),[23] dimethyl phosphines (-$P(CH_3)_2$),[25] methyl sulfides (-SCH_3),[25] dicarbodithionic acids (-CS_2H),[26] and carboxylic acids (-CO_2H),[23] revealed that the contact resistance is highly dependent on the surface linkers. In the case of most organic thiols, high work function metals increase currents due to reduced transport barrier height.[22,27]

However, most junction studies focused on aliphatic systems while more attractive aromatic molecules are not well understood yet. When compared to aliphatic molecules, aromatic molecules are expected to give higher conductance due to stronger electronic coupling via closer HOMO or LUMO bands to E_{Fermi}. Systematic studies of aromatic thiols addressing the effects of key parameters, i.e. energy level alignment, contact effect, and metal work function are scarce. Here we measure junction properties based on the oligoacene thiols and dithiols using CP-AFM (see Figure 5.2). These molecules feature the highly conjugated and rigid backbones with varying length. We compare monothiols vs. dithiols on three metals (Ag, Au, and Pt). We aim to understand the correlation between energy level alignment and junction resistance.

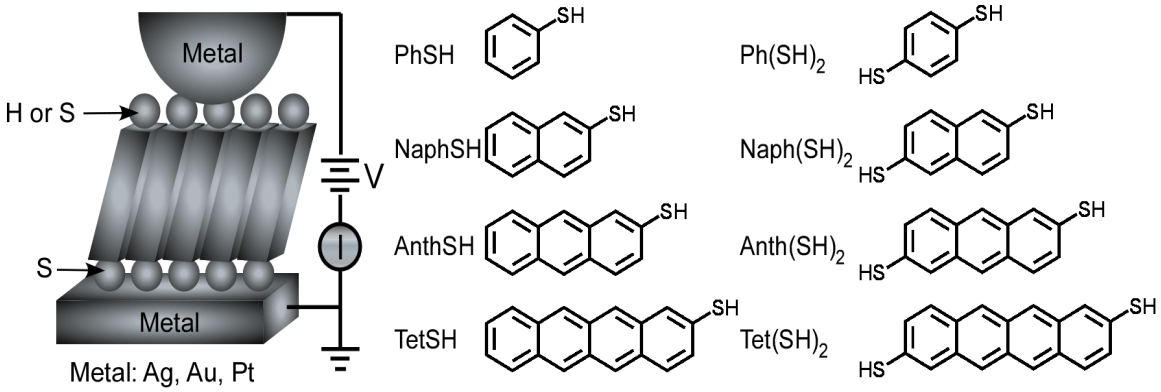

Figure 5.2. Schematic representation of a CP-AFM junction on the left. A metal-coated (Ag, Au, or Pt) AFM tip is brought into contact with a SAM of oligoacene thiols or dithiols of various length on a metal substrate at load of 1 nN. Voltage is swept at the tip and current-voltage characteristics are recorded. The molecular structures are shown on the right.

5.3 Experimental

Materials. Gold nuggets (99.999% pure) were purchased from Mowrey, Inc. (St. Paul, MN). Evaporation boats and chromium evaporation rods were purchased from R. D. Matthis (Long Beach, CA). Platinum and titanium for e-beam evaporation were purchased from Kamis, Inc. (Mahopac Falls, NY). Silicon (100) wafers were purchased from WaferNet (San Jose, CA). Contact mode AFM tips (DNP or NP silicon nitride probes) were purchased from Veeco Instruments (Camarillo, CA). Absolute ethanol was purchased from Fisher Scientific.

Synthesis of Oligoacene Thiols and Dithiols. Benzenethiol (PhSH) and naphthalene-2-thiol (NaphSH) were purchased from Aldrich, and the rest molecules in Figure 5.2 were synthesized as shown in Scheme 5.1. Chemicals for the synthesis of the molecules were purchased from Aldrich if not mentioned. In case of tetracene-2-thiol and oligoacene dithiols, molecules were synthesized with thiol groups capped by acetyl (Ac) groups to increase solubility of molecules and avoid disulfide formation. Upon monolayer growth the acetyl groups were deprotected with an appropriate amount of bases. THF and triethylamine (TEA) were dried following procedures in the literature.[28]

All the other solvents were spectrophotometric or reagent grade and were used without further purification. ^{1}H NMR spectra were obtained on a Varian VI-300 spectrometer. Proton chemical shifts are referenced to tetramethylsilane (TMS). Infrared spectra were taken on a Nicolet Magna 550 FTIR. High-resolution mass spectra (HRMS) were recorded on a Finnigan FTMS 2001 mass spectrometer or a Bruker Biotof II mass spectrometer.

1,4-Di(acetylthio)benzene (Ph(SAc)$_2$): Benzene-1,4-dithiol (**1**) (0.5 g, 3.5 mmol, Alfa Aesar) and acetyl chloride (1.0 g, 1.3 mmol) were dissolved in 100 mL of dry THF. To this solution was added triethylamine (1.3 g, 1.3 mmol) slowly. The reaction mixture was vigorously stirred at room temperature overnight. After the evaporation of the solvent under reduced pressure, the residual mixture was dissolved in 100 mL of CH_2Cl_2, and washed with 100 mL of H_2O (3×) in a separatory funnel. The organic layer was separated, and the solvent was removed. The crude product was purified by column chromatography (silica gel, dichloromethane-hexane (1:1 v/v), yielding 0.75 g (92%). ^{1}HNMR (300 MHz, $CDCl_3$): δ 7.47 (s, 4H), 2.46 (s, 6H) ppm. ^{13}CNMR (300 MHz, $CDCl_3$): δ 193.3, 134.9, 129.7, 30.4 ppm. HRMS Calcd. for C10H10O2S2: 226.0122. Found: 226.0141.

Naphthalene-2,6-disulfonyl chloride (3): 2,6-Naphthalenedisulfonic acid disodium salt (1.0 g**,** 3.0 mmol) and phosphorus pentachloride (1.5 g, 7.2 mmol) were mixed and vigorously stirred at 120 ^{o}C for 2 h. After cooling the reaction mixture down to room temperature, 100 mL of $CHCl_3$ was added and refluxed for 1 h. While the solution is hot, the reaction mixture is filtered and washed with 100 mL of H_2O (3×) in a separatory funnel. The organic layer was then separated and the solvent was then removed under pressure till the solution becomes almost saturated. To the solution, 100 mL of methanol was poured with stirring and white precipitate was formed and filtered with rinsing with methanol. The product was dried at room temperature, yielding 0.86 g (88%). ^{1}HNMR (300 MHz, $CDCl_3$): δ 8.75 (d, J=2.1 Hz, 2H), 8.34 (d, J=9 Hz, 2H), 8.24 (dd, J=9.0, 1.8 Hz, 2H) ppm. ^{13}CNMR (300 MHz, $CDCl_3$): δ 132.4, 128.6, 124.0 ppm.

Scheme 5.1. Synthesis of Oligoacene thiols and dithiols

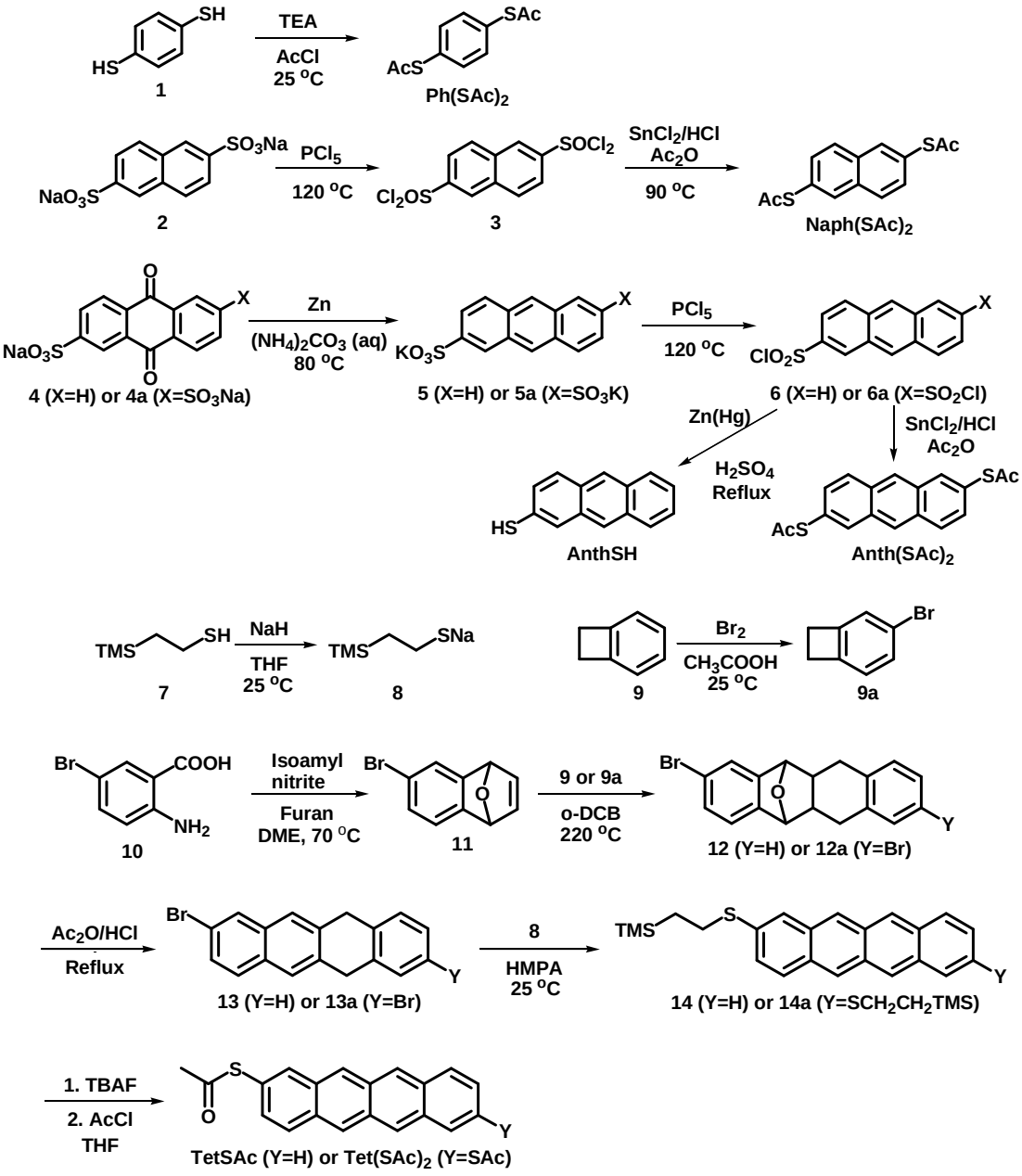

2,6-Di(acetylthio)naphthalene (Naph(SAc)$_2$): Stannous chloride dihydrate (2.0 g, 4.4 mmol) was dissolved in a mixture of 10 mL of acetic anhydride and 2 mL of concentrated HCl. The mixture was heated to 90 ^{o}C and naphthalene-2,6-disulfonyl

chloride (**3**) (0.067 g, 0.31 mmol) was added. The reaction mixture was vigorously stirred at 90 ^{o}C for 2 h, and then allowed to cool down to room temperature. After addition of 100 mL of H_2O to the reaction mixture, the product was extracted with 100 mL of CH_2Cl_2 (3×) in a separatory funnel. The solvent was then dried and the crude product was purified by column chromatography (silica gel, dichloromethane-hexane (2:1 v/v), yielding 0.048 g (56%). ^{1}HNMR (300 MHz, $CDCl_3$): δ 7.98 (d, *J*=1.5 Hz, 2H), 7.87 (d, *J*=8.7 Hz, 2H), 7.51 (dd, *J*=8.4, 1.5 Hz, 2H), 2.48 (s, 6H) ppm. ^{13}CNMR (300 MHz, $CDCl_3$): δ 193.9, 134.5, 131.7, 128.9, 127.0, 30.43 ppm. HRMS Calc. for C14H12O2S2: 276.0279. Found: 299.0170 ($[M+Na]^+$).

Anthracene-2-sulfonic acid potassium salt (5): 9,10-anthraquinonesulfonic acid sodium salt monohydrate (**4**) (11.5 g, 35.0 mmol) and ammonium carbonate (16.0 g, 167 mmol) were added to 150 mL of H_2O and heated to 80 ^{o}C with vigorous stirring. Zn metal (20 g) activated with 3 % HCl was added to the reaction mixture, and the reaction temperature was kept at 80 ^{o}C for 3 d. After cooling down, the reaction mixture was slowly neutralized with concentrated H_2SO_4. The white precipitate was filtered, rinsed with cold acetone, and then recrystallized with a solution containing 200 mL of H_2O and 15 g of KCl. The white product was filtered, rinsed with cold acetone, and dried, yielding 9.0 g (87%). ^{1}HNMR (300 MHz, DMSO-d_6): δ 8.65 (s, 1H), 8.56 (s, 1H), 8.30 (s, 1H), 8.12-8.07 (m, 2H), 8.04 (d, *J*=9.0 Hz, 1H), 7.00 (dd, *J*=8.7, 1.5 Hz, 1H), 7.56-7.50 (m, 2H) ppm. ^{13}CNMR (300 MHz, DMSO-d_6): δ 145.4, 132.1, 132.0, 131.3, 130.8, 128.62, 128.59, 128.3, 127.5, 126.3, 126.2, 124.49, 124.45 ppm. HRMS Calcd. for C14H9KO3S: 295.9909. Found: 257.0272 ($[M-K]^-$).

Anthracene-2,6-disulfonic acid dipotassium salt (5a): This compound was prepared using similar procedures as for **5** using 9,10-anthraquinone-2,6-disulfonic acid disodium salt and double equivalent of reaction agents (yield: 48%). ^{1}HNMR (300 MHz, DMSO-d_6): δ 8.62 (s, 2H), 8.29 (s, 2H), 8.03 (d, *J*=8.7 Hz, 2H), 7.69 (dd, *J*=9.0, 1.8 Hz, 2H) ppm. ^{13}CNMR (300 MHz, DMSO-d_6): δ 145.6, 131.6, 131.2, 128.3, 127.3, 124.6, 124.5 ppm. HRMS Calcd. for: C14H8K2O6S2: 413.9036. Found: 452.8673 ($[M+K]^+$).

Anthracene-2-sulfonyl chloride (6): Anthracene-2-sulfonic acid potassium salt (**5**) was first converted to anthracene-2-sulfonyl chloride (**6**) using similar procedures as for compound **3** (yield: 50%). ^{1}HNMR (300 MHz, $CDCl_3$): δ 8.85 (s, 1H), 8.70 (s, 1H), 8.58 (s, 1H), 8.22 (d, *J*=9.0 Hz, 1H), 8.13-8.07 (m, 2H), 7.92 (d, *J*=9.0 Hz, 1H), 7.70-7.60 (m, 2H). HRMS Calcd. for C14H9ClO2S: 276.0006. Found: 276.0015.

Anthracene-2,6-sulfonyl chloride (**6a**): anthracene-2,6-disulfonic acid dipotassium salt (**5a**) was first converted to anthracene-2,6-sulfonyl chloride (**6a**) using similar procedures as for compound **3**. (yield: 94%). ^{1}HNMR (300 MHz, $CDCl_3$): δ 8.88 (d, *J*=1.5 Hz, 2H), 8.83 (s, 2H), 8.35 (d, *J*=9 Hz, 2H), 8.07 (dd, *J*=9, 1.8 Hz, 2H) ppm. ^{13}CNMR (300 MHz, $CDCl_3$): δ 131.5, 130.7, 130.2, 121.5 ppm. ^{1}HNMR (300 MHz, DMSO-d_6): δ 8.65 (s, 2H), 8.32 (s,2H), 8.05 (d, *J*=9.0 Hz, 2H), 7.70 (dd, *J*=8.7, 1.5 Hz, 2H) ppm. ^{13}CNMR (300 MHz, DMSO-d_6): δ 145.1, 131.6, 131.2, 128.4, 127.4, 124.6, 124.4 ppm. HRMS Calcd. for C14H8Cl2O4S2: 373.9236. Found: 373.9263.

Anthcene-2-thiol (AnthSH): The anthracene-2-sulfonyl chloride (**6**) (0.5 g, 1.8 mmol) and a freshly prepared Zn(Hg) amalgam (20 g) were added to a solution of 50 mL of 30% H_2SO_4 (aq) with vigorous stirring. The reaction mixture was refluxed for 2 h. The crude product was extracted with 50 mL of CH_2Cl_2 (3×). The solvent was then under reduced pressure and the white product was purified by column chromatography (silica gel, dichloromethane-hexane (1:4 v/v), yielding 0.35 g (92%). ^{1}HNMR (300 MHz, $CDCl_3$): δ 8.38 (s, 1H), 8.27 (s, 1H), 7.99 (d, J=8.7 Hz, 2H), 7.92 (s, 1H), 7.91 (d, J=8.7Hz, 1H), 7.51-7.43 (m, 2H), 7.31 (dd, J=8.7, 1.8 Hz, 1H), 3.65 (s, 1H) ppm. ^{13}CNMR (300 MHz, $CDCl_3$): δ 129.1, 128.3, 128.2, 127.8, 127.7, 126.7, 126.5, 125.9, 125.5, 124.8 ppm. HRMS Calcd. for C14H10S: 210.0503. Found: 210.0506.

2,6-Di(acetylthio)anthracene (Anth(SAc)$_2$): The anthracene-2,6-disulfonyl chloride (**6a**) (1.3 g, 3.5 mmol) was converted to 2,6-Di(acetylthio)anthracene (**Anth2SAc**) using similar procedures as for **Naph2SAc** (yield: 62%). ^{1}HNMR (300 MHz, $CDCl_3$): δ 8.44 (s, 2H), 8.14 (d, *J*=1.8 Hz, 2H), 8.05 (d, *J*=9.0 Hz, 2H), 7.45 (dd, *J*=9.0, 1.8 Hz, 2H), 2.51 (s, 6H) ppm. ^{13}CNMR (300 MHz, $CDCl_3$): δ 194.3, 134.7,

132.2, 131.4, 130.5, 129.3, 126.9, 125.9, 30.5 ppm. HRMS Calcd. for C18H14O2S2: 326.0430. Found: 326.0447.

Sodium 2-(trimethylsilyl)ethanethiolate (8): Sodium hydride (0.2 g, 8.3 mmol) was added to 10 mL of dry THF solution containing 2-(trimethylsilyl)ethanethiol (**7**) (1.12 g, 8.3 mmol, Fluka) with vigorous stirring for 1 h. Removal of the solvent yielded white pure product **8**. ^{1}HNMR (300 MHz, $CDCl_3$): δ 2.79-2.72 (m, 2H), 0.98-0.90 (m, 2H), 0.03 (s, 9H) ppm. ^{13}CNMR (300 MHz, $CDCl_3$): δ 34.9, 17.2, -1.65 ppm.

9a: This compound was prepared as described in the literature.[29]

11: To a three-necked round bottomed flask with a condenser and two dropping funnels were added furan (10 g, 146 mmol) and 20 mL of 1,2-dimethoxyethane (DME). The two dropping funnels contained isoamyl nitrite (3.5 g, 29.4 mmol) diluted with 10 mL of DME and 2-amino-5-bromobenzoic acid (6.35 g, 29.4 mmol) dissolved in 10 mL of DME, respectively. The reaction mixture was heated to 70 ^{o}C in a water bath. While vigorously stirring, the isoamyl nitrite solution and the 2-amino-5-bromobenzoic acid solution were dropped slowly over 10 minutes. The reaction temperature was kept at 70 ^{o}C for 1 h, and cooled down to room temperature. The solvent was removed under reduced pressure, and the crude product was purified by column chromatography (silica gel, dichloromethane-hexane (1:3 v/v), yielding 4.1 g of light yellow liquid (62%). ^{1}HNMR (300 MHz, $CDCl_3$): δ 7.40 (s, 1H), 7.13 (d, J=1.2 Hz, 1H), 7.12 (s, 2H), 7.03 (dd, J=3.9, 1.5 Hz, 1H), 5.70 (s, 2H) ppm. ^{13}CNMR (300 MHz, $CDCl_3$): δ 151.9, 148.3, 143.3, 142.7, 127.7, 124.1, 121.6, 118.8, 82.2 ppm.

12: To a sealed tube were added **11** (1.07 g, 4.8 mmol) and benzocyclobutene **9** (0.5 g, 4.8 mmol) and 2 mL of *o*-dichlorobenzene (*o*-DCB). The sealed tube was placed in a 220 ^{o}C preheated bath and vigorously stirred for 6 h. After cooling down, the solvent was removed under reduced pressure, and the crude product was purified by column chromatography (silica gel, dichloromethane-hexane (1:5 v/v), yielding 1.0 g of white solid (64%). ^{1}HNMR (300 MHz, $CDCl_3$): δ 7.41 (d, J=1.5 Hz, 1H), 7.31 (dd, J=7.8, 1.5 Hz, 1H), 7.17 (s, 4H), 7.14 (d, J=7.8 Hz, 1H), 5.13 (s, 2H), 3.08-2.98 (m, 2H), 2.81-2.69

(m, 2H), 2.08-1.97 (m, 2H) ppm. ^{13}CNMR (300 MHz, $CDCl_3$): δ 148.1, 144.7, 138.8, 129.5, 127.1, 127.0, 126.4, 122.7, 120.7, 120.4, 84.39, 84.37, 42.72, 33.03 ppm.

12a: This compound was prepared using similar procedures as for **12** with compounds **11** and **9a** (yield: 57%). ^{1}HNMR (300 MHz, $CDCl_3$): δ 7.40 (d, *J*=1.8 Hz, 1H), 7.31 (dd, *J*=8.1, 1.8 Hz, 1H), 7.28 (s, 1H), 7.27 (d, *J*=6.6 Hz, 1H), 7.14 (d, *J*=7.8 Hz, 1H), 7.01 (d, *J*=7.8 Hz, 1H), 5.12 (s, 2H), 3.03-2.94 (m, 2H), 2.75-2.60 (m, 2H), 2.06-1.95 (m, 2H) ppm. ^{13}CNMR (300 MHz, $CDCl_3$): δ 147.9, 144.5, 141.0, 137.6, 129.9, 129.6, 129.3, 128.6, 122.7, 120.7, 120.5, 119.7, 84.25, 42.54, 42.42, 32.81, 32.49 ppm.

13: The compound **12** (0.7 g, 2.1 mmol) was mixed with 18 mL of acetic anhydride. To the mixture was added 4 mL of concentrated HCl slowly and the reaction mixture was refluxed for 6 h. After cooling down, ice cold water was added to the reaction mixture. The white precipitate was filtered and rinsed with methanol. The crude product was reprecipitated in a solution of CH_2Cl_2 and methanol, yielding 0.6 g of white solid (76%). ^{1}HNMR (300 MHz, $CDCl_3$): δ 7.96 (d, *J*=1.8 Hz, 1H), 7.74 (s, 1H), 7.67 (s, 1H), 7.670 (d, *J*=9.0 Hz, 1H), 7.674 (s, 1H), 7.50 (dd, *J*=9.0, 1.8 Hz, 1H), 7.38-7.34 (m, 2H), 7.26-7.22 (m, 2H), 4.10 (s, 2H), 4.08 (s, 2H) ppm. ^{13}CNMR (300 MHz, $CDCl_3$): δ 136.8, 129.3, 129.0, 128.7, 127.3, 126.5, 125.2, 124.4, 36.9 ppm. HRMS Calcd. for C18H13Br: 308.0201. Found: 308.0153.

13a This compound was prepared using similar procedures as for **13** (yield: 52%). ^{1}HNMR (300 MHz, $CDCl_3$): δ 7.96 (d, *J*=1.8 Hz, 1H), 7.73 (s, 1H), 7.67 (s, 1H), 7.68 (d, *J*=9 Hz, 1H), 7.50 (s, 1H), 7.51 (dd, *J*=8.7, 1.8 Hz, 1H), 7.36 (dd, *J*=8.1, 1.8 Hz, 1H), 7.22 (d, *J*=8.1 Hz, 1H), 4.05 (d, *J*=6 Hz, 2H), 4.03 (d, *J*=6 Hz, 2H) ppm. ^{13}CNMR (300 MHz, $CDCl_3$): δ 130.3, 129.4, 128.9, 125.4, 124.5, 36.6, 36.3 ppm. HRMS Calcd. for C18H12Br2: 385.9306. Found: 385.9292.

2-(2-(Trimethylsilyl)ethylthio)tetracene 14: The compound **13** (0.20 g, 0.65 mmol) was added to 10 mL of hexamethylphosphoramide (HMPA). While vigorously stirring, sodium 2-(trimethylsilyl)ethanethiolate (0.92 g, 5.9 mmol) was added and kept at room temperature for 10 min. To this reaction mixture was added 40 mL of H_2O and 1

mL of concentrated HCl and red precipitate was formed. The precipitate was collected via gravity filteration, and purified by column chromatography (silica gel, dichloromethane-hexane (1:2 v/v), yielding an inseparable mixture of 0.1 g of red solid composing **14** (~82%), tetracene, and 2-bromotetracene. The most impurities were sublimed away at 170 ^{o}C for 2 h under 100 mTorr, leaving pure reddish orange solid **14** (0.1 g, 43%). *Note that this compound is sensitive to light and O_2.* ^{1}HNMR (300 MHz, CD_2Cl_2): δ 8.68 (s, 2H), 8.65 (s, 1H), 8.05-8.02 (m, 2H), 7.94 (d, *J*=9.0 Hz, 1H), 7.78 (s, 1H), 7.45-7.42 (m, 2H), 7.29 (dd, *J*=9.0, 1.5 Hz, 1H), 3.21-3.15 (m, 2H), 1.11-1.05 (m, 2H), 0.14 (s, 9H) ppm. HRMS Calcd. for C23H24SSi: 360.1368. Found: 360.1370.

2,8-Di(2-(trimethylsilyl)ethylthio)tetracene 14a: This compound was prepared using similar procedures as for **14** with **13a** and double equivalent of **8** (yield: 24%). *Note that this compound is sensitive to light and O_2.* ^{1}HNMR (300 MHz, CD_2Cl_2): δ 8.60 (s, 2H), 8.52 (s, 2H), 7.93 (d, *J*=9.0 Hz, 2H), 7.77 (s, 2H), 7.28 (dd, *J*=9.0, 1.8 Hz, 2H), 3.21-3.15 (m, 2H), 1.11-1.05 (m, 2H), 0.14 (s, 9H) ppm. HRMS Calcd. for C28H36S2Si2: 492.1797, Found: 492.1768.

2-(Acetylthio)tetracene (TetSAc): To a solution of **14** (0.1 g, 0.28 mmol) and 50 mL of dry THF was added dropwise 1 mL of 1.0 M tetrabutylammonium fluoride (TBAF) solution in THF. The reaction mixture was stirred for 20 min and the solution turned to dark purple. With dropwise addition of 0.43 mL of anhydrous acetyl chloride (Fluka), the solution turned to orange. After another 20 min, the solvent was removed till the amount reduced to about 10 mL, and 50 mL of methanol was added with vigorous stirring. The resulting reddish orange precipitate was collected by gravity filteration and dried. The precipitate was redissolved in 100 mL of CH_2Cl_2 and undissolved precipitate was removed by gravity filteration. The filterate solution was concentrated and the product was purified by column chromatography (silica gel, dichloromethane-hexane (1:2 v/v), yielding a pure reddish orange solid (0.015 g, 18%). *Note that this compound is sensitive to light and O_2.* ^{1}HNMR (300 MHz, CD_2Cl_2): δ 8.75 (s, 3H), 8.73 (s, 1H), 8.17

(s, 1H), 8.08-8.05 (m, 3H), 7.49-7.45 (m, 2H), 7.36 (dd, *J*=9.0, 1.8 Hz, 1H), 2.51 (s, 3H) ppm. HRMS Calcd. for C20H14OS: 302.0765, Found: 302.0759.

2,8-Di(acetylthio)tetracene (Tet(SAc)$_2$): This compound was prepared using similar procedures as for **TetSAc** with **14a** and double equivalent of TBAF and acetyl chloride (yield: 16%). *Note that this compound is sensitive to light and O_2.* ^{1}HNMR (300 MHz, CD_2Cl_2): δ 8.73 (s, 2H), 8.71 (s, 2H), 8.16 (s, 2H), 8.02 (d, *J*=13 Hz, 2), 7.38 (d, *J*=9 Hz), 2.52 (s, 6H) ppm. HRMS Calcd. for C22H16O2S2: 376.0586, Found: 376.0604.

Monolayer Growth and Characterization. The Ag or Au substrates were 1000 Å thick thin films on silicon (with a 50 Å Cr adhesion layer) prepared in a Balzers thermal evaporator at a rate of 1.0 Å/s at a base pressure of $\leq 2\times10^{-6}$ Torr. The Pt substrates were 1000 Å films on silicon prepared in an e-beam evaporator (SEC 600) with a 50 Å Ti adhesion layer. The metal surfaces were immersed in 10 ml of 0.1-0.01 mM solutions of the thiol molecule in argon purged absolute ethanol. SAMs of PhSH, NaphSH, and AnthSH were grown for 18-24 h. For the preparation of SAMs of tetracene thiol, we added 30 μL of triethylamine (TEA) to the tetracene-2-thioacetate (TetSAc) solution for deprotection and SAM growth on Ag substrates (36 h) or 10 μL of concentrated ammonia aqueous solution for SAM growth on Au and Pt substrates (24 h). In case of dithiol molecules, 30 μL TEA was added in the solution of acetyl capped molecule for deprotection and SAM growth (15-24 h). After removing the samples from the solutions and rinsing with toluene and ethanol, we reimmersed each sample in 10 mL of pure absolute ethanol with 20 μL of TEA for another 24h to ensure the complete removal of acetyl groups on the outer terminus of the SAMs. All SAM samples were rinsed thoroughly with toluene and ethanol and stored in argon purged absolute ethanol for less than 12 h and dried under a stream of N_2 before all measurements. Detailed conditions are summarized in Table 5.1. Note that longer growing or usage of higher amount of bases lead to multilayer formation.

Table 5.1. Monolayer growing conditions

	Deprotecting Agent and Period		Deprotecting Agent and Period
PhSH	No deprotection, grown for 24 h	$Ph(SAc)_2$	(i) 30 μL of TEA, grown for 15 h (ii) 20 μL TEA in pure ethanol for 24 h
NaphSH	No deprotection, grown for 24 h	$Naph(SAc)_2$	(i) 30 μL of TEA, grown for 15 h (ii) 20 μL TEA in pure ethanol for 24 h
AnthSH	No deprotection, grown for 24 h	$Anth(SAc)_2$	(i) 30 μL of TEA, grown for 24 h (ii) 20 μL TEA in pure ethanol for 24 h
TetSAc	• 10 μL of NH_3 for Au/Pt (24 h) • 10 μL of TEA for Ag (36 h)	$Tet(SAc)_2$	(i) 30 μL of TEA, grown for 24 h (ii) 20 μL TEA in pure ethanol for 24 h

We characterized the SAMs using spectroscopic ellipsometry and XPS. Ellipsometry measurements were carried out on a VASE spectroscopic ellipsometer (J. A. Woolam Co., Inc.). Measurements of the polarization angles (Ψ and Δ) were taken as a function of wavelength (λ) between 600 and 1000 nm at an incident angle of 65^o. The indices of refraction ($n(\lambda)$) and extinction coefficients ($k(\lambda)$) of the metal-coated substrates were determined by measurement of the polarization angles prior to monolayer deposition. The instrument software converted these values to $n(\lambda)$ and $k(\lambda)$ of metal films and saved them as a material file. After monolayer formation on metal substrates, the polarization angles were measured again and the film thicknesses were determined by a built-in algorithm. $n(\lambda)$ and $k(\lambda)$ of the SAMs were assumed to be 1.55 and 0, respectively, over the wavelength range.

We acquired XPS spectra on a Perkin-Elmer Phi 5400 spectrometer. The Mg K_α x-ray (1253.6 eV) anode was operated at 200 W. Photoelectron detection was accomplished with a hemispherical analyzer pass energy set at a pass energy of 89.45 eV for survey scans and 17.9 eV for high-resolution scans. Each sample was transferred into the ultra high vacuum chamber immediately after drying under a stream of nitrogen to minimize contamination or oxidation. To obtain monolayer thicknesses, we carried out XPS measurements on SAMs of alkanethiols ($CH_3(CH_2)_nSH$, n = 7, 9, 11, 13, 15) on each metal and obtained calibration curves for the relative peak areas of the metal (Ag

$3d_{5/2}$, Au $4f_{7/2}$, or Pt $4f_{7/2}$) and the C 1s peaks, using known thicknesses of these SAMs from the literature.[30,31] These calibration curves were used to obtain the thicknesses of the oligoacene thiol SAMs.

Determination of Molecular Energy Levels. To probe the electronic structure of the SAMs on metals (Ag, Au, and Pt), we acquired UPS spectra on a Perkin-Elmer Phi-5400 spectrometer equipped with a He I ($h\nu$ = 21.2 eV) radiation source at an incident angle of 50^{o} from the sample normal. Photoemitted electrons were collected at normal emission with a pass energy of 4.45 eV. All spectra were acquired at an applied bias of -7 V on the sample and the energy scale was referenced to the metal Fermi level (E_{Fermi}). The intensities of the raw spectra were normalized at E_{Fermi}. The onsets of the highest occupied molecular orbitals were determined from the UPS spectra. After magnifying the first increasing peak near the metal Fermi level, we found the onset point from the cross-point between two trend lines (one is placed on the baseline and the other on the slope of the first peak). Optical gaps were determined from the onset of UV-Visible absorption spectra using a similar procedure to the determinations of UPS onsets. The optical gap corresponds to the lowest gap between the lowest occupied molecular orbital band and the highest occupied molecular orbitals. UV-Visible absorption spectra were obtained on a Hewlett-Packard 8453 UV-vis spectrophotometer from chloroform solutions of PhSH, NaphSH, AnthSH, and acetyl protected molecules (in place of TetSH and dithiols) at a concentration of $\sim 10^{-5}$ M (the maximum absorbance was ~ 1).

Preparation of Metal-Coated AFM Tips and Flat Metal Substrates. To prepare metallized tips, we coated contact mode AFM tips with 250 Å Ag or Au on a 30 Å Cr adhesion layer or with 80 Å Pt film on a 30 Å Ti adhesion layer. Template stripped flat metal substrates were used to grow monolayers for reproducible electrical measurement. Flat metal substrates were prepared by the following steps. For flat Ag or Au substrates, 5000 Å of Ag or Au was first deposited onto clean Si wafers on an e-beam evaporator. We then glued Si chips (0.5 cm × 0.5 cm) onto the metal surface using epoxy (EPO-TEK 377, Epoxy Technologies, MA). The epoxy layer was cured by placing the

wafers in an oven at 120 ^{o}C for 1 h. For flat Pt substrates, 3000 Å of Pt was sputter-coated onto a clean Si wafer on a Perkin Elmer 2400 DC sputter at a rate of ~3 Å/s. On top of the Pt film, subsequent depositions of 300 Å of Cr and 2000 Å of Au were followed on a thermal evaporator. Note that the Cr layer prevented the penetration of Au atom into Pt film. The Au film enhanced the yield of flat Pt substrates due to better adhesion with the cured epoxy layer. The rest of the steps were the same as for flat Ag or Au substrates. The flat metal substrates were peeled off from the silicon surface and immersed immediately in the thiol or dithiol solution for SAM growth.

Current-Voltage (*I*-*V*) Measurements. We formed the junctions by contacting a SAM on flat Ag, Au, or Pt substrates with a Ag-, Au-, or Pt-coated AFM tip at a load of 1 nN using a Digital Instruments Multimode AFM in a glove box (O_2 < 8 ppm), as illustrated in Figure 5.2. Current-voltages measurements were carried out using a Keithley model 236 electrometer with a DC voltage applied to the AFM tip as controlled with LabVIEW software. For the length dependence experiments, each metal-molecule-metal junction was examined over a voltage range of ±0.2 V. 5-10 *I*-*V* traces were collected for each molecular junction. A tip radius of ~50 nm was used in all experiments, and the number of molecules in each junction was estimated to be ~100.[32] Linear fits to each *I*-*V* trace yielded low-bias (±0.1 V) resistances that were then averaged for each molecule. Extrapolation of this low-bias average resistance versus the number of benzene rings to zero benzene ring gave the contact resistance (R_0) and the β value. For high voltage (up to ±1 V) experiments, 5-10 *I*-*V* traces were collected and averaged for each SAM and the average *I*-*V* trace were used to find V_{trans} values in the Fowler-Nordheim plot.

5.4 Results and Discussion

Monolayer Characterization. Monolayer thicknesses measured by XPS and ellipsometry are summarized in Table 5.2. Both measurements gave comparable thicknesses for a given monolayer. Figure 5.3 plots monolayer thickness versus estimated

molecular length. The latter was calculated from molecular modeling within the Cambridge Scientific Chem3D software (MM2). We define the molecular length as the sum of the metal-S bond length (2.35 Å) and the distance between the terminal H on the aromatic ring to S atom on the opposite end in a monothiol or between S and S in dithiols. For each SAM, the thickness increases linearly with molecular length, suggesting that the molecules are predominantly in an upright orientation on each metal surface.

Table 5.2. Thicknesses of the SAMs (unit: Å)

	Estimated Molecular Length[a]	XPS[b]			Ellipsometry[b]		
		Ag	Au	Pt	Ag	Au	Pt
PhSH	8.1	8.5	5.5	8.0	7.9	6.1	8.8
NaphSH	10.3	10.4	8.2	10.9	11.2	8.5	11.2
AnthSH	12.6	11.6	11.7	12.3	13.0	11.1	12.8
TetSH	15.0	14.2	15.4	14.2	15.0	14.2	15.2
$Ph(SH)_2$	8.8	8.4	8.2	9.3	9.3	8.6	8.9
$Naph(SH)_2$	11.0	11.6	10.2	10.3	11.7	10.3	11.1
$Anth(SH)_2$	13.3	12.3	11.5	11.5	12.8	12.6	13.8
$Tet(SH)_2$	15.7	14.8	14.7	15.3	15.3	14.1	14.7

[a] Molecular length was estimated with the Cambridge Scientific Chem3D software (MM2). Molecular length is the terminal H to S or S to S distance plus the metal-S bond length (2.35 Å) for monothiols and dithiols, respectively. [b] Standard deviations are typically 1-2 Å.

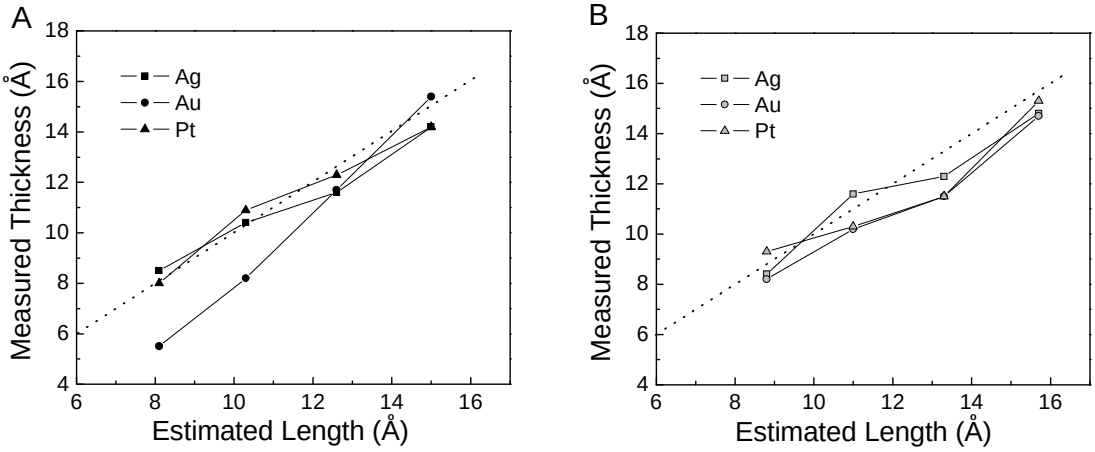

Figure 5.3. Plots of monolayer thicknesses (from XPS) versus estimated molecular lengths for oligoacene thiols (A) and dithiols (B) on Ag (squares), Au (circles), and Pt (triangles) surfaces. The dotted line shows the estimated molecular length from molecular modeling.

In addition to measuring film thicknesses, we used high resolution XPS spectra in the carbon (1s) and sulfur (2p) region to determine detailed molecular binding characters in the SAMs and also, in the case of dithiols, to calculate the percentage of doubly bound molecules (DBM) of which both thiol groups are bound to the metal surface (see Figure 5.4A). All binding energy scale were referenced to those of the metal substrate (Ag $3d_{5/2}$ at 368.3 eV, Au $4f_{7/2}$ at 84.0 eV, and Pt $4f_{7/2}$ at 71.2 eV).[33] We fitted each spectrum using a combination of Gaussian and Lorentzian line shapes. Each C 1s spectrum can be decomposed into two line shapes, **(i)** and **(ii)** at 284.5 and 286.5 eV, respectively. As examples, C 1s spectra of Tet$(SH)_2$ monolayers on Ag, Au, and Pt are shown in Figure 5.4B. Peak **(i)** is assigned to C atoms in the aromatic backbone, and peak **(ii)** is assigned to a shake-up process in the aromatic matrix and/or to the emission of carbon bound to sulfur.[34] The fitting is not perfect around 288.0 eV due likely to a small amount of adventitious surface contaminants.[35]

The S 2p doublet (S $2p_{1/2}$ and S $2p_{3/2}$) spectra were decomposed with a pair of peaks with the same full-width-at-half-maximum (FWHM) and the standard spin-orbit

splitting of 1.18 eV.[33] For instance, high resolution spectra in the S 2p region of $Tet(SH)_2$ monolayers on Ag, Au, and Pt are displayed in Figure 5.4C. The S $2p_{3/2}$ peak of bound thiol appeared at approximately 162.0 eV and that of unbound thiol at 163.6 eV with nearly equivalent intensities.[34] For the estimation of the percentage of doubly bound molecules, we considered the attenuation of photoemission intensity from bound S atom by the aromatic backbone on the basis of Lambert-Beer's law:[36]

$$I(162.0eV) = I(163.6eV)\exp(-\frac{d}{\lambda}) \tag{5.1}$$

where I is the peak intensity and λ is the attenuation length of 33 Å through the hydrocarbon film.[37] We then calculated the percentage of doubly bound dithiols from equation (5.2): [38]

$$\%DBM = \frac{\left[S2p(unbound) - S2p(bound)\right]/2}{S2p(unbound) + \left[S2p(unbound) - S2p(bound)\right]/2} \tag{5.2}$$

Average positions of the C 1s and S 2p peaks and the percentages of doubly bound molecules are compiled in Table 5.3. The experimental error associated with the determination of binding energies is ±0.2 eV and that in the S 2p percentage of doubly bound molecules is ±10%. We concluded from the data in Table 5.3 that (i) C1s and S 2p peaks of the SAMs are nearly the same across the series of metals and (ii) the percentage of doubly bound molecule indicates that molecules are mostly standing upright.

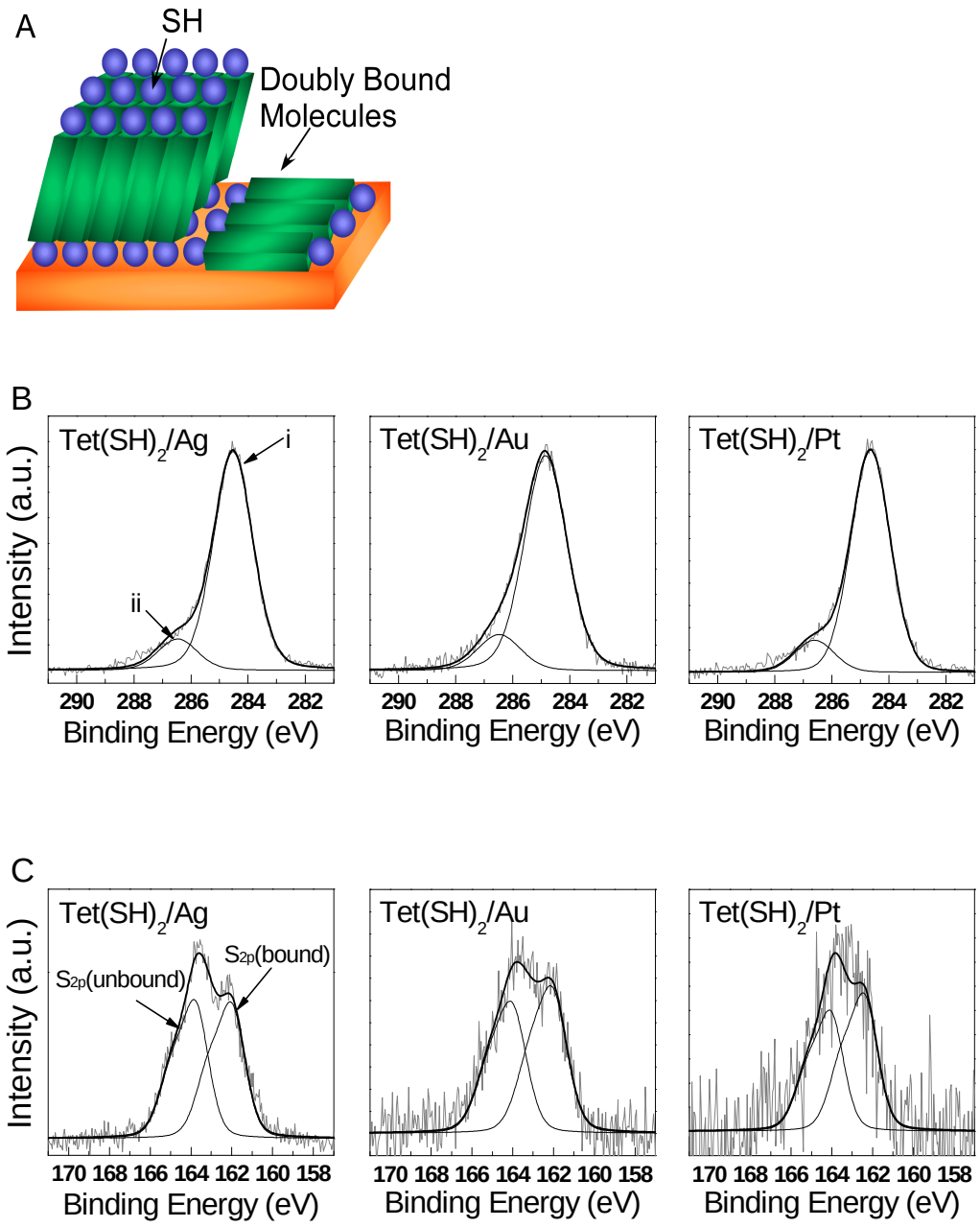

Figure 5.4. (A) Schematic representation of monolayers (●: thiol group (SH), ▬: backbone). Doubly bound molecules lie down with both thiol groups bound on the metal substrate. (B) High resolution XPS spectra in the C 1s region for $Tet(SH)_2$ SAMs on Ag, Au, and Pt. (C) High resolution XPS spectra in the S 2p region for $Tet(SH)_2$ SAMs on Ag, Au, and Pt. In each scan, gray lines represent experimental data, and thin and thick black lines show individual contributions and overall fit, respectively.

Table 5.3. Summary of average peak positions and percentages of doubly bound dithiols from high resolution C 1s and S 2p spectra

		C1s	S2p		DBM
		Peak **(i)**(eV)	Unbound (eV)	Bound (eV)	(%)
$Ph(SH)_2$	Ag	284.7	163.7	162.1	33
	Au	284.4	163.6	162.0	25
	Pt	284.3	163.3	162.3	17
$Naph(SH)_2$	Ag	284.5	163.7	162.1	27
	Au	284.5	163.7	161.9	11
	Pt	284.3	163.8	162.3	11
$Anth(SH)_2$	Ag	284.5	163.7	162.0	23
	Au	284.4	163.7	162.0	17
	Pt	284.4	163.7	162.5	14
$Tet(SH)_2$	Ag	284.6	163.8	162.0	26
	Au	284.6	163.7	161.9	21
	Pt	284.5	163.8	162.2	20

Energy Level Alignment. Valence electronic structures of SAMs were probed by UPS and HOMO-LUMO gaps of the isolated thiol molecules by UV-Visible absorption. We determined the onsets of the highest occupied molecular orbitals ($E_{HOMO,Onset}$) with respect to the metal Fermi level from UPS spectra. UPS spectra of all SAMs are provided in Figure 5.5-5.7. $E_{HOMO,Onset}$ levels of all molecules with respect to the metal Fermi level are compiled in Table 5.4 and the positions are displayed in Figure 5.10. The experimental error associated with $E_{HOMO,Onset}$ level is ±0.1 eV. Note that we use the onset instead of peak postion of $E_{HOMO,}$ because the latter is difficult to determine from UPS spectra. Figure 5.8 also shows direct comparison of AnthSH and $Anth(SH)_2$ on Ag, Au, and Pt surfaces. For a given molecule/metal combination, the valence structure in the UPS spectra appear similar on all three metal surfaces, in agreement with previous reports.[11] These features are different from those of physisorbed aromatic molecules.[39,40]

This implies that energy level alignment is strongly dependent on chemical bond formation at the metal/molecule due to the presence of significant interface dipole (discussed below). Nevertheless, the onsets of HOMO bands lie closer to the metal Fermi level as metal work function increases, in agreement with a previous report.[11] In the case of oligoacene dithiols, HOMO bands lie closer to the metal Fermi level than the corresponding monothiols molecular bands. This trend is more obvious for short molecules (benzenes and naphthalenes) and less distinct for longer molecules.

Figure 5.9 shows UV-Visible absorption spectra of oligoacene molecules. As the number of benzene ring increases, the absorption peaks are red-shifted, as expected from the decreased HOMO-LUMO gap due to improved conjugation. The optical gaps, determined from the onsets of UV-Visible absorption spectra were found to decrease linearly with increasing number of fused benzene rings, as shown in insets of Figure 5.9.

The surface work functions of SAM-coated metals (φ_{SAM}s) were determined from the cut-off of UPS photoemission, Table 5.5. The metal work function change ($\Delta\varphi=\varphi_{SAM} - \varphi_{Metal}$) is -0.3 (±0.1), -1.0 (±0.1), -1.5 (±0.2) eV for Ag, Au, and Pt, respectively. The observed work function change is consistent with reported experimental results and theoretical calculations.[3,11] The work function change upon the formation of monolayers is given by

$$\Delta\varphi = \Delta V + D \tag{5.3}$$

where ΔV is the potential shift associated with the aligned dipole moments of the molecules within the monolayer and D is the interface dipole formed upon chemical bond formation. The interface dipole depends on many factors, e.g. surface coverage, bonding geometry, bonding type, charge transfer, and polarization at the metal/organic interface. For a given series of molecules, the number of benzene rings are believed to be not important to the total work function change because molecular intrinsic dipoles across the series are almost equivalent as for the case of alkanethiols.[3,5] The very similar binding energies of C 1s and S 2p across the metal series suggests that no significant charge transfer at the interface occurs,[41] as consistent with published results.[3,42] The potential

shift associated with slightly different monolayer quality of SAMs would be very small.[11,17] Therefore, the interface dipole change can be attributed to the sulfur-metal bond formation. The chemical contacts induce significant local charge redistribution at the interface, and the effect are strongly dependent on metal type (Ag<Au<Pt).

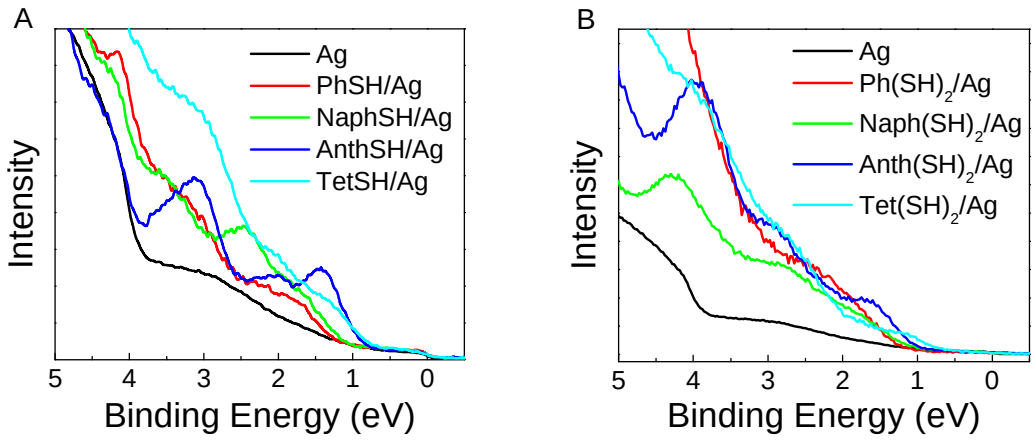

Figure 5.5. UPS spectra of oligoacene thiols (A) and dithiols (B) on Ag.

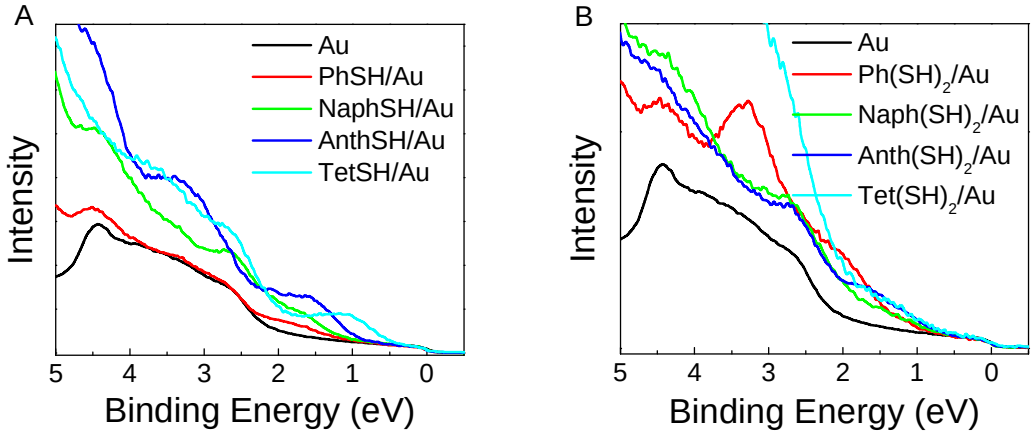

Figure 5.6. UPS spectra of oligoacene thiols (A) and dithiols (B) on Au.

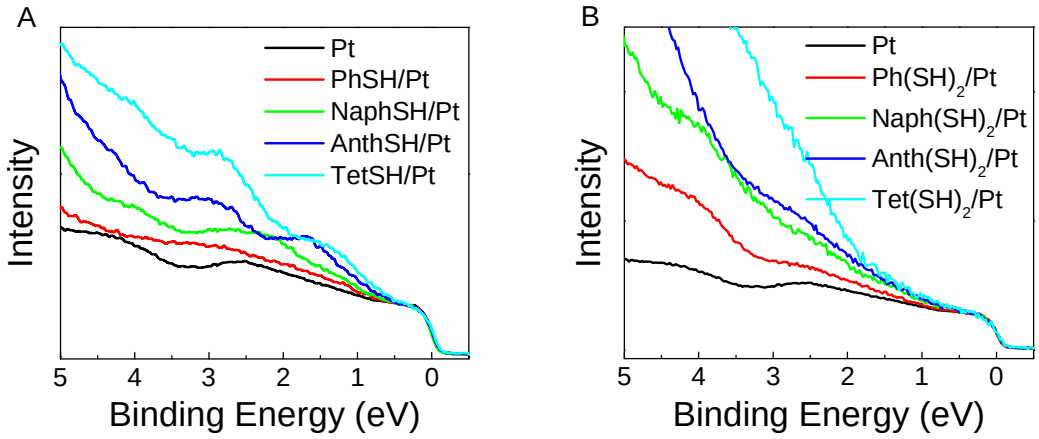

Figure 5.7. UPS spectra of oligoacene thiols (A) and dithiols (B) on Pt.

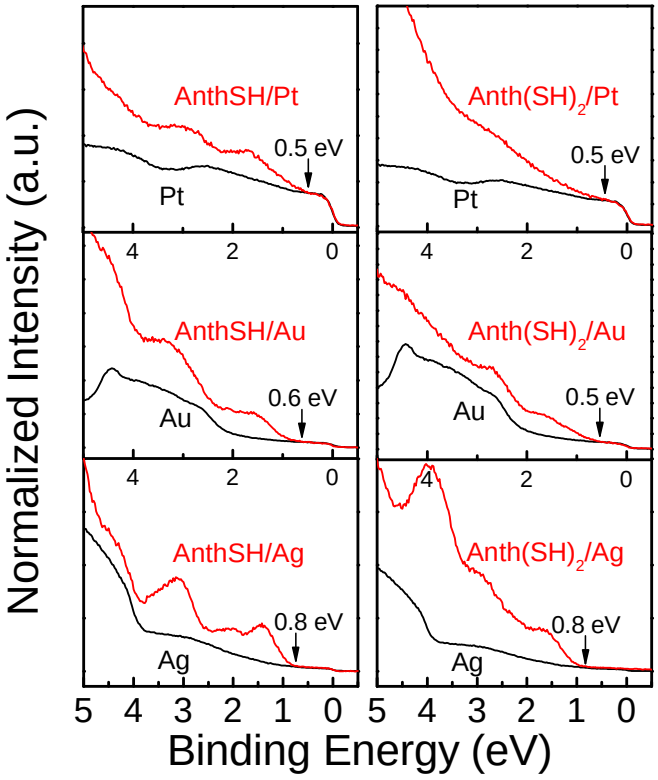

Figure 5.8. UPS spectra of AnthSH and Anth$(SH)_2$ on Ag, Au, and Pt near the metal Fermi level. Arrows indicate the onsets of the HOMOs.

Table 5.4. Summary of E_{Fermi}-$E_{HOMO,Onset}$ values obtained from UPS spectra (unit: eV)

	E_{Fermi}-$E_{HOMO,Onset}$				E_{Fermi}-$E_{HOMO,Onset}$		
	Ag	Au	Pt		Ag	Au	Pt
PhSH	1.2	1.1	0.8	$Ph(SH)_2$	1.1	0.9	0.8
NaphSH	1.1	0.9	0.6	$Naph(SH)_2$	0.9	0.6	0.5
AnthSH	0.8	0.6	0.5	$Anth(SH)_2$	0.8	0.5	0.5
TetSH	0.7	0.4	0.4	$Tet(SH)_2$	0.6	0.4	0.4

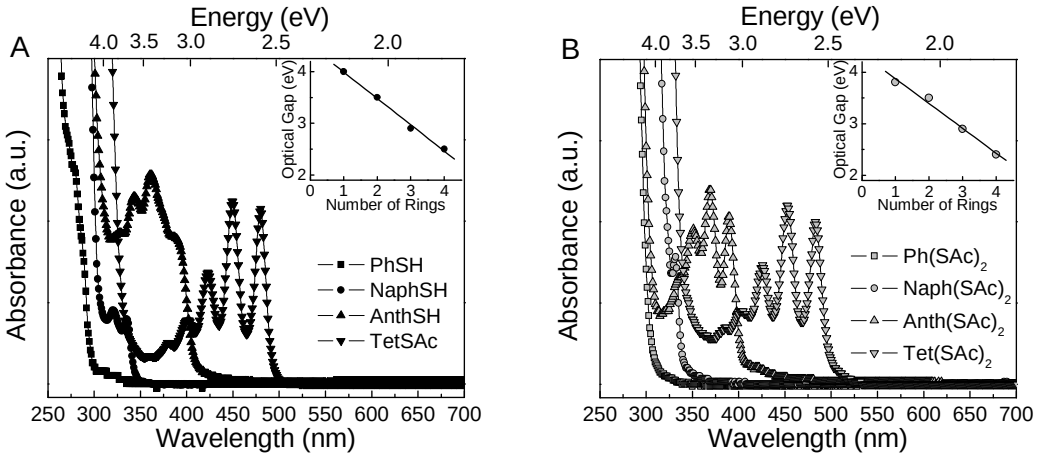

Figure 5.9. UV-Visible absorption spectra of oligoacene thiols (A) and dithiols (B). Insets display the plot of optical gap versus number of rings. The spectra were taken from chloroform solutions of molecules at a concentration of ~10^{-5} M.

Table 5.5. Summary of film work function obtained from UPS spectra (unit: eV)

	Film Work Function				Film Work Function		
	Ag (4.26)	Au (5.20)	Pt (5.65)		Ag (4.26)	Au (5.20)	Pt (5.65)
PhSH	3.9 (±0.1)	4.4 (±0.1)	4.0 (±0.1)	$Ph(SH)_2$	3.8 (±0.1)	4.3 (±0.1)	4.5 (±0.1)
NaphSH	4.0 (±0.1)	4.4 (±0.1)	4.0 (±0.1)	$Naph(SH)_2$	4.0 (±0.1)	4.1 (±0.2)	4.3 (±0.1)
AnthSH	3.9 (±0.1)	4.2 (±0.1)	4.1 (±0.1)	$Anth(SH)_2$	4.1 (±0.2)	4.3 (±0.1)	4.2 (±0.1)
TetSH	3.9 (±0.1)	4.1 (±0.1)	4.1 (±0.1)	$Tet(SH)_2$	4.1 (±0.1)	4.0 (±0.2)	4.2 (±0.1)

Figure 5.10 shows energy level diagram of oligoacene molecules on Ag, Au, and Pt based on the UPS and UV-Vis data (Table 5.4, Table 5.5, and Figure 5.9). The onsets of the lowest unoccupied molecular orbitals (LUMO) levels are constructed with optical gaps determined from UV-Visible absorption data, assuming that the optical gaps of the SAMs are the same as those of molecules in solution and independent of metal substrates.[10,12,13] Note that due to exciton binding energy in films, actual LUMO positions can be varied by ~1.0 eV.[13] For instance, in the case of 4,4'-ethynylphenyl-1-benzenethiol (OPE-SH, one of the most well studied molecules), optical gap is 3.3 eV,[12] and $E_{HOMO,Onset} - E_{LUMO,Onset}$ is about 2.4 eV.[18] From the constructed energy level alignment, HOMO lies much closer to the metal Fermi level and is mainly responsible for junction conductance.

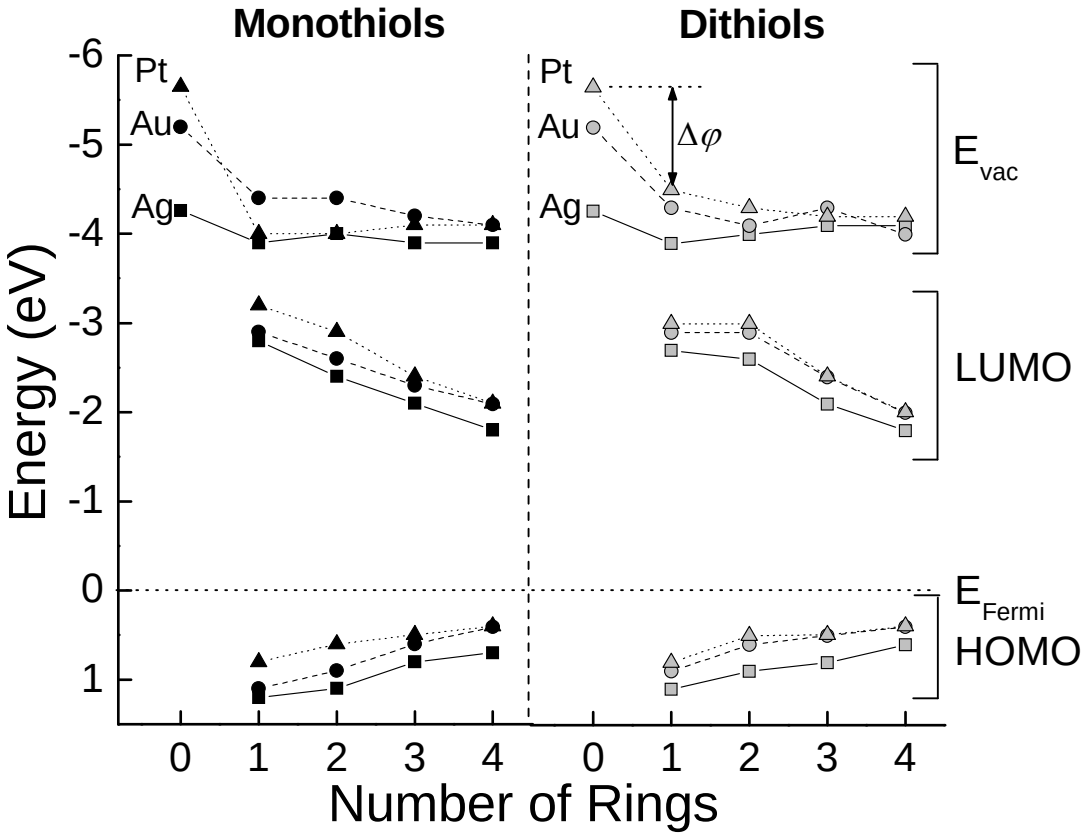

Figure 5.10. Energy level diagram of oligoacene thiols and dithiols from the data in Table 5.4, Table 5.5, and Figure 5.9 for Ag (squares), Au (circles), and Pt (triangles) surfaces.

General *I-V* Behavior. Figure 5.11 shows representative *I-V* characteristics of Au-oligoacene thiol-Au and Au-oligoacene dithiol-Au junctions. Each *I-V* trace has sigmoidal shape and is nearly symmetric with respect to zero bias. For a given voltage, current scales exponentially with length in the low bias regime. These attributes indicated that non-resonant tunneling is the principal transport mechanism in these junctions.[6,7] High bias *I-V* characteristics are discussed later.

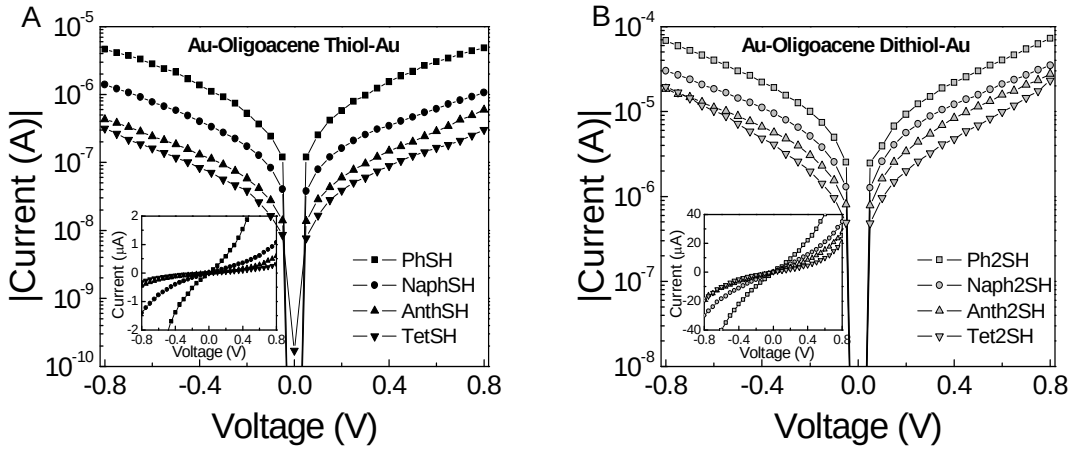

Figure 5.11. Representative semilog plot of average *I-V* traces of Au-oligoacene thiol-Au (A) and Au-oligoacene dithiol-Au (B) junctions. Insets show sigmoidal *I-V* behavior on linear axes. The error bars are not shown for clarity.

Low Bias Junction Characteristics. We examine the molecular length dependence in junction resistance in the low bias region (±0.1 V) based on the average of 5-10 *I-V* traces. Figure 5.12 shows semilog plots of resistance versus number of rings for oligoacene thiol and dithiol junctions. Note that we were not able to measure some of the Ag-oligoacene dithiol-Ag junctions because of junction instability. This is perhaps because Ag atoms are liable to migrate between electrodes under bias through SAMs.[43,44] The linear relationships indicated that the data is well described by the nonresonant tunneling:

$$R = R_0 \exp(\beta \bullet n) \tag{5.4}$$

where R_0 is the contact resistance, n is the number of fused benzene rings (or barrier thickness), and β the length-dependent tunneling attenuation factor:

$$\beta = \sqrt{\frac{8m_e\phi}{\eta^2}} \tag{5.5}$$

where m_e is the electron mass and ϕ is the tunneling barrier height dictated by the energy offset between metal Fermi level and the closest frontier molecular energy level (e.g. E_{Fermi}-$E_{HOMO,Onset}$). Note that due to ambiguity on the exact length of metal-molecule

physical contact in monothiol junctions we prefer to analyze data in terms of the number of benzene rings. From the slope of the linear fits, we extracted β values, Figure 5.13. The average β value is 1.0 (±0.15) per ring or 0.5/Å for monothiols and 0.5 (±0.07) per ring or 0.2/Å for dithiols. This observation is somewhat surprising in that molecular backbones are the same. However, the lower $E_{HOMO,Onset}$ data for dithiols suggest that electronic coupling in the dithiol junctions should be stronger than the monothiol junctions, leading to a lower tunneling barrier. Also, the low β value in the dithiol junctions is consistent with the data of reported aromatic dithiols or diamines.[45-48] Moreover, the measured β values are also nearly independent of metal work function within experimental error. For both thiols and dithiols, the independence of β values on metal work function is presumably a result of too small difference between metal series to be measured by CP-AFM and is consistent with the bias dependence of β value at low bias regime (details are discussed below).

We obtained contact resistances from the *y*-intercept in the semilog plot of resistance versus number of rings, as shown in Figure 5.12. All contact resistances are plotted as a function of metal work function in Figure 5.14. A few important observations can be made: (i) contact resistance increases with increasing metal work function which suggests HOMO-assisted tunneling, (ii) dithiol contacts have much lower contact resistance than monothiol contacts at a given set of metal electrodes, (iii) molecular junctions incorporating a pair of mixed metal electrodes (*e.g.* Ag tip/ Au substrate and Au tip/Ag substrate) have almost the same contact resistances, and (iv) the dependence of R_0 as well as β on the contact type suggest that a barrier is present at the metal/molecule contacts.

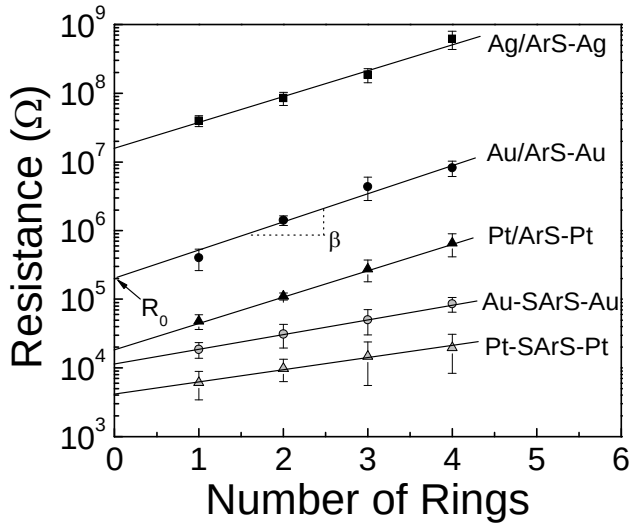

Figure 5.12. Semilog plot of resistance versus number of rings for oligoacene thiol and dithiol junctions. Resistances were calculated from the average of 10-20 *I-V* traces within ±0.1 V. The error bars represent one standard deviation from the mean.

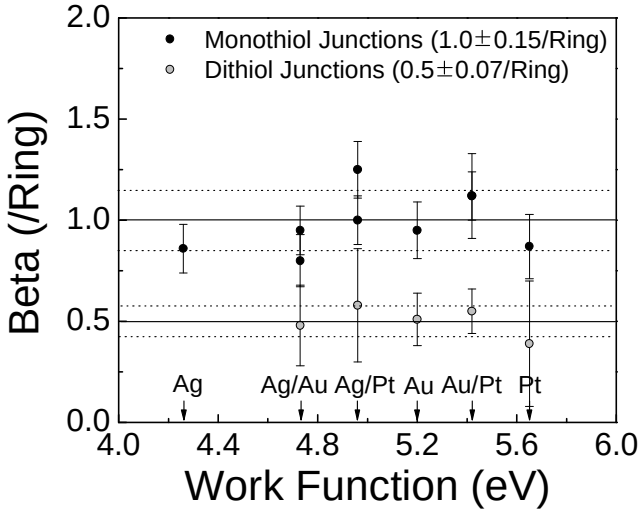

Figure 5.13. β as a function of electrode metal work function for junctions composed of oligoacene thiols and dithiols. For both thiols and dithiols, β values appear independent of metal work function. The solid line is the average of each series and dotted lines are one standard deviation above and below the average.

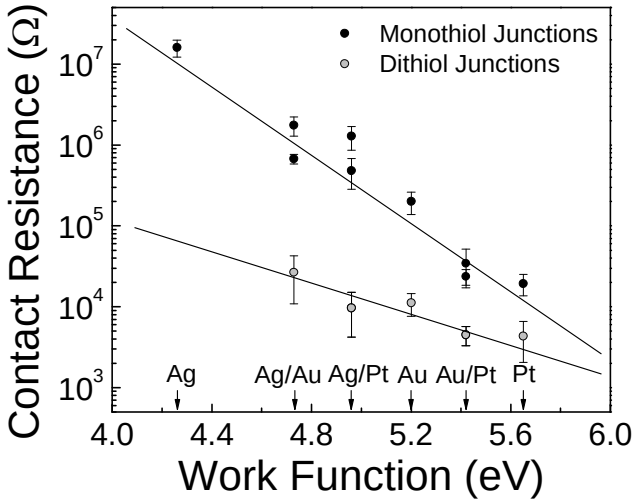

Figure 5.14. Contact resistance as a function of electrode metal work function for junctions composed of oligoacene monothiol and dithiols. The solid lines are guides for the eye.

High Bias Junction Characteristics. Junction properties (β, R_0, and V_{trans}) were examined up to junction breakdown voltages (0.8-1.2 V depending on molecules). Figure 5.15 shows the dependence of β and R_0 on the applied bias. As discussed earlier, the β values for dithiol junctions are nearly a factor of two lower than those of monothiol junctions. In both cases, the β value is nearly constant in the low bias regime, but decreases at higher biases. This behavior suggests that the effective tunneling barrier is lowered and/or thinned due to the high field. The abrupt lowering of β values after 0.6 V in monothiol junctions is consistent with the barrier thinning effect, as revealed below in the V_{trans} analysis. In addition, the thinning begins at a lower voltage for dithiol junctions because the effective barrier is already low. This β value change within the range of ±1.0 V reflects a much lower tunneling barrier in these oligoacene molecular junctions when compared with alkane thiols or dithiols junctions in which β values show no dependence up to even higher voltages. This observation is consistent with energy alignment of molecules reported here and in the literature,[5,49] *i.e.* much deeper HOMO levels in the

case of alkanethiols. R_0 is also gradually decreased because of the effective tunneling barrier lowering for either case.

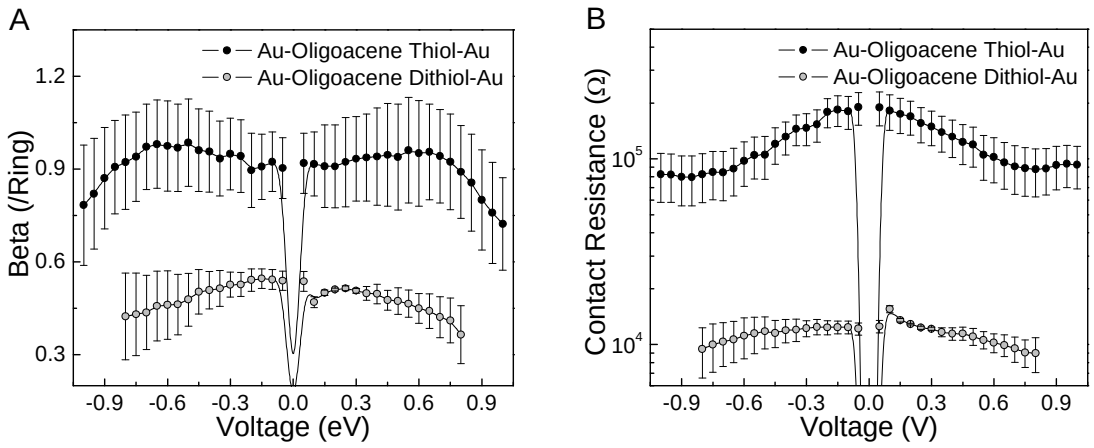

Figure 5.15. β (A) and R_0 (B) as a function of tip bias from a representative Au-oligoacene thiol-Au and Au-oligoacene dithiol-Au junctions.

Details of the barrier lowering were further scrutinized from the analysis of V_{trans} in each molecular junction. With increasing voltages, nonresonant tunneling transitions to field emission and at the same time, the tunneling barrier shape transforms from square/trapezoidal barrier to triangular barrier at the voltage of V_{trans}.[6,20,21,50] Therefore, at lower biases than V_{trans}, the tunneling current is given by the standard nonresonant tunneling equation:

$$I \propto V \exp(-\frac{2s\sqrt{2m_e\phi}}{\eta}) \tag{5.6}$$

where s is the barrier width (i.e. molecular length) and m_e is the electron effective mass. At higher biases, current-voltage characteristics follow the Fowler Nordheim (field emission) equation:

$$\ln(\frac{I}{V^2}) \propto \frac{-4s\sqrt{2m_e\phi^3}}{3\eta q}(\frac{1}{V}) \tag{5.7}$$

where q is the elementary charge. Figure 5.16 shows an example of this mechanistic transition in the Au-tetracene thiol-Au junction. The plot of $ln\ (I/V^2)$ versus $1/V$ (so called, Fowler Nordheim plot) demonstrates that the negative slope is evident at higher voltages than V_{trans}, as expected. The effective barrier change is also depicted.

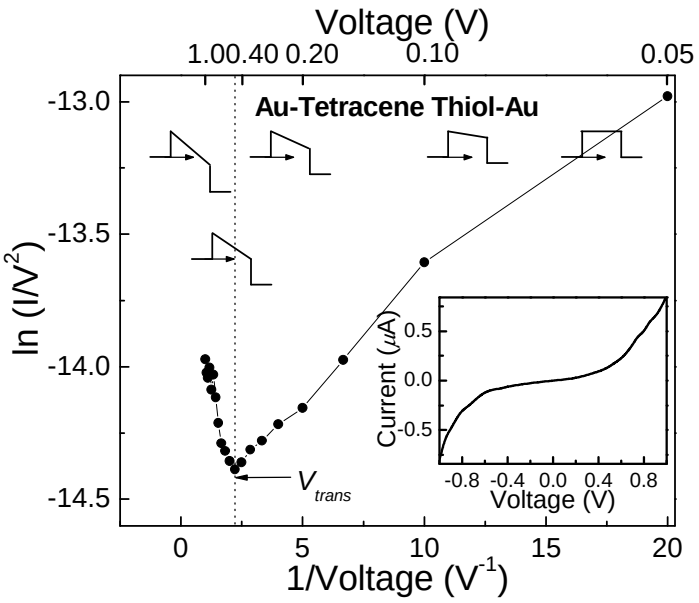

Figure 5.16. Fowler-Nordheim plot of a Au-Tetracene Thiol-Au junction measured by CP-AFM. Solid circles represent the average of 20 *I-V* curves. Gradual transition of averaged tunneling barrier shapes is illustrated. The dotted line corresponds to the voltage where the tunneling barrier transition from trapezoidal to triangular. The inset shows current-voltage characteristics on standard axes.

Figure 5.17 shows V_{trans} behavior as a function of electrode work function. For a pair of mixed metal junctions (e.g. Ag tip/Au substrate or Au tip/Ag substrate), V_{trans} values were very similar to each other. The lines indicate trends of V_{trans} values depending on electrode work function. In general, although the slopes are different, it is obvious that V_{trans} values decrease with increasing work function. In addition, at a given set of electrodes, V_{trans} values decreases with molecular length. The linear relationship

between V_{trans} and $E_{HOMO,Onset}$ in Au-molecule-Au junctions can also be found in Figure 5.18, consistent with our previous reports.[10,21]

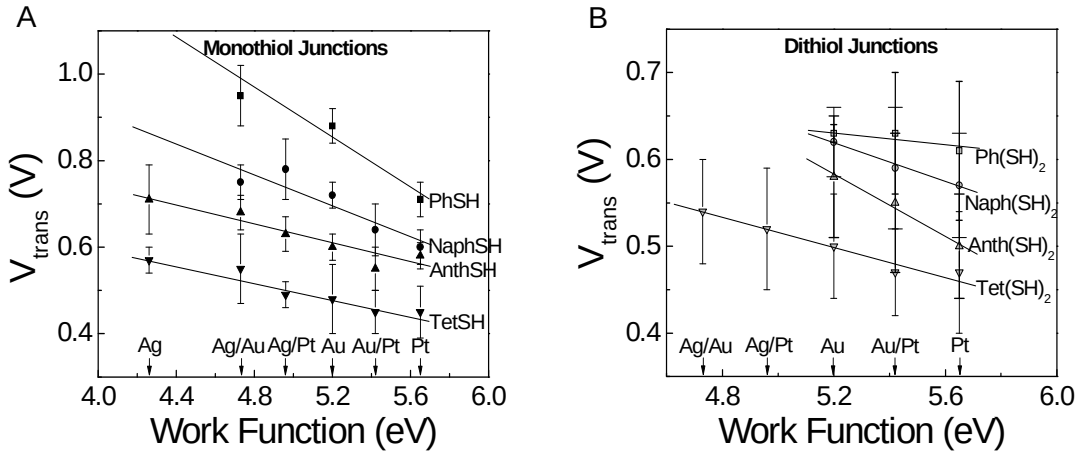

Figure 5.17. V_{trans} as a function of electrode work function for junctions composed of oligoacene thiols (A) and dithiols (B).

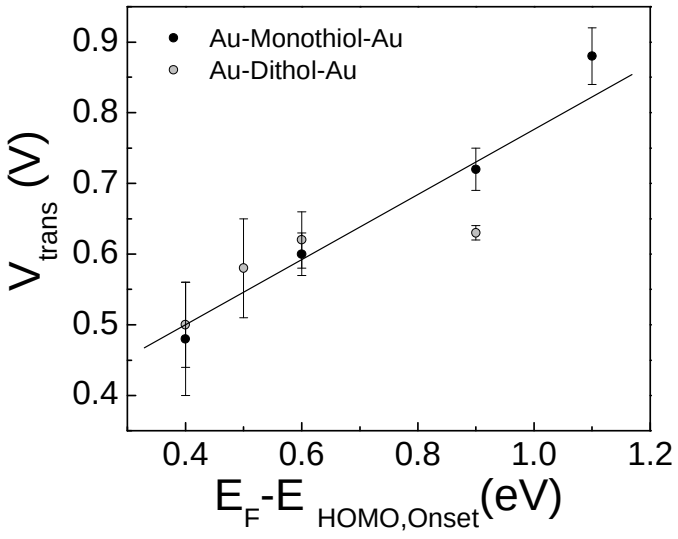

Figure 5.18. V_{trans} as a function of energy offset (E_F-$E_{HOMO,Onset}$).

Determination of Transmission. Junction properties can be understood on the basis of quantum mechanical transmission model.[7,22] According to Landauer formalism,[51] the resistance (R) of the junction is described as follows:

$$R = \frac{h}{2e^2 NT} \tag{5.8}$$

where N is the number of molecules in the junction and T is the transmission. The model assumes that the molecules are resistors in parallel with no intermolecular interaction and that the molecules are well contacted with electrodes. Figure 5.19 shows schematic representation of transmission (T) in oligoacene thiol or dithiol junctions. The transmission is partitioned into three overlaps, the tip metal-molecule (T_{tip}), the molecular backbone (T_{mol}), and the molecule-substrate metal (T_{sub}) with a relationship:

$$T = T_{tip} \bullet T_{mol} \bullet T_{sub} \tag{5.9}$$

Further, the T_{mol} corresponds to $(T_{ph})^n$ where T_{ph} is transmission through a benzene ring. Substitution of equation (5.9) into equation (5.8) yields:

$$R = \frac{h}{2e^2 N} \bullet \frac{1}{T_{tip}} \bullet \frac{1}{T_{sub}} \bullet \left(\frac{1}{T_{ph}}\right)^n \tag{5.10}$$

When compared to equation (5.4), R_0 and β can be expressed by

$$R_0 \equiv \frac{h}{2e^2 N} \bullet \frac{1}{T_{tip}} \bullet \frac{1}{T_{sub}} \tag{5.11}$$

$$\exp(\beta n) \equiv \left(\frac{1}{T_{ph}}\right)^n \tag{5.12}$$

The transmission values of each component were estimated using equation (5.11) and (5.12). From the β values in Figure 5.13, T_{ph} was estimated to be 0.61 and 0.37 for monothiol junctions and dithiol junctions, respectively. T_{sub} and T_{tip} were calculated from the contact resistance data in Figure 5.14 assuming that T_{sub} values in dithiol junctions are the same as T_{tip} values and T_{sub} values in monothiol junctions are the same as in dithiol junctions. Figure 5.20 shows the estimated transmission against the number of molecules in the junction. We found that the transmission efficiency of contacts decreases in the

order Pt–S–Ph>Au–S–Ph>Ag–S–Ph>Pt/Ph>Au/Ph>Ag/Ph ("–" represents chemical contact and "/" physical contact).

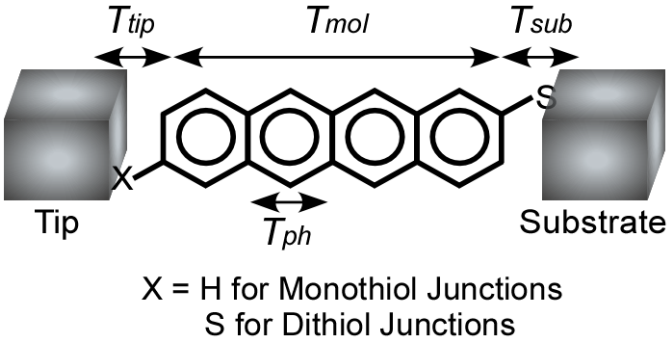

Figure 5.19. Schematic representation of transmission (T) in oligoace thiol or dithiol junctions. The transmission is partitioned into three overlaps, the tip metal-molecule (T_{tip}), the molecular backbone (T_{mol}), and the molecule-substrate metal (T_{sub}) with a relationship of $T = T_{tip} \bullet T_{mol} \bullet T_{sub}$. Further, the T_{mol} corresponds to $(T_{ph})^n$ where T_{ph} is transmission through a benzene ring.

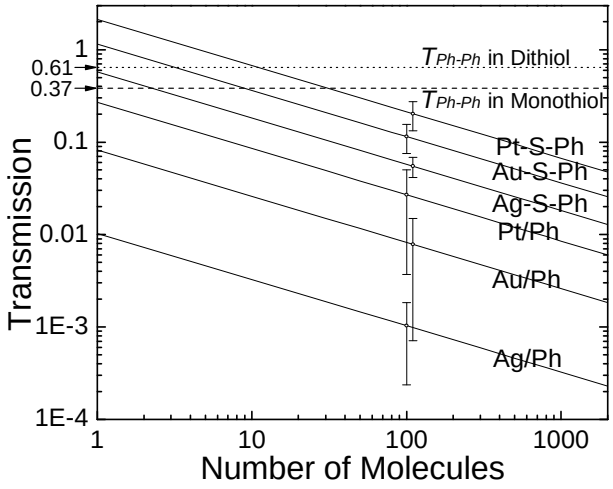

Figure 5.20. Contact transmissions (solid lines) interpolated from the data in Figure 5.14 as a function of molecules present in our CP-AFM experiment. Choosing an estimate for the number of molecules present in our junctions allows for prediction of the transmission for each of the six different contacts. The dashed line represents the transmission of molecular backbone (or oligoacene) as determined from the averaged β values in Figure 5.13.

5.5 Conclusion

We investigated junctions of highly conjugated oligoacene molecular wires having mono thiols and dithiols with a systematic change in molecular length. The length dependency in junction resistance was found to be affected by the surface linking types (chemical/physical vs. bichemical contact). The tunneling attenuation factor, β, was 1.0 per ring or 0.5/Å for monothiol series and 0.5 per ring or 0.2/Å for dithiol series, and contact resistance, R_0, was 10-100 times lower for dithiol junctions, indicating bichemical contacts reduce both the averaged tunneling barrier height and contact resistance significantly. When a combination of metals (Ag, Au, and Pt) were employed as electrodes in the junctions, β values were rather independent of metal work function while contact resistances were significantly reduced with metal work function. From the detailed analysis on resistances, transmission efficiency, T, of contacts was reduced in the order Pt–S–Ph>Au–S–Ph>Ag–S–Ph>Pt/Ph>Au/Ph>Ag/Ph ("–" represents chemical contact and "/" physical contact), and the transmission per ring was calculated to be 0.37 per ring in monothiols and 0.61 per ring in dithiols. Moreover, V_{trans}, a characteristic voltage where a transition from nonresonant tunneling to field emission occurs, was investigated. V_{trans} values are linearly dependent on energy offsets between the metal Fermi level (E_F) and the onset of the highest occupied molecular orbital ($E_{HOMO,Onset}$) values. The V_{trans} analysis also revealed the tunneling barrier lowering with increasing work function as well as bichemical contact.

5.6 Acknowledgment

We thank NSF (CHE-0315165) for the financial support.

5.7 References

(1) Hamadani, B. H.; Corley, D. A.; Ciszek, J. W.; Tour, J. M.; Natelson, D. *Nano Lett.* **2006**, *6*, 1303.

(2) Campbell, I. H.; Rubin, S.; Zawodzinski, T. A.; Kress, J. D.; Martin, R. L.;

Smith, D. L.; Barashkov, N. N.; Ferraris, J. P. *Phys Rev B* **1996**, *54*, 14321.
(3) Heimel, G.; Romaner, L.; Zojer, E.; Bredas, J. L. *Nano Lett.* **2007**, *7*, 932.
(4) Paniagua, S. A.; Hotchkiss, P. J.; Jones, S. C.; Marder, S. R.; Mudalige, A.; Marrikar, F. S.; Pemberton, J. E.; Armstrong, N. R. *J. Phys. Chem. C* **2008**, *112*, 7809.
(5) Alloway, D. M.; Hofmann, M.; Smith, D. L.; Gruhn, N. E.; Graham, A. L.; Colorado, R.; Wysocki, V. H.; Lee, T. R.; Lee, P. A.; Armstrong, N. R. *J. Phys. Chem. B* **2003**, *107*, 11690.
(6) Simmons, J. G. *J. Appl. Phys.* **1963**, *34*, 1973.
(7) Nitzan, A. *Annu. Rev. Phys. Chem.* **2001**, *52*, 681.
(8) Nitzan, A.; Ratner, M. A. *Science* **2003**, *300*, 1384.
(9) Kim, B.-S.; Beebe, J. M.; Jun, Y.; Zhu, X.-Y.; Frisbie, C. D. *J. Am. Chem. Soc.* **2006**, *128*, 4970.
(10) Zangmeister, C. D.; Beebe, J. M.; Naciri, J.; Kushinerick, J. G.; van Zee, R. D. *Small* **2008**, *4*, 1143.
(11) Zangmeister, C. D.; Picraux, L. B.; van Zee, R. D.; Yao, Y. X.; Tour, J. M. *Chem. Phys. Lett.* **2007**, *442*, 390.
(12) Zangmeister, C. D.; Robey, S. W.; van Zee, R. D.; Kushmerick, J. G.; Naciri, J.; Yao, Y.; Tour, J. M.; Varughese, B.; Xu, B.; Reutt-Robey, J. E. *J. Phys. Chem. B* **2006**, *110*, 17138.
(13) Zangmeister, C. D.; Robey, S. W.; vanZee, R. D.; Yao, Y.; Tour, J. M. *J. Am. Chem. Soc.* **2004**, *126*, 3420.
(14) Xue, Y. Q.; Datta, S.; Ratner, M. A. *J Chem Phys* **2001**, *115*, 4292.
(15) Venkataraman, L.; Park, Y. S.; Whalley, A. C.; Nuckolls, C.; Hybertsen, M. S.; Steigerwald, M. L. *Nano Lett.* **2007**, *7*, 502.
(16) Quinn, J. R.; Foss, F. W.; Venkataraman, L.; Breslow, R. *J. Am. Chem. Soc.* **2007**, *129*, 12376.
(17) Heimel, G.; Romaner, L.; Bredas, J. L.; Zojer, E. *Phys. Rev. Lett.* **2006**, *96*, 196806.
(18) Watkins, N. J.; Zangmeister, C. D.; Chan, C. K.; Zhao, W.; Ciszek, J. W.; Tour, J. M.; Kahn, A.; van Zee, R. D. *Chem. Phys. Lett.* **2007**, *446*, 359.

(19) Beebe, J. M.; Engelkes, V. B.; Miller, L. L.; Frisbie, C. D. *J. Am. Chem. Soc.* **2002**, *124*, 11268.
(20) Beebe, J. M.; Kim, B.-S.; Frisbie, C. D.; Kushmerick, J. G. *Acs Nano* **2008**, *2*, 827.
(21) Beebe, J. M.; Kim, B.-S.; Gadzuk, J. W.; Frisbie, C. D.; Kushmerick, J. G. *Phys. Rev. Lett.* **2006**, *97*, 026801.
(22) Engelkes, V. B.; Beebe, J. M.; Frisbie, C. D. *J. Am. Chem. Soc.* **2004**, *126*, 14287.
(23) Chen, F.; Li, X.; Hihath, J.; Huang, Z.; Tao, N. *J. Am. Chem. Soc.* **2006**, *128*, 15874.
(24) Fujii, S.; Akiba, U.; Fujihira, M. *Chem Lett* **2008**, *37*, 408.
(25) Park, Y. S.; Whalley, A. C.; Kamenetska, M.; Steigerwald, M. L.; Hybertsen, M. S.; Nuckolls, C.; Venkataraman, L. *J. Am. Chem. Soc.* **2007**, *129*, 15768.
(26) Tivanski, A. V.; He, Y. F.; Borguet, E.; Liu, H. Y.; Walker, G. C.; Waldeck, D. H. *J. Phys. Chem. B* **2005**, *109*, 5398.
(27) Kiguchi, M.; Miura, S.; Hara, K.; Sawamura, M.; Murakoshi, K. *Appl. Phys. Lett.* **2007**, *91*, 053110.
(28) Armarego, W. L. F.; Chai, C. L. L. *Purification of Laboratory Chemicals* **2003**, *5th edition*, Butterworth Heinemann.
(29) Lloyd, J. B. F.; Ongley, P. A. *Tetrahedron* **1965**, *21*, 245.
(30) Ulman, A. *Chem Rev* **1996**, *96*, 1533.
(31) Li, Z. Y.; Chang, S. C.; Williams, R. S. *Langmuir* **2003**, *19*, 6744.
(32) Salomon, A.; Cahen, D.; Lindsay, S.; Tomfohr, J.; Engelkes, V. B.; Frisbie, C. D. *Adv. Mater.* **2003**, *15*, 1881.
(33) Moulder, J. F.; Bomben, K. D.; Sobol, P. E.; Stickle, W. F. *Handbook of X-ray Photoelectron Spectroscopy* **1995**, Physical Electronics, Inc.
(34) Shaporenko, A.; Elbing, M.; Baszczyk, A.; von Hanisch, C.; Mayor, M.; Zharnikov, M. *J. Phys. Chem. B* **2006**, *110*, 4307.
(35) We found a peak from adventitious surface contaminants around 288.0 eV even in the C 1s spectra of alkanethiols on metal surfaces as others did (Himmelhaus, M. *et al. J. Electron Spectrosc. Relat. Phenom.* **1998**, *92*, 139-149, and Petrovykh, D. Y. *et al. Langmuir* **2006**, *22*, 2578-2587).

(36) Weckenmann, U.; Mittler, S.; Naumann, K.; Fischer, R. A. *Langmuir* **2002**, *18*, 5479.

(37) Laibinis, P. E.; Bain, C. D.; Whitesides, G. M. *J. Phys. Chem.* **1991**, *95*, 7017; the attenuation length is also confirmed by our experiment.

(38) Beebe, J. M.; Engelkes, V. B.; Liu, J. Q.; Gooding, J.; Eggers, P. K.; Jun, Y.; Zhu, X. Y.; Paddon-Row, M. N.; Frisbie, C. D. *J. Phys. Chem. B* **2005**, *109*, 5207.

(39) Diao, L.; Frisbie, C. D.; Schroepfer, D. D.; Ruden, P. P. *J. Appl. Phys.* **2007**, *101*, 014510.

(40) Amy, F.; Chan, C.; Kahn, A. *Org. Electron.* **2005**, *6*, 85.

(41) Crispin, X.; Geskin, V.; Crispin, A.; Cornil, J.; Lazzaroni, R.; Salaneck, W. R.; Bredas, J. L. *J. Am. Chem. Soc.* **2002**, *124*, 8131.

(42) De Renzi, V.; Rousseau, R.; Marchetto, D.; Biagi, R.; Scandolo, S.; del Pennino, U. *Phys. Rev. Lett.* **2005**, *95*, 046804.

(43) Beebe, J. M.; Kushmerick, J. G. *Appl. Phys. Lett.* **2007**, *90*, 083117.

(44) Terabe, K.; Hasegawa, T.; Nakayama, T.; Aono, M. *Nature* **2005**, *433*, 47.

(45) Liu, K.; Li, G. R.; Wang, X. H.; Wang, F. S. *J. Phys. Chem. C* **2008**, *112*, 4342.

(46) Yamada, R.; Kumazawa, H.; Noutoshi, T.; Tanaka, S.; Tada, H. *Nano Lett.* **2008**, *8*, 1237.

(47) Tada, T.; Nozaki, D.; Kondo, M.; Hamayama, S.; Yoshizawa, K. *J. Am. Chem. Soc.* **2004**, *126*, 14182.

(48) Quinn, J. R.; Foss, F. W.; Venkataraman, L.; Hybertsen, M. S.; Breslow, R. *J. Am. Chem. Soc.* **2007**, *129*, 6714.

(49) Duwez, A. S.; Pfister-Guillouzo, G.; Delhalle, J.; Riga, J. *J. Phys. Chem. B* **2000**, *104*, 9029.

(50) Gundlach, K. H.; Kadlec, J. *J. Appl. Phys.* **1975**, *46*, 5286.

(51) Landauer, R. *Phys. Lett. A* **1981**, *85*, 91-93.

6 Transition from Direct Tunneling to Field Emission in Metal-Molecule-Metal Junctions[†]

6.1 Abstract

Current-voltage measurements of metal-molecule-metal junctions formed from π-conjugated thiols exhibit an inflection point on a plot of $ln\ (I/V^2)$ *vs.* $1/V$, consistent with a change in transport mechanism from direct tunneling to field emission. The transition voltage was found to scale linearly with the offset in energy between the Au Fermi level and the highest occupied molecular orbital as determined by ultraviolet photoelectron spectroscopy. Asymmetric voltage drops at the two metal-molecule interfaces cause the transition voltage to be dependent on bias polarity.

6.2 Introduction

The overarching goal of molecular electronics is the design and implementation of nanoscale circuit elements based on the nonlinear current-voltage characteristics of molecules. A number of intriguing current-voltage characteristics have been observed for two-terminal metal-molecule-metal junctions, including negative differential resistance[1,2] and molecular switching.[3–5] Each of these behaviors could potentially prove useful for a range of electronics applications. The ability to rationally design molecular electronic components hinges on a fundamental understanding of the charge transport mechanism in such junctions.[6] To that end, Wang *et al.* have clearly demonstrated that for the case of alkyl-based junctions the charge transport mechanism is direct tunneling over a ± 1 V range.[7] Direct tunneling refers to nonresonant tunneling that occurs when the applied bias is less than the barrier height. The dominance of direct tunneling in alkyl systems is not surprising, due to their large (~8 eV) highest occupied molecular orbital–lowest unoccupied molecular orbital (HOMO-LUMO) gaps. In these junctions, a transition to hopping or diffusive transport is difficult, because field-induced breakdown occurs prior

[†] Reproduced with permission from Beebe, J. M.; Kim, B.-S.; Gadzuk, J. W.; Frisbie, C. D.; Kushmerick, J. G. *Phys. Rev. Lett.* **2006**, *97*, 026801/1-4. Copyright 2006 American Physical Society

to reaching the bias necessary to bring about the change in mechanism.[8,9] In contrast to the alkyl case, the mechanism of charge transport in junctions containing π-conjugated molecules is still under debate. In particular, Selzer *et al.* have demonstrated that the local environment and the means in which molecules are contacted can determine whether tunneling or a thermally activated process dominates charge transport for an oligo(phenyleneethynylene) derivative.[10] In a more general sense, the decreased HOMO-LUMO gap of the conjugated species increases the likelihood of accessing different transport mechanisms, such as resonant tunneling or electron hopping, prior to device breakdown. In this chapter, we provide evidence for a mechanistic transition from direct tunneling to field emission[11] at moderate bias (≤1 V) for a number of π-conjugated thiols. This change in mechanism can be described by the transition from a trapezoidal to a triangular tunneling barrier. By combining the transport results with photoelectron spectroscopy experiments, we are able to correlate the voltage at which the mechanistic transition occurs with the energy level alignment for a given molecular junction.

6.3 Results and Discussion

As mentioned above, direct tunneling is the dominant charge transport mechanism in junctions incorporating alkanes[7] and π-conjugated[10] monolayers. The simplest way to model the current-voltage behavior of a molecular junction is as an arbitrary tunnel barrier within the Simmons approximation[12]:

$$I = \frac{qA}{4\pi^2 \eta d^2}\left\{\left(\phi - \frac{qV}{2}\right)\exp\left(-\frac{2d\sqrt{2m_e}}{\eta}\sqrt{\phi - \frac{qV}{2}}\right) - \left(\phi + \frac{qV}{2}\right)\exp\left(-\frac{2d\sqrt{2m_e}}{\eta}\sqrt{\phi + \frac{qV}{2}}\right)\right\} \quad (6.1)$$

where A is the junction area, d is the barrier width, m_e is the electron effective mass, ϕ is the barrier height, and q is the electronic charge. In molecular junctions, the barrier width corresponds to the molecular length, and the barrier height can be approximated by the energy offset between the electrode Fermi level and the nearest molecular orbital. Equation (6.1) describes a trapezoidal barrier when the applied bias is less than the barrier height. In the zero-bias limit, the barrier is rectangular, and Eq. (6.1) reduces to

$$I \propto V \exp\left(-\frac{2d\sqrt{2m_e\phi}}{\eta}\right) \tag{6.2}$$

At the opposite limit, when the applied bias exceeds the barrier height, the barrier transitions from trapezoidal to triangular, and the current-voltage dependence can be described as follows:

$$I \propto V^2 \exp\left(-\frac{4d\sqrt{2m_e\phi^3}}{3\eta qV}\right) \tag{6.3}$$

Tunneling in the high-voltage regime is synonymous with tunneling through a triangular barrier and with the terms field emission and Fowler-Nordheim tunneling.[13] To extract meaningful information from the high-voltage regime, it is useful to linearize Eq. (6.3):

$$\ln\left(\frac{I}{V^2}\right) \propto -\frac{4d\sqrt{2m_e\phi^3}}{3\eta qV}\left(\frac{1}{V}\right) \tag{6.4}$$

From Eq. (6.4), it is obvious that a plot of *ln* (I/V^2) against $1/V$ will yield a line, the slope of which will depend on the barrier height. Because field emission experiments generally involve barriers with both substantial width and height, no measurable current flows prior to the onset of field emission. Therefore, a transition from direct tunneling to field emission will only be seen for the case of a small barrier height and width, such as is found in metal-molecule-metal junctions. To experimentally examine the transition from direct tunneling to field emission requires recasting Eq. (6.2) in terms of the variables *ln* (I/V^2) and $1/V$ so it can be directly compared to Eq. (6.4). The resulting equation is as follows:

$$\ln\left(\frac{I}{V^2}\right) \propto \ln\left(\frac{1}{V}\right) - \frac{2d\sqrt{2m_e\phi}}{\eta} \tag{6.5}$$

From Eq. (6.5), a plot of *ln* (I/V^2) against $1/V$ will exhibit a logarithmic growth in the low-bias regime. When the applied bias is near the barrier height, the mechanisms compete, causing a transition from logarithmic growth to linear decay. This transition corresponds to the voltage required to change the shape of the barrier from trapezoidal to

triangular. We choose to refer to this special value of applied bias as the transition voltage, or V_{trans}. It should be noted that measurement of V_{trans} provides a means of experimentally estimating the height of the original rectangular barrier. Because the Simmons equation as outlined in Eq. (6.1) does not explicitly account for voltage drops at the contacts or the image potential of the tunneling electron, V_{trans} remains an estimate, and not an exact measure of the barrier height.

To examine the current-voltage behavior of molecular junctions, two platforms were employed: conducting probe–atomic force microscopy (CP-AFM)[8,14–16] and crossed-wire tunnel junctions[17,18] (Figure 6.1). In both techniques, molecules are self-assembled onto one electrode using thiol-Au chemistry. The second electrode is then placed into soft mechanical contact with the molecular layer, thereby avoiding the

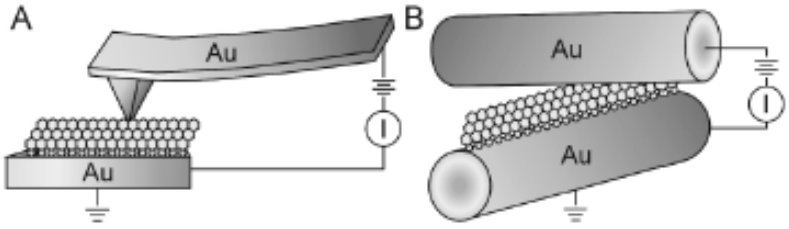

Compound	Structure	$V_{transition}$ [a] CP-AFM (V)	$V_{transition}$ [a] Crossed-Wire (V)	E_F-E_{HOMO} (eV)
Ph-SH		0.95, ***	[b]	2.0
Naph-SH	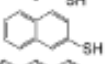	0.76, ***	0.71, ***	1.8
Anth-SH	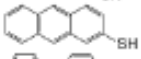	0.62, -0.85	0.57, -0.85	1.6
BP-SH		0.82, ***	0.79, ***	1.9
TP-SH		0.67, -0.82	0.66, -0.92	1.7

[a] Bias applied at the top electrode. Positive bias is electron injection at the Au-S contact.
*** No transition reached within the 0 to -1V bias range.
[b] Ph-SH is too short to be measured in the crossed-wire junction.

Figure 6.1. Schematic representation of (A) CP-AFM and (B) crossed-wire molecular junctions. The table included within the figure shows our adopted nomenclature as well as the structures, transition voltages, and energy level offsets for each of the molecules used in this study. Positive bias corresponds to electron (hole) injection at the Au-S (Au-phenyl) interface.

damage that can be induced by evaporated top contacts.[19,20] In both platforms, a bias (±1.0 V) is swept at the top electrode, the bottom electrode is held at ground, and the current through the junction is measured. Reported values are the averages of 20–100 *I-V* traces per self-assembled monolayer. In this chapter, we focus on a collection of π-conjugated molecules terminated in thiol linkers (Figure 6.1). The method of assembly, monolayer characterization, and low-bias currentvoltage behavior of these molecules has been previously reported.[21] All molecules studied are known to form monolayers of similar surface coverage on Au surfaces.

Figure 6.2 shows the average of 100 *I-V* traces for a Au-anthracenethiol-Au junction collected using CP-AFM, plotted on the axes specified by Eq. (6.4). The inset displays the same data plotted on standard current-voltage axes. Though a systematic study of the temperature dependence of the current-voltage data is necessary to unambiguously assign a charge transport mechanism, it is likely that the mechanism is direct tunneling at low bias. This assertion is supported by the conclusions of Selzer *et al.*

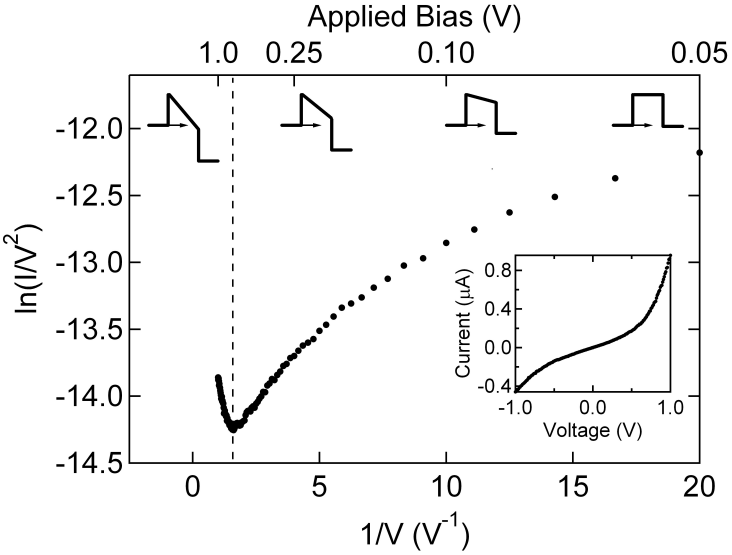

Figure. 6.2. Solid circles represent the average of 100 *I-V* curves for a Au-anthracenethiol-Au junction measured by CP-AFM. The dashed line corresponds to the voltage at which the tunneling barrier transitions from trapezoidal to triangular (V_{trans}). Also shown are representations of the barrier shape at various values of applied bias. The inset shows current-voltage data on standard axes.

regarding π-conjugated monolayers,[10] the sigmoidal shape of the *I-V* curve shown in Figure 6.2, and the previously observed exponential dependence of resistance on molecular length.[21] The dashed line in Figure 6.2 denotes the voltage required for transition from direct tunneling to field emission (V_{trans}) for anthracenethiol. The shape of the curve in the two bias regions matches the shape predicted by Eqs. (6.4) and (6.5) (linear decrease at high bias and logarithmic growth at low bias). There is no evidence of negative differential resistance at any point in the curve, suggesting that the mechanistic transition is not one of nonresonant to resonant tunneling. Each molecule employed in this study exhibited a data curve qualitatively similar to that shown for anthracenethiol. Measurements on alkanethiol junctions (not shown) do not exhibit a V_{trans} inflection point over the same ± 1 V range, consistent with the conclusions of Wang *et al.*[7] that direct tunneling is the charge transport mechanism in such junctions. Transition voltages for each of the π-conjugated molecules are compiled in Figure 6.1. Note the excellent agreement of V_{trans} measured in the CP-AFM and crossed-wire geometries.

Figure 6.3 shows linear scaling of V_{trans} with the difference in energy between the Au Fermi level and molecular HOMO. In this graph, the *x* coordinates were determined from ultraviolet photoelectron spectroscopy (UPS).[21] The linear scaling matches the behavior expected if the barrier height was set by the E_{Fermi}-E_{HOMO} offset and demonstrates that V_{trans} corresponds to a *molecular signature*. Although linear scaling is observed between V_{trans} and the E_{Fermi}-E_{HOMO} offset, there is a significant discrepancy between the barrier heights predicted by these two methods. The effective barrier lowering observed in the charge transport measurements can be attributed to a number of factors. Primarily, we are modeling the tunnel barrier as a simple geometric shape (rectangular, trapezoidal, triangular), and are not taking into account the image potential, which would effectively reduce the area of the potential barrier by rounding off the corners and reducing the thickness.[12] Proper modeling of these systems should use a molecularly derived potential barrier.[22] Another reason for the difference between the value of V_{trans} and E_{Fermi}-E_{HOMO} is that the position of the HOMO level was determined

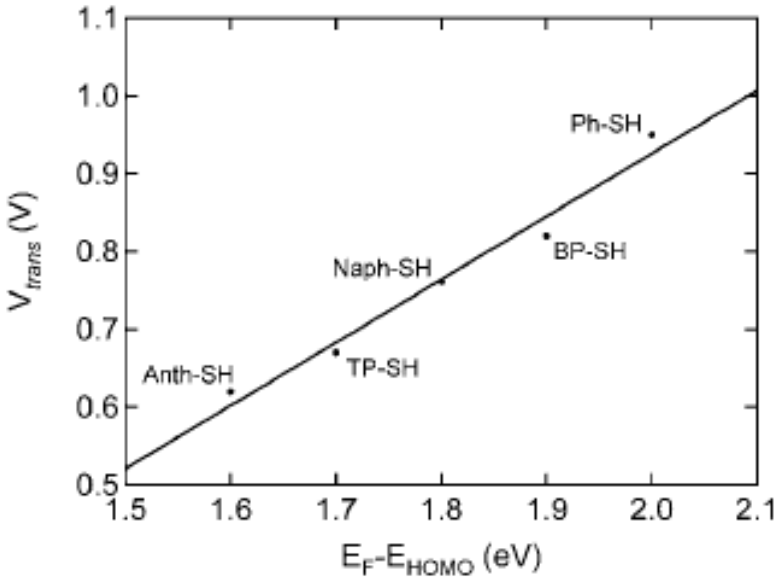

Figure. 6.3. V_{trans} (CP-AFM) versus E_{Fermi}-E_{HOMO} energy difference (UPS).

from the peak maxima in the UPS.[21] The onset of the UPS peak would yield a better match with V_{trans}; however, the difficulty in unambiguously assigning this value precludes its use.

It is important to note that there is a strong dependence of V_{trans} on bias polarity (Figure 6.1). In all cases, V_{trans} is lower when a positive bias is applied to the Au-phenyl interface. We attribute this directly to the asymmetry in the two metal-molecule contacts. We have previously shown how such contact asymmetries can lead to rectification in molecular junctions due to unequal voltage drops at the two interfaces.[17,23] Similarly, we have demonstrated that symmetric dithiols exhibit lower contact resistance (less voltage drop) than asymmetric monothiols.[24] Figure 6.4 shows schematically how V_{trans} is affected by asymmetric voltage drops at the two metal-molecule interfaces. The energy diagrams are drawn to correspond to the specific (hypothetical) case of a drop of 50% of the applied bias at the left contact, and 50% across the molecule, with no voltage drop at the right contact. In Figures. 6.4(B) and 6.4(C), the magnitude of the applied bias is constant, but the polarity is opposite. In Figure 6.4(B), enough bias is applied to cause a transition from a trapezoidal barrier to a triangular barrier. From the diagram in Figure

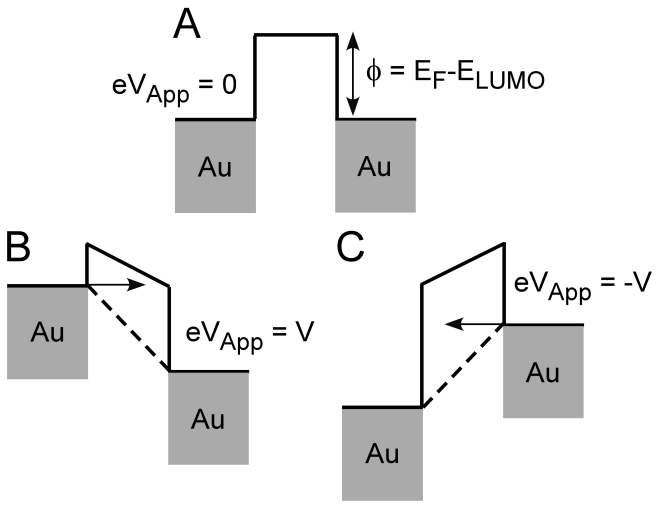

Figure. 6.4. Effect of asymmetric voltage drops on V_{trans}. Note that the figure is drawn for LUMO-mediated electron tunneling, but the model also applies for HOMO-mediated hole tunneling. See text for full description.

6.4(C), it is obvious that the barrier has not yet become triangular. The monothiol molecules used in this study lead to an inherent asymmetric voltage drop at the two metal-molecule contacts. Reexamination of the data in Reference (18) shows that symmetric dithiols with phenylene-vinylene and phenylene-ethynylene backbones exhibit identical values of V_{trans} for both bias polarities. This confirms that the observed polarity dependence of V_{trans} is a direct consequence of the asymmetric metal-molecule contacts.

A final point is that the barrier shape transition model holds for different test platforms. As shown in Figure 6.1, the transition voltage as measured by CP-AFM agrees well with that measured by crossed-wire junctions for a given molecule. We determine the standard deviation of the transition voltage to be 0.07 V. Therefore, the slight differences between V_{trans} measured by CP-AFM and by crossed-wire junctions are within the measurement uncertainty. This cross-platform agreement highlights the fact that the observed behavior depends on the identity of the molecule in the junction, and not on the manner in which the junction was fabricated. The junction area, electrode roughness, and applied load are different for the two platforms, yet both techniques measure the same value of V_{trans} for a given molecule. In a field where measurement of

the same molecule in different device platforms often yields widely varying data, this result supports not only the validity of the model, but also the quality of data obtained from both test structures.

6.4 Summary

We have demonstrated that Au-molecule-Au junctions formed from π-conjugated thiols exhibit current-voltage behavior consistent with a transition from a trapezoidal barrier to a triangular barrier at moderate bias. The voltage required to bring about this transition was found to depend linearly on the energy offset between the junction Fermi level and molecular HOMO as measured by UPS. The linear dependence of V_{trans} on the HOMO position demonstrates that this measurement provides an alternative method to determine the apparent height of the tunneling barrier in molecular junctions. The observed shift in V_{trans} with bias polarity demonstrates the importance of interfacial voltage drops in determining the current-voltage behavior of molecular devices. We are currently examining the effect of varying the metal at either contact, as changing the metal will change the alignment of the molecular HOMO relative to the junction Fermi level.[25] Preliminary results show V_{trans} to be temperature dependent, and we are currently exploring the implications of this temperature dependence on the proposed mechanism. Further, we are developing a more detailed numerical treatment of the observed tunneling barrier transition in order to directly incorporate the effects of voltage drops at the metal-molecule interfaces.

6.5 Acknowledgment

We thank the financial support of DARPA and NSF (CHE-0315165).

6.6 References

(1) Chen, J.; Reed, M. A.; Rawlett, A. M; Tour, J. M. *Science* **1999**, *286*, 1550.

(2) Gorman, C. B.; Carroll, R. L.; Fuierer, R. R. *Langmuir* **2001**, *17*, 6923.

(3) Reed, M. A.; Chen, J.; Rawlett, A. M.; Price, D.W.; Tour, J. M. *Appl. Phys. Lett.* **2001**,

78, 3735.

(4) Blum, A. S.; Kushmerick, J. G.; Long, D. P.; Patterson, C. H.; Yang, J. C.; Henderson, J. C.; Yao, Y.; Tour, J. M.; Shashidhar, R.; Ratna, B. R. *Nat. Mater*. **2005**, *4*,167.

(5) Cai, L.; Cabassi, M. A.; Yoon, H.; Cabarcos, O. M.; McGuiness, C. L.; Flatt, A. K.; Allara, D. L.; Tour, J. M.; Mayer, T. S. *Nano Lett.* **2005**, *5*, 2365.

(6) Nitzan, A.; Ratner, M. A. *Science* **2003**, 300, 1384.

(7) Wang, W.; Lee, T.; Reed, M. A. *Phys. Rev. B* **2003**, *68*, 035416.

(8) Wold, D. J.; Frisbie, C. D. *J. Am. Chem. Soc.* **2001**, *123*, 5549.

(9) Holmlin, R. E.; Haag, R.; Chabinyc, M. L.; Ismagilov, R. F.; Cohen, A. E.; Terfort, A.; Rampi, M. A.; Whitesides, G. M. *J. Am. Chem. Soc.* **2001**, *123*, 5075.

(10) Selzer, Y.; Cai, L.; Cabassi, M. A.; Yao, Y.; Tour, J. M.; Mayer, T. S.; Allara, D. L. *Nano Lett.* **2005**, *5*, 61.

(11) Young, R.; Ward, J.; Scire, F. *Phys. Rev. Lett.* **1971**, *27*, 922.

(12) Simmons, J. G. *J. Appl. Phys.* **1963**, *34*,1793.

(13) Gadzuk, J.W.; Plummer, E.W. *Rev. Mod. Phys.* **1973**, *45*, 487.

(14) Leatherman, G.; Durantini, E. N.; Gust, D.; Moore, T. A.; Moore, A. L.; Stone, S.; Zhou, Z.; Rez, P.; Liu, Y. Z.; Lindsay, S. M. *J. Phys. Chem. B* **1999**, *103*, 4006.

(15) Engelkes, V. B.; Beebe, J. M.; Frisbie, C. D. *J. Phys. Chem. B* **2005**, *109*, 16801.

(16) Wold, D. J.; Frisbie, C. D. *J. Am. Chem. Soc*. **2000**, *122*, 2970.

(17) Kushmerick, J. G.; Holt, D. B.; Yang, J. C.; Naciri, J.; Moore, M. H.; Shashidhar, R. *Phys. Rev. Lett.* **2002**, *89*, 086802.

(18) Kushmerick, J. G. ; Holt, D. B.; Pollack, S. K.; Ratner, M. A.; Yang, J. C.; Schull, T. L.; Naciri, J.; Moore, M. H.; Shashidhar, R. *J. Am. Chem. Soc.* **2002**, *124*, 10654.

(19) Walker, A.V.; Tighe, T. B.; Haynie, B. C.; Uppili, S.; Winograd, N.; Allara, D. L. *J. Phys. Chem. B* **2005**, *109*, 11263.

(20) Richter, C. A.; Hacker, C. A.; Richter, L. J. *J. Phys.Chem. B* **2005**, 109, 21836.

(21) Kim, B.-S.; Beebe, J. M.; Jun, Y.; Zhu, X.Y.; Frisbie, C. D. *J. Am. Chem. Soc.* **2006**, 128, 4970.

(22) Xue, Y. Q.; Ratner, M. A. *Phys. Rev. B* **2003**, *68*, 115406.

(23) Kushmerick, J. G. *Mater. Today* **2005**, *8*, 26.

(24) Engelkes, V. B.; Beebe, J. M.; Frisbie, C. D. *J. Am. Chem. Soc.* **2004**, *126*, 14287.

(25) Beebe, J. M.; Engelkes, V. B.; Miller, L. L.; Frisbie, C. D. *J. Am. Chem. Soc.* **2002**, 124, 11268.

7 Measuring Relative Barrier Heights in Molecular Electronic Junctions with Transition Voltage Spectroscopy[†]

7.1 Abstract

Though molecular devices exhibiting potentially useful electrical behavior have been demonstrated, a deep understanding of the factors that influence charge transport in molecular electronic junctions has yet to be fully realized. Recent work has shown that a mechanistic transition occurs from direct tunneling to field emission in molecular electronic devices. The magnitude of the voltage required to enact this transition is molecule-specific, and thus measurement of the transition voltage constitutes a form of spectroscopy. Here we determine that the transition voltage for a series of alkanethiol molecules is invariant with molecular length, while the transition voltage of a conjugated molecule depends directly on the manner in which the conjugation pathway has been extended. Finally, by examining the transition voltage as a function of contact metal, we show that this technique can be used to determine the dominant charge carrier for a given molecular junction.

7.2 Introduction

The field of molecular electronics is driven by the perceived opportunity to use molecules as active elements in electronic circuits. Instances of two-state switching[1–4] and Coulomb blockading[5–7] have been demonstrated in a small number of molecule-based devices, but realization of a practical device technology will require a detailed understanding of the transport mechanisms. We have recently demonstrated that the charge transport mechanism in electronic junctions of a series of π-conjugated molecules undergoes a transition from direct tunneling (rectangular barrier) to field emission (triangular barrier) upon increasing the applied bias. The voltage at which this transition

[†] Reproduced with permission from Beebe, J. M.; Kim, B.-S.; Frisbie, C. D.; Kushmerick, J. G. *ACS nano* **2008**, *2*, 827-832. Copyright 2008 American Chemical Society

occurs (V_{trans}) is linearly correlated with the energy offset between the metal Fermi level and the highest occupied molecular orbital (HOMO),[8] a feature that allows us to probe the effective energy barrier to charge transport by measuring V_{trans} for a series of structurally distinct molecular junctions. We refer to this barrier height measurement as transition voltage spectroscopy, or TVS.

One of the most salient attributes of TVS is that V_{trans} is a measurable quantity and therefore does not require any assumptions or fit parameters for its determination. Other advantages of TVS include the following: (1) TVS is simple to implement and requires only basic mathematical transformation of the acquired data; (2) TVS is sensitive to the metal-molecule contact chemistry at each interface, and therefore inherently reflects the contact resistance; (3) the measured V_{trans} is independent of contact area, which eliminates problems associated with comparing current densities between different device architectures.[9] Though V_{trans} is a single experimental observable, its value is sensitive to the molecular topology, metal-molecule linking group, and electrode composition, as will be demonstrated within. Understanding of TVS is facilitated by a simple barrier picture for charge tunneling in a junction, Figure 7.1B. While this barrier description is known to be deficient in capturing quantitative aspects of tunneling through molecules, it allows us to understand in a straightforward manner the cause of the transition in transport mechanism that we observe in molecular junctions; more sophisticated approaches based on the Landauer formalism do not readily lend themselves to prediction of a switch in mechanism. Therefore, we model the electronic structure of our metal-molecule- metal junctions as a rectangular tunneling barrier with a height (ϕ) set by the energy offset between the metal Fermi level and the closest molecular orbital, and a width (d) determined by the length of the molecule incorporated into the junction, as shown in Figure 7.1B. In molecular junctions incorporating thiols, a variety of spectroscopic[10,11] and electrical[12–14] measurements predict that the occupied molecular orbitals lie closer in energy to the metal Fermi level than to the unoccupied

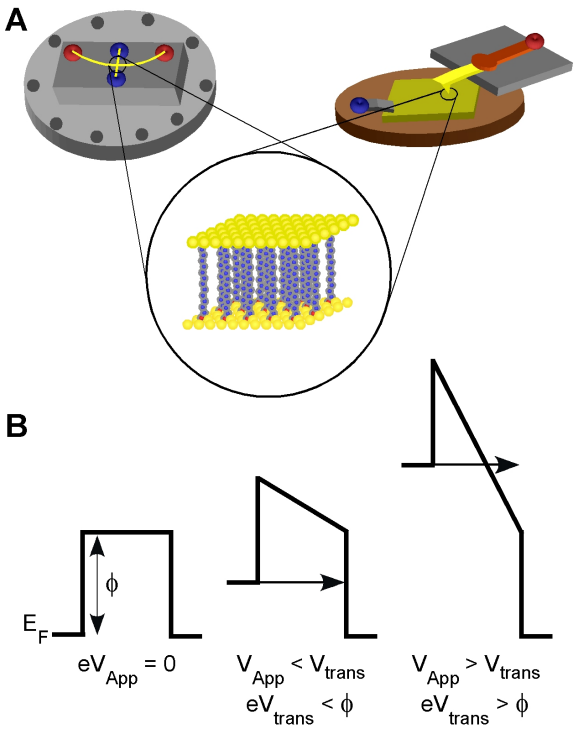

C

Molecule	Structure	V_{trans}
Ph-SH		0.95 ± 0.11
Naph-SH		0.71 ± 0.12
Anth-SH	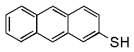	0.60 ± 0.18
BP-SH	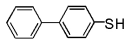	0.81 ± 0.11
TP-SH	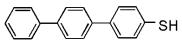	0.67 ± 0.14
OPE(2)-SH	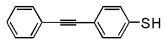	0.93 ± 0.13
OPE(3)-SH	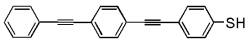	0.80 ± 0.13
OPV(2)-SH	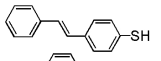	0.79 ± 0.12
OPV(3)-SH	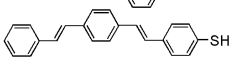	0.57 ± 0.07
C_6-SH		1.24 ± 0.07
C_8-SH		1.28 ± 0.12
C_{10}-SH	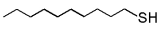	1.27 ± 0.13
C_{12}-SH	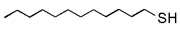	1.20 ± 0.08
C_{16}-SH		1.15 ± 0.11
C_{18}-SH		1.26 ± 0.08

Figure 7.1. (A) Schematic representation of crossed-wire and CP-AFM junctions. Both techniques measure an ensemble of molecules that are chemically bound to the bottom electrode and physically contacted by the top electrode (magnified region). (B) (left) At an applied bias smaller than V_{trans}, the tunneling barrier height (ϕ) is set by the Fermi level-molecular orbital energy offset, and the barrier width (d) corresponds to the length of the molecule in the junction. (center) For biases less than the barrier height, the shape of the barrier is trapezoidal. (right) At an applied bias greater than V_{trans}, the barrier shape becomes triangular, and the transport mechanism changes to field emission. Note that our cartoons are drawn for the case of electron transport mediated by an unoccupied orbital; hole transport mediated by an occupied orbital is equivalent. (c) Our adopted nomenclature and the chemical structure of each of the molecules used in this study, along with their corresponding V_{trans} values. Standard deviations are determined by using the 10 measured values of V_{trans} for each junction type. The overall average standard deviation is 0.11 V.

molecular orbitals. Although the energy diagram (Figure 7.1B) is drawn for electron transport mediated by an unoccupied orbital, the following argument also applies for hole transport mediated by an occupied state.

When a bias is applied to the junction, the overall voltage drop across the junction

is equal to the magnitude of the applied bias. The details of the electrostatic potential profile across the junction are unknown, and voltage drop can occur at both metal-molecule contacts as well as across the molecular bridge.[15,16] If the voltage is dropped only at the contacts (the weak coupling limit often achieved in scanning tunneling microscope experiments), then the barrier remains rectangular, and the electrode Fermi level can be swept through the molecular orbitals, resulting in resonant tunneling.[17,18] If, however, a significant fraction of the bias is dropped across the molecular bridge, then the barrier *shape* will change from rectangular to trapezoidal. At a threshold voltage defined by the barrier height and the distribution of voltage drops, the barrier becomes triangular (Figure 7.1B), and the functional dependence of current on applied voltage changes due to a change in transport mechanism. We refer to the voltage required to enact this transition as V_{trans}, which can be directly determined from a plot of $ln\ (I/V^2)$ against $1/V$.[8]

As already noted, for the sake of simplicity we are referring to the potential barrier as a simple geometric shape (rectangular, trapezoidal, triangular). The true barrier of course is much more complex and is determined by the electronic structure of the molecule. Although these barriers are oversimplifications, this approximation does not affect our results because the true barrier shape is not important for TVS analysis. Rather, the important feature is the prediction of a transition from direct tunneling through a barrier (trapezoidal type) to field emission through the top of the barrier (triangular type). In more complex treatments, the true barrier shape is required as an input parameter to a series of equations that fully describe the electronic state of the junction. One of our key findings is that the simple barrier model qualitatively explains the change in the functional form of the current-voltage behavior.

7.3 Experimental

Monolayer Deposition and Characterization. The method of assembly and monolayer characterization for the molecules examined in this paper have been

previously described.[22,32,40,41] Briefly, the self-assembled monolayers were prepared on commercially available 10 μm diameter wires. Prior to monolayer deposition, the wires were cleaned in 30% H_2O_2 for at least 10 min to remove any adsorbates; ~1 mM solutions of each of the molecules were prepared in an Ar glovebox from suitable solvents (ethanol for the alkanes and CH_2Cl_2/EtOAc for the aromatic molecules). Monolayers were allowed to assemble overnight, and the resulting monolayer-coated wires were rinsed by placing them in a vial of ethanol (for alkanes) or CH_2Cl_2 (for aromatics) to remove any physisorbed molecules.

Current-Voltage Measurements. For each molecule used in this study, a total of 200 *I-V* traces were collected using either the crossed-wire or the CP-AFM junction geometry. In both cases, a voltage is swept at the top (bare) electrode, the bottom (monolayer-containing) electrode is held at ground, and the current through the junction is measured. For each molecule, the top electrode was brought into contact with the molecular monolayer, 20 *I-V* traces were collected, and the top contact was removed from the monolayer surface. The inherent noise in the current-voltage data can make it somewhat difficult to determine V_{trans} for an individual current-voltage trace. Twenty *I-V* traces per junction formation were averaged together toprovide a more robust value of V_{trans} that was less influenced by current fluctuations. This process was repeated 10 times for each molecule, thereby providing a statistical sampling across various spatial regions of the monolayer.

Transition Voltage Determination. Each 20-trace data set was geometrically averaged, and transformed onto axes of $ln\ (I/V^2)$ against $1/V$. The position of the transition voltage was determined manually for each data set. The mean value of the 10 data sets was then reported as V_{trans} for that molecule. This process was then repeated for each of the 15 molecules used in this study. The standard deviation in V_{trans} measured across 10 data sets is approximately 0.1 V. Two types of data were rejected during V_{trans} analysis. One exclusion criterion was any junction that resulted in a short circuit. Because the top electrode is placed into soft contact with the monolayer, only a very small number

of junctions (<5%) exhibited this condition. A second rejection criterion was for cases where we were unable to unambiguously determine V_{trans}. Ambiguity in V_{trans} occurs for junctions with a higher level of noise in the *I-V* data, which causes the appearance of multiple possible V_{trans} values. Rather than arbitrarily choosing between these values, we simply made an extra set of measurements in cases where this problem occurred. With the exception of these exclusion criteria, no data selection was performed.

Transition Voltage as a Function of Metal Electrode. For the investigation of metal-molecule contact effects, monolayers of OPE(3)-SH and OPE(3)-NC were deposited on 10 μm diameter wires of the different metals. The crossed-wire apparatus was then used with a Au top electrode to measure the *I-V* characteristics and transition voltage as described above. Because H_2O_2 oxidizes the Ag wires (and potentially the Pt wires), a change in preparation technique was required for this set of experiments. Wires were first affixed to a stainless steel block inside an Ar plasma chamber that was located inside an Ar glovebox. Wires were cleaned *via* exposure to a 25-W Ar plasma for 10 min. After plasma cleaning, wires were placed into molecule-containing solutions inside the glovebox, and thus the wires were never exposed to ambient conditions after plasma exposure. For consistency, wires of all metal types involved in this series of experiments were cleaned using the Ar plasma method.

7.4 Results and Discussion

We employ two distinct but complementary test structures to measure the current-voltage properties of molecules: conducting probe atomic force microscopy (CP-AFM)[19,20] and crossed-wire tunnel junctions[21,22] (Figure 7.1A). Each technique features a soft, physically placed top electrical contact, which avoids potential damage from evaporated metal sources.[23,24] In both test structures, a self-assembled monolayer of a molecule of interest is formed on the bottom (Au) contact. The top (Au) electrode is then brought into physical contact with the molecular layer. Voltage is swept at the top contact, the bottom electrode is held at ground, and the current through the junction is measured.

To begin, we will look at two series of molecules which have been carefully chosen such that the contact chemistry remains constant throughout a given molecular series. For all molecules in these two series, the bottom contact is Au-S, and the top contact is Au/phenyl for the π-conjugated molecules and Au/methyl for the alkanes. Measurement of V_{trans} in a Au/C8-SH/Au junction is illustrated in Figure 7.2. To generate Figure 7.2, the average of 20 current-voltage traces (as shown in Figure 7.2, inset) is transformed to axes of *ln* (I/V^2) against *1/V*. To arrive at a composite V_{trans} for each molecule,[10] separate metal-molecule-metal junctions are formed, generating 10 spectra of the type found in Figure 7.2. The average value of the inflection point voltage across these junction formations is then used as V_{trans} for a given molecule. The results across each molecular series are summarized numerically in Figure 7.1C and graphically in Figure 7.3 (alkanethiols) and Figures 7.4 and 7.5 (π-conjugated thiols). The alkanethiols

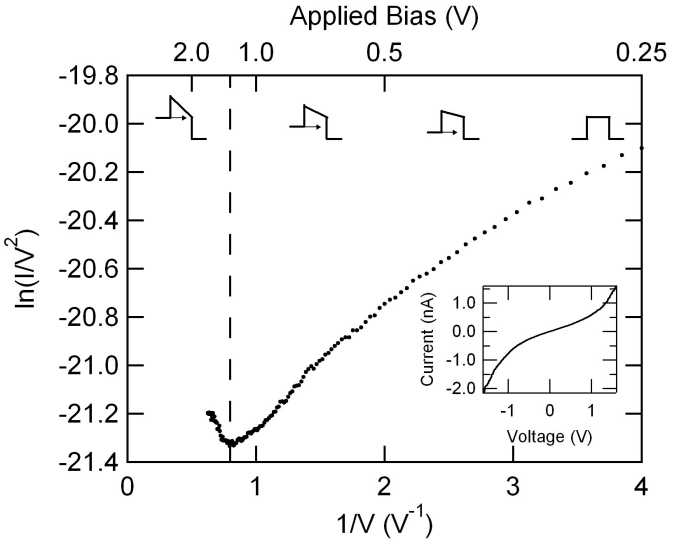

Figure 7.2. Solid circles represent the average of 20 *I-V* curves for a Au/C8-SH/Au junction measured by CP-AFM. The dashed line corresponds to the voltage required to change the functional dependence of current on applied voltage (V_{trans}). Also shown are representations of the barrier shape at various values of applied bias. The inset shows current-voltage data on standard axes. Note that only a small portion of the field emission regime can be sampled in molecular junctions contacted directly by electrodes on both sides because field-dependent breakdown of the junction occurs at biases ranging from ~1.5-2.0 V, depending on the length of a given molecule.

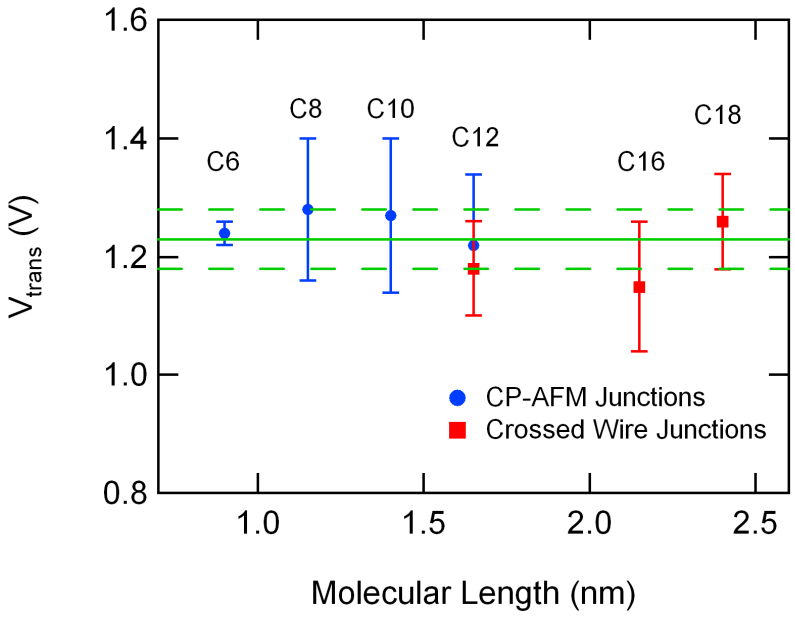

Figure 7.3. V_{trans} as a function of molecular length for a series of alkanethiols. Shorter molecules were measured using CP-AFM (circles) because the small contact areas enabled measurement of current at higher bias than was attainable in the crossed-wire geometry (squares). The solid line represents the mean alkanethiol barrier height, and the dashed lines show the standard deviation across the seven individual measurements. The numbers above each data point display the number of carbon atoms in each molecule.

constitute an important control series in molecular electronic experiments, because their HOMO-LUMO gap remains effectively constant as the number of methylene repeat units is increased, and it has been unambiguously determined that nonresonant tunneling is the transport mechanism for small applied biases.[12] Similarly, ultraviolet photoelectron spectroscopy measurements have shown that the E_{Fermi}-E_{HOMO} offset for alkanethiols is nearly independent of molecular length.[25,26] Therefore, we expect that V_{trans} would also be constant across the alkanethiol series. The average value of V_{trans}, represented by the solid line in Figure 7.3, falls within the standard deviation of measured values for each of the molecules, thereby illustrating that V_{trans} is indeed independent of molecular length in alkanethiols. Another important feature of Figure 7.3 is the excellent agreement between V_{trans} as determined by CP-AFM and V_{trans} obtained from the crossed-wire geometry. We have previously observed similar cross-platform agreement for acenes(Naph-SH,

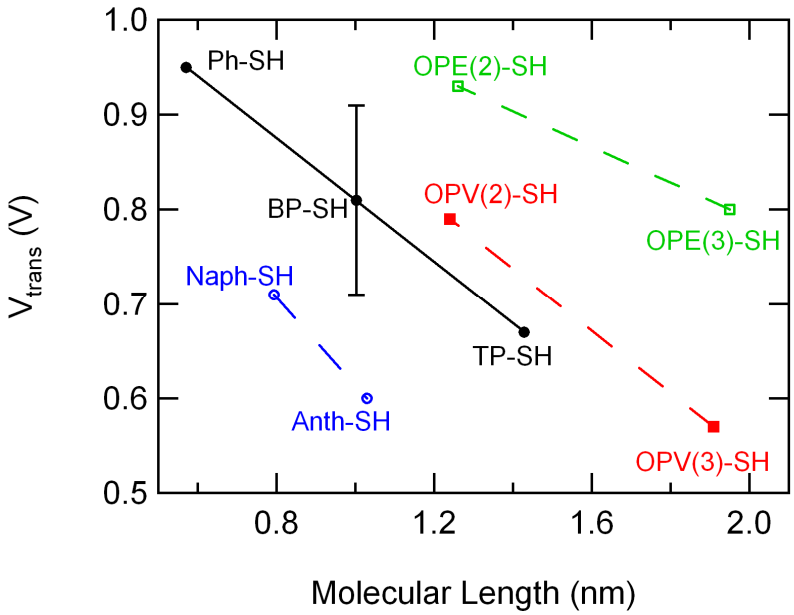

Figure 7.4. V_{trans} as a function of molecular length for four different pathways for extending conjugation. Dashed lines connecting molecules within the OPE series (open squares), OPV series (filled squares), and acene series (open circles) have been added to guide the eye. The solid black line is a linear fit to the three points in the phenylene series (filled circles). The standard deviation in V_{trans} for each molecule is given in Figure 7.1, for clarity only the uncertainty in the BP-SH measurement is shown here.

Anth-SH) and phenylenes (BP-SH, TP-SH).[8] Here, one junction, Au/C12-SH/Au, was chosen for measurement in both test structures. As shown in Figure 7.3, the measured values of V_{trans} agree within 5%, demonstrating the independence of V_{trans} on junction area. We note that one must be careful when performing this type of analysis in junctions with evaporated metal contacts, as the metal evaporation step likely perturbs the physical structure of the molecules[23] and therefore the electronic structure of the resulting junction.[24] In contrast to the alkane series, the HOMO-LUMO gap of π-conjugated molecules is known to decrease with an increase in conjugation length.[27] We would therefore expect longer conjugated molecules to exhibit a smaller value of V_{trans} than shorter conjugated molecules. However, as shown in Figure 7.4, V_{trans} does not decrease monotonically with molecular length for all aromatic thiols. Rather, V_{trans} is observed to decrease with molecular length within a given molecular series (*i.e.*, $V_{trans,OPV(2)\text{-}SH}$

$<V_{trans,OPV(3)\text{-}SH}$). The molecules explored here represent four distinct ways of extending conjugation within a molecular series. The solid black line in Figure 7.4 is a linear least-squares fit to the molecules in the phenylene series. The second (BP-SH) and third (TP-SH) molecules in this series have a structural repeat unit that is strikingly similar to benzenethiol, and therefore it is unsurprising that V_{trans} exhibits a monotonic dependence on length for this series. All other aromatic families have a repeat structure that does not neatly reduce to benzenethiol. The OPV and OPE series have repeat structures that are longer than benzenethiol, while the molecules in the acene series (Naph-SH, Anth-SH) have a repeat unit that is smaller than Benzenethiol by two carbon atoms, and therefore extrapolation of V_{trans} for these molecular families down to a single repeat unit results in a barrier that is larger and smaller respectively than that measured for benzenethiol. The scaling of V_{trans} with molecular conjugation is demonstrated in Figure 7.5 where V_{trans} is plotted *versus* the calculated HOMO-LUMO gap. This scaling is supported by prior experimental examinations of the efficiency of charge transport through aromatic bridges.[21,28–30]

The measured transition voltage for a molecular junction is also sensitive to the nature of the metal-molecule linkage. For example, the value of V_{trans} is bias polarity-dependent in molecular junctions incorporating asymmetric metal-molecule contacts such as afforded by monothiols, but is polarity independent in symmetric junctions incorporating dithiols.[8] This behavior illustrates that V_{trans} simultaneously probes both the barrier height and the voltage drop or spectral overlap at each metal-molecule contact. While a number of studies have examined how contact asymmetry can lead to charge transport rectification[22,31] or how the chemistry of the metal-molecule contact can affect the contact resistance,[14,32] TVS can provide added insight into these investigations. By measuring the transition voltage for OPE(3) moieties attached through thiolate and isocyanide linkages on four different metal electrodes (Ag, Pd, Au, and Pt), we are able to explore how the metal-molecule contact influences the so-called “band lineup” problem.[33] Band lineup refers to the position of the metal electrodes Fermi level with

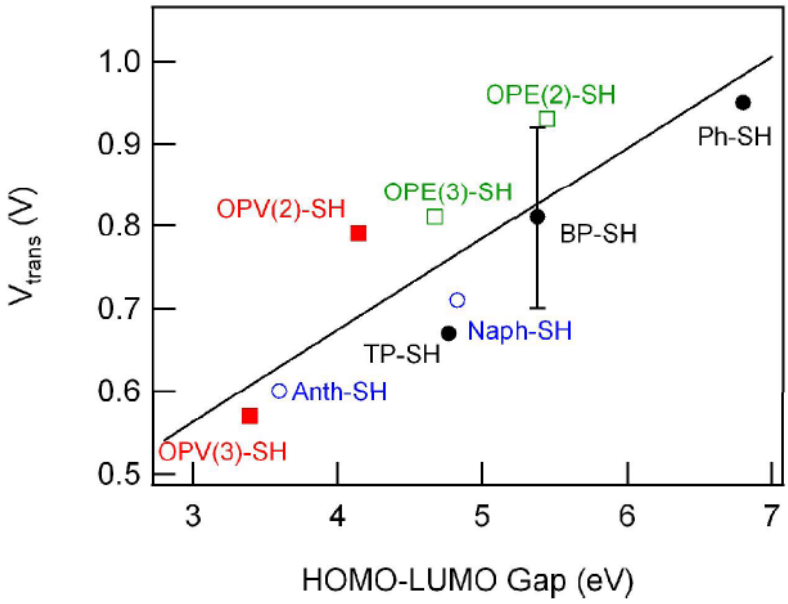

Figure 7.5. V_{trans} as a function of calculated HOMO-LUMO gap for the conjugated thiols studied. Density functional theory (DFT) methods at the B3LYP/6-31G* level of theory were used to calculate the HOMO-LUMO gap of the aromatic molecules studied.[42] The molecular cores with the thiol linkage group replaced with a hydrogen atom were used. All calculations were done for the energy minimized structures with the exception of the OPE derivatives which had their rings fixed in a perpendicular orientation. The solid black line is a linear least-squares fit of the data. The standard deviation in V_{trans} for each molecule is given in Figure 7.1, for clarity only the uncertainty in the BP-SH measurement is shown here.

respect to the occupied and unoccupied molecular orbitals. In its simplest form if the Fermi level is energetically closer to an unoccupied orbital, electron tunneling would be the dominate conduction channel. Conversely for a band lineup in which occupied orbitals are closer to the Fermi level hole conduction is expected.

Figure 7.6 plots V_{trans} *versus* electrode work function[34] for the systems measured. Focusing first on the OPE(3)-SH system, we see that V_{trans} decreases as the electrode work function increases. As the work function of a metal increases, the energy difference between the Fermi level and the HOMO decreases, and therefore the observed correlation suggests that charge transport in these aromatic thiol systems is modulated by charge carriers interacting with an occupied molecular level (hole tunneling). Hole conduction

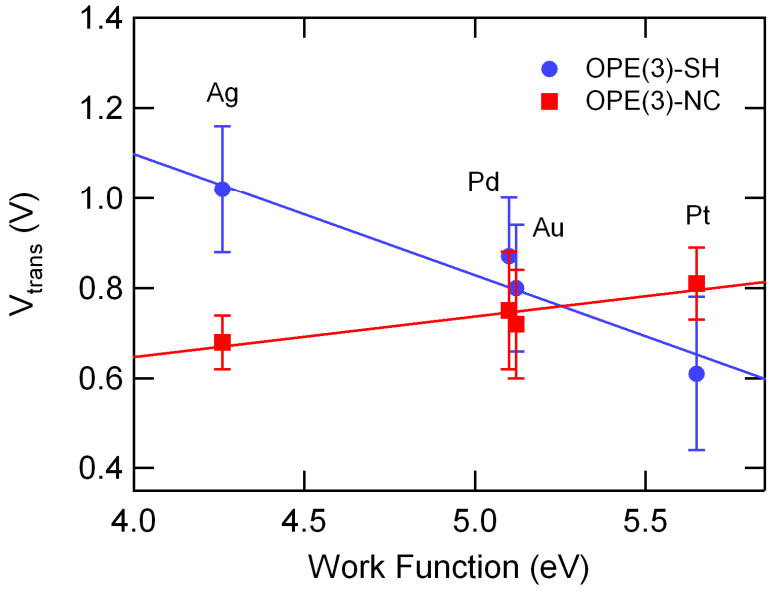

Figure 7.6. V_{trans} as a function of work function for OPE(3) thiol (circles) and isocyanide (squares) molecules on Ag, Pd, Au, and Pt electrodes. V_{trans} decreases (increases) as the work function increases for thiol (isocyanide)-coupled molecules, suggesting that hole (electron) transport is dominant. Values of the work function for the metal electrodes used are from reference 34.

for aromatic thiols has been previously suggested by a number of experimental and theoretical studies,[32] and recently confirmed by thermoelectric measurements.[35] What is more interesting is the dependence of V_{trans} for isocyanide-coupled OPE(3) across the metal series. The fact that V_{trans} for OPE(3)-NC monolayer junctions increases as the electrode work function increases clearly suggests that LUMO-mediated tunneling is the dominant channel in these systems. The reason for the difference in the absolute value of the slopes of the thiol and isocyanide data is not immediately apparent, but likely occurs due to the manner in which each functional group influences the energy level alignment when adsorbed to a metal. In general, the alignment caused by a molecular adsorbate on a metal surface will lie somewhere between the Schottky-Mott limit (vacuum level alignment) and Fermi-level pinning, depending on the contact chemistry between metal and molecule.[36] At the Schottky-Mott limit the offset between the molecular orbitals and

the Fermi level will shift rigidly with the metal work function, while Fermi-level pinning would produce a constant offset regardless of metal work function. Since for both the thiol and isocyanide linkages the change in V_{trans} is smaller than the change in work function it is clear that some extent of charge transfer occurs forming a dipole at the interface and thus causing a deviation from the Schottky-Mott limit. The fact that the magnitude of the slopes is different– V_{trans} of the thiol junctions is more strongly coupled to the metal work function than the isocyanide junctions–suggests that there is a difference in how this interface dipole changes with metal type for the two linkages.[37,38]

The idea that different charge carriers (holes for thiols and electrons for isocyanides) are dominant is also supported by photoemission measurements of the orbital alignment in aromatic thiol and isocyanide systems.[32,37] On the basis of these measurements, one should choose either the Pt-S or Ag-CN to minimize the barrier to charge transport for holes or electrons, respectively, in a molecular device. This is in some conflict with theoretical calculations that suggest that the Pd-S and Pd-CN should be the best linkage pairs.[39] The fact that an experimentally simple test method can provide us with information on the charge carrier in molecular electronic junctions and determine which contact chemistry provides the lowest barrier to charge transport highlights the utility and power of transition voltage spectroscopy.

7.5 Summary

We have demonstrated that the measurement of V_{trans} for a molecular junction–a technique we term transition voltage spectroscopy–can be used as a direct probe of charge transport in molecular systems, even in the absence of more traditional spectroscopic measurements. Further, because the magnitude of V_{trans} does not depend on junction area, information about the charge transport properties, namely, the effective barrier height, of a molecule can be garnered without specific knowledge of the number of molecules in the junction. The most direct application of transition voltage spectroscopy is to measure the effective barrier to charge transport across a molecular

junction. We have shown that the effective barrier height is constant across the alkane series and decreases with the extent of electron delocalization across π-conjugated molecules. We have also demonstrated how transition voltage spectroscopy can be used to investigate metal–molecule contacts, and in the specific case of OPE(3)-SH *versus* OPE(3)-NC, provide information on the dominant charge carrier. In future work, our goal is to develop a more complete theoretical framework for transition voltage spectroscopy so that this formalism can find wider use in understanding charge transport in molecular electronic systems.

7.6 Acknowledgment

We thank the financial support of DARPA and NSF (CHE-0616427).

7.7 References

(1) Donhauser, Z. J.; Mantooth, B. A.; Kelly, K. F.; Bumm, L. A.; Monnell, J. D.; Stapleton, J. J., Jr.; Rawlett, A. M.; Allara, D. L.; Tour, J. M. *Science* **2001**, *292*, 2303.

(2) Reed, M. A.; Chen, J.; Rawlett, A. M.; Price, D. W.; Tour, J. M. *Appl. Phys. Lett.* **2001**, *78*, 3735.

(3) Szuchmacher Blum, A.; Kushmerick, J. G.; Long, D. P.; Patterson, C. H.; Yang, J. C.; Henderson, J. C.; Yao, Y.; Tour, J. M.; Shashidhar, R.; Ratna, B. R. *Nat. Mater.* **2005**, *4*, 167.

(4) Lortscher, E.; Ciszek, J. W.; Tour, J.; Riel, H. *Small* **2006**, *2*, 973.

(5) Kubatkin, S.; Danilov, A.; Hjort, M.; Cornil, J.; Bredas, J. L.; Stuhr-Hansen, N.; Hedegard, P.; Bjornholm, T. *Nature* **2003**, *425*, 698.

(6) Park, J.; Pasupathy, A. N.; Goldsmith, J. I.; Chang, C.; Yaish, Y.; Petta, J. R.; Rinkoski, M.; Sethna, J. P.; Abruna, H. D.; McEuen, P. L. *Nature* **2002**, *417*, 722–725.

(7) Yu, L. H.; Zangmeister, C. D.; Kushmerick, J. G. *Nano Letters* **2006**, *6*, 2515.

(8) Beebe, J. M.; Kim, B.-S.; Gadzuk, J. W.; Frisbie, C. D.; Kushmerick, J. G. *Phys. Rev. Lett.* **2006**, *97*, 026801.

(9) Salomon, A.; Cahen, D.; Lindsay, S. M.; Tomfohr, J.; Engelkes, V. B.; Frisbie, C. D.

Adv. Mater. **2003**, *15*, 1881.

(10) Muntwiler, M.; Lindstrom, C. D.; Zhu, X. Y. *J. Chem. Phys.* **2006**, *124*, 081104.

(11) Zangmeister, C. D.; Robey, S. W.; van Zee, R. D.; Yao, Y. X.; Tour, J. M. *J. Am. Chem. Soc.* **2004**, *126*, 3420.

(12) Wang, W.; Lee, T.; Reed, M. A. *Phys. Rev. B* **2003**, *68*, 035416.

(13) Engelkes, V. B.; Beebe, J. M.; Frisbie, C. D. *J. Am. Chem. Soc.* **2004**, *126*, 14287.

(14) Beebe, J. M.; Engelkes, V. B.; Miller, L. L.; Frisbie, C. D. *J. Am. Chem. Soc.* **2002**, *124*, 11268.

(15) Mujica, V.; Roitberg, A. E.; Ratner, M. A. *J. Chem. Phys.* **2000**, *112*, 6834.

(16) Liang, G. C.; Ghosh, A. W.; Paulsson, M.; Datta, S. *Phys. Rev. B* **2004**, *69*, 115302.

(17) Andres, R. P.; Bein, T.; Dorogi, M.; Feng, S.; Henderson, J. I.; Kubiak, C. P.; Mahoney, W.; Osifchin, R. G.; Reifenberger, R. *Science* **1996**, *272*, 1323.

(18) Datta, S.; Tian, W.; Hong, S.; Reifenberger, R.; Henderson, J.; Kubiak, C. P. *Phys. Rev. Lett.* **1997**, *79*, 2530.

(19) Cui, X. D.; Zarate, X.; Tomfohr, J.; Sankey, O. F.; Primak, A.; Moore, A. L.; Moore, T. A.; Gust, D.; Harris, G.; Lindsay, S. M. *Nanotechnology* **2002**, *13*, 5.

(20) Wold, D. J.; Frisbie, C. D. *J. Am. Chem. Soc.* **2000**, *122*, 2970.

(21) Kushmerick, J. G.; Holt, D. B.; Pollack, S. K.; Ratner, M. A.; Yang, J. C.; Schull, T. L.; Naciri, J.; Moore, M. H.; Shashidhar, R. *J. Am. Chem. Soc.* **2002**, *124*, 10654.

(22) Kushmerick, J. G.; Holt, D. B.; Yang, J. C.; Naciri, J.; Moore, M. H.; Shashidhar, R. *Phys. Rev. Lett.* **2002**, *89*, 086802.

(23) Walker, A. V.; Tighe, T. B.; Stapleton, J. J.; Haynie, B. C.; Upilli, S.; Allara, D. L.; Winograd, N. *Appl. Phys. Lett.* **2004**, *84*, 4008.

(24) Yu, L. H.; Zangmeister, C. D.; Kushmerick, J. G. *Phys. Rev. Lett.* **2007**, *98*, 206803.

(25) Alloway, D. M.; Hofmann, M.; Smith, D. L.; Gruhn, N. E.; Graham, A. L.; Colorado, R, Jr.; Wysocki, V. H.; Lee, R.; Lee, P. A.; Armstrong, N. *J. Phys. Chem. B* **2003**, *107*, 11690.

(26) Duwez, A. S.; Pfister-Guillouzo, G.; Delhalle, J.; Riga, J. *J. Phys. Chem. B* **2000**, *104*, 9029.

(27) O'Neill, L.; Byrne, H. J. *J. Phys. Chem. B* **2005**, *109*, 12685.

(28) Szuchmacher Blum, A.; Kushmerick, J. G.; Pollack, S. K.; Yang, J. C.; Moore, M. H.; Naciri, J.; Shashidhar, R.; Ratna, B. *J. Phys. Chem. B* **2004**, *108*, 18124.

(29) Szuchmacher Blum, A.; Yang, J. C.; Shashidhar, R.; Ratna, B. *Appl. Phys. Lett.* **2003**, *82*, 3322.

(30) Holmlin, R. E.; Ismagilov, R. F.; Haag, R.; Mujica, V.; Ratner, M. A.; Rampi, M. A.; Whitesides, G. M. *Angew. Chem., Int. Ed.* **2001**, *40*, 2316.

(31) Kushmerick, J. G.; Whitaker, C. M.; Pollack, S. K.; Schull, T. L.; Shashidhar, R. *Nanotechnology* **2004**, *15*, S489.

(32) Kim, B.-S.; Beebe, J. M.; Jun, Y.; Zhu, X.-Y.; Frisbie, C. D. *J. Am. Chem. Soc.* **2006**, *128*, 4970.

(33) Xue, Y.; Datta, S.; Ratner, M. A. *J. Chem. Phys.* **2001**, *115*, 4292.

(34) Michaelson, H. B. *J. Appl. Phys.* **1977**, *48*, 4729.

(35) Reddy, P.; Jang, S.-Y.; Segalman, R. A.; Majumdar, A. *Science* **2007**, *315*, 1568.

(36) Salaneck, W. R.; Seki, K.; Kahn, A.; Pireaux, J.-J. *Conjugated Polymer and Molecular Interfaces: Science and Technology for Photonic and Optoelectronic Applications*; Marcel Dekker: New York, **2001**.

(37) Zangmeister, C. D.; Robey, S. W.; van Zee, R. D.; Kushmerick, J. G.; Naciri, J.; Yao, Y.; Tour, J. M.; Varughese, B.; Xu, B.; Reutt-Robey, J. E. *J. Phys. Chem. B* **2006**, *110*, 17138.

(38) Zangmeister, C. D.; Picraux, L. B.; van Zee, R. D.; Yao, Y.; Tour, J. M. *Chem. Phys. Lett.* **2007**, *442*, 390.

(39) Seminario, J. M.; De La Cruz, C. E.; Derosa, P. A. *J. Am. Chem. Soc.* **2001**, *123*, 5616.

(40) Stapleton, J. J.; Daniel, T. A.; Upilli, S.; Cabarcos, O. M.; Naciri, J.; Shashidhar, R.;

Allara, D. L. *Langmuir* **2005**, *21*, 11601.

(41) Stapleton, J. J.; Harder, P.; Daniel, T. A.; Reinard, M. D.; Yao, Y.; Price, D. W.; Tour, J. M.; Allara, D. L. *Langmuir* **2003**, *19*, 8245.

(42) Frisch, M. J.; Trucks, G. W.; Schlegel, H. B.; Scuseria, G. E.; Robb, M. A.; heeseman, J. R.; Montgomery, J., J. A.; Vreven, T.; Kudin, K. N.; Burant, J. C. *et al. Gaussian 03, Revision C.02*, Gaussian, Inc.: Wallingford CT, **2004**.

8 Temperature and Length Dependence of Charge Transport in Redox-Active Molecular Wires Incorporating Ruthenium (II) Bis(σ-arylacetylide) Complexes

8.1 Abstract

We report the electrical transport behavior of a series of redox-active conjugated molecular wires as a function of temperature and molecular length. The wires consist of covalently coupled ruthenium (II) bis (*σ*-arylacetylide) complexes (**Ru1** – **Ru3**) and range in length from 2.4 - 4.9 nm. The molecules are unique in that they contain multiple metal-redox centers that are well-coupled by conjugated ligands. The molecules were self-assembled and their films were extensively characterized using ellipsometry, x-ray photoelectron spectroscopy, reflection-absorption infrared spectroscopy, and cyclic voltammetry. We probed their electrical properties using conducting probe atomic force microscopy and crossed-wire junctions. At room temperature, we found a very weak dependence of the wire resistance with molecular length, consistent with a high degree of electronic communication along the molecular backbone. In low temperature (5 K) experiments, Coulomb blockade-like behavior was observed in junctions incorporating **Ru3**; direct tunneling appears to be the dominant transport mechanism in **Ru1** and **Ru2** junctions.

8.2 Introduction

Ongoing investigations of electrical transport in molecules are motivated by the discovery of intriguing transport phenomena including Coulomb blockades,[1-4] Kondo resonances,[4-7] current rectification,[8,9] switching,[10,11] and negative differential resistance.[12-14] In the field of molecular electronics, there is also significant interest in understanding transport in "molecular wires", *i.e.*, highly conjugated molecules that can

† Reproduced with permission from Kim, B.-S.; Beebe, J. M.; Olivier, C.; Rigaut, S.; Touchard, D.; Kushmerick, J. G.; Zhu, X.-Y.; Frisbie, C. D. *J. Phys. Chem. C* **2007**, *111*, 7521-7526. Copyright 2007 American Chemical Society

conduct large currents between metal contacts (*e.g.*, polyenes,[15] polyacenes,[16] and poly(phenylenevinylene)s).[17,18] Implicit in the concept of a molecular wire is the idea that charge can be transported efficiently along the molecule over relatively long distances. The precise dependence of the wire resistance on molecular length, however, depends on the electronic structure of the molecule and on the charge transport mechanism (*e.g.*, tunneling versus hopping). To date, few studies have specifically addressed the length dependence of resistance (or conductance) in molecular wires connecting metal electrodes.[15-17,19-21]

Here we report the transport behavior of a series of redox-active, conjugated molecular wires as a function of temperature and molecular length. The wire molecules consist of covalently coupled ruthenium (II) bis(σ-arylacetylide) complexes and range in length from 2.4 - 4.9 nm; their structures are shown in Figure 8.1(a). We note that **Ru3** is the longest molecular wire probed in molecular junction studies to date. Wires incorporating metal complexes are particularly interesting for molecular electronics studies because they offer multiple redox and spin states that can lead to unusual current-voltage (*I*-*V*) characteristics as well as efficient charge conduction.

Prior to junction formation, the SAMs on Au substrates were extensively characterized using ellipsometry, x-ray photoelectron spectroscopy (XPS), reflection-absorption infrared spectroscopy (RAIRS), and cyclic voltammetry. The results of the structural characterization studies indicated a loosely packed monolayer with a surface coverage of 1-2 $\times$ 10^{13} molecules/cm^2 for all three complexes. To examine the conductance of the organometallic wires endcapped with isocyanide (-N≡C) surface linking groups, we have employed two different molecular junction test beds, conducting probe atomic force microscopy (CP-AFM)[16] and crossed-wire (X-wire) junctions,[11,22] (Figure 8.1(b),(c)). At room temperature, we found a very weak dependence of the wire resistance with molecular length, consistent with a high degree of electronic communication along the molecular backbone. Low temperature (5 K) experiments indicated a difference in transport mechanism for the longest wire **Ru3** versus **Ru1** and

Ru2. Specifically, Coulomb blockade-like behavior was observed in junctions incorporating **Ru3** whereas direct tunneling is the likely transport mechanism through **Ru1** and **Ru2**. Overall, these studies demonstrate the important connection between charge transport mechanism and transport length in molecular wires. This work also opens the opportunities to probe transport through linked metal centers as a function of redox states.

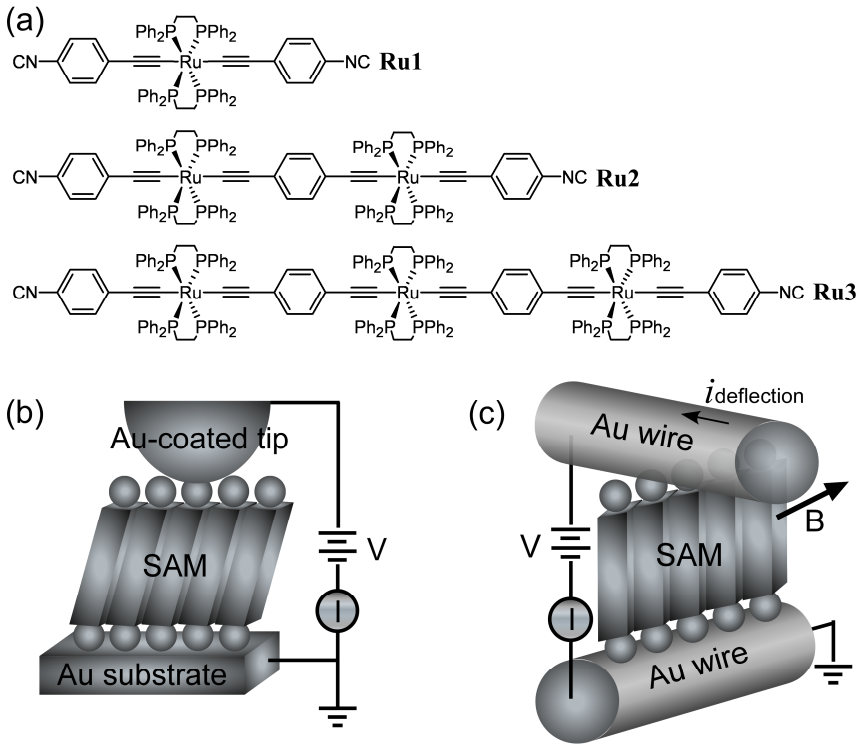

Figure 8.1. Molecular structures (a) and schematic representations of the CP-AFM (b) and the X-wire (c) junction test structures. In both test structures, the top Au electrode was brought into contact with a SAM of ruthenium complexes formed on the bottom Au electrode. *I-V* traces were obtained over ±1.0 V.

8.3 Experimental

Sample Preparation The synthetic route for these complexes will be reported elsewhere. To incorporate these molecules into electronic junctions, we self-assembled them on Au surfaces using Au-isocyanide chemistry.[16,23,24] The general procedure of self-

assembled monolayer (SAM) preparation involves immersing Au substrates into 5×10^{-2} mg/mL solutions in toluene for 3-6 h. After this growth period, SAM-coated Au substrates were rinsed thoroughly with dichloromethane, toluene, and acetonitrile, and then dried under a gentle stream of nitrogen.

SAM characterization. SAMs were characterized using ellipsometry, XPS, RAIRS, and cyclic voltammetry. To determine monolayer thicknesses by ellipsometry, measurements of the polarization angles Ψ and Δ were taken as a function of wavelength (λ) between 400 and 700 nm at an incident angle of 75°. The indices of refraction (n) and extinction coefficient (k) of Au substrates were determined by measurement of the polarization angles prior to monolayer deposition. The instrument software converted these values to n and k by assuming that the substrate is of infinite thickness. After SAM deposition, the polarization angles were again measured and film thicknesses determined by the instrument software. n and k values of the SAM were assumed to be 1.5 and 0.0, respectively.

XPS spectra were acquired using the Mg K_α x-ray (1253.6 eV) from an anode source incorporating a hemispherical analyzer in an ultrahigh vacuum system. The x-ray anode was operated at 200 W and the analyzer pass energy was 17.9 eV for high-resolution scans. The binding energy scales of all spectra were referenced to the Au $4f_{7/2}$ peak (84.0 eV). The SAM thickness was calculated using the relative areas of the Au 4f and the C 1s peaks and using hexadecanethiol SAM on Au as a reference (d = 1.86 nm). Assuming the same attenuation length of the gold (λ_{Au} = 3.46 nm) and carbon (λ_C = 3.02 nm) photoelectrons for the SAMs, the calculation based on equation (8.1) yielded the thickness.

$$\frac{\frac{I_c}{I_{Au}}(sample)}{\frac{I_c}{I_{Au}}(reference)} = \frac{\left\{1-\exp(-\frac{d_{sample}}{\lambda_c})\right\}\exp(-\frac{d_{reference}}{\lambda_{Au}})}{\exp(-\frac{d_{sample}}{\lambda_{Au}})\left\{1-\exp(-\frac{d_{reference}}{\lambda_c})\right\}} \qquad (8.1)$$

where I_C = the area of C 1s peaks, I_{Au} = the area of Au 4f peaks, and d is the thickness.

The isocyanide (N≡C) stretching modes in SAMs of the ruthenium complexes were monitored by reflection-absorption infrared spectroscopy. In these experiments, the infrared beam was incident at an 84° angle with respect to the surface normal. A total of 1000 scans were collected at 1.0 cm^{-1} resolution.

Cyclic voltammetry (CV) experiments were undertaken to determine the redox states of the ruthenium complexes and to measure surface coverage. In these experiments, a three-neck electrochemical cell was utilized. A clean o-ring (1.2 cm diameter) in a cylindrical cavity surrounding a hole in the bottom of the cell was placed between the cell and a SAM-coated Au substrate, which comprised the working electrode. The cell was filled with 0.2 M tetrabutylammonium hexafluorophosphate (Bu_4NPF_6) in CH_2Cl_2. A Pt gauze was used as the counter electrode and the cell was referenced to Ag/AgCl. Prior to examining the monolayer oxidation potentials, the system was calibrated to the ferrocene oxidation potential. For each molecule, the scan rate was 50 mV/s and the CV curves were reproducible and stable to electrochemical cycling within the range of 0.0 – 0.9 V. In addition, surface coverage (Γ) was determined according to the following equation (8.2):

$$\Gamma = \frac{Q}{nFA} \tag{8.2}$$

where Q is the charge injected into the SAM, n is the number of electrons involved in the electron transfer process, F is the faraday constant, and A is the surface area of the monolayer examined, i.e. the inside area of o-ring. Q was obtained by integration of the area under forward cyclic voltammogram using the first oxidation wave for each of the molecules.

***I-V* measurements.** To probe the electrical properties of the ruthenium complexes, we employed two test beds: CP-AFM and X-wire junctions, Figure 8.1. In CP-AFM junctions, Au-coated AFM tips and template-stripped flat Au substrates were prepared as previously described.[25] The molecular junction was formed by bringing an Au-coated AFM tip into contact with the SAM at an applied load of 2 nN, as illustrated in Figure 8.1(b). A tip radius of ~50 nm was used in all experiments, and the number of

molecules in each junction was estimated to be a few tens of molecules. *I-V* characteristics were recorded by sweeping the tip voltage (±1.0 V) with the SAM-coated Au substrate held at ground. It should be emphasized that the CP-AFM test platform is particularly well-suited to measure the dependence of current on molecular length because the junction area and applied load can be held constant across the measurement series. To further examine the current-voltage properties, we formed X-wire junctions (Figure 8.1(c)), the details of which have been discussed previously.[11,22] In the present study, current was measured for each molecule both at room temperature and in a liquid helium environment, while conductance was simultaneously recorded using lock-in techniques. *I-V* characteristics obtained from the X-wire geometry at room temperature are compared with them as found in CP-AFM experiments. This duplicate junction formation was conducted in order to prove both reproducibility and acquisition of intrinsic molecular properties, not complicated with junction fabrication methods.

8.4 Results and Discussion

Monolayer Characterization. The SAMs on Au substrates were extensively characterized in order to investigate monolayer formation, surface coverage, and redox properties. First, ellipsometry and XPS were used to measure film thickness. Both methods revealed that the thicknesses of each SAM increase linearly with the number of Ru centers in the molecular chain, and that the thicknesses are slightly shorter than the estimated molecular lengths (Table 8.1), indicating that the molecules are tilted. In addition, high-resolution XPS spectra are displayed in Figure 8.2. We find good correlation between the intensity of each element and the molecular stoichiometry. With increase of molecular length, the total numbers of Ru, C, and P atoms increase and the number of N atoms is approximately constant. The intensity of the Au substrate is attenuated, as expected.

Table 8.1. Thickness values for SAMs of ruthenium complexes on Au determined by ellipsometry and XPS (unit: nm)

SAM	Estimated thickness[a]	Measured thickness	
		Ellipsometry	XPS
Ru1	2.2	2.1 (±0.3)	1.9 (±0.2)
Ru2	3.4	3.3 (±0.4)	3.2 (±0.3)
Ru3	4.7	4.4 (±0.2)	4.1 (±0.4)

[a] The terminal C (unbound isocyanide) to Au, unbound molecular length plus Au-isocyanide bond length (0.19 nm). Molecular length with *trans* conformations for all C≡C bonds was estimated through the molecular mechanics energy minimization using the Cambridge Scientific Chem3D software.

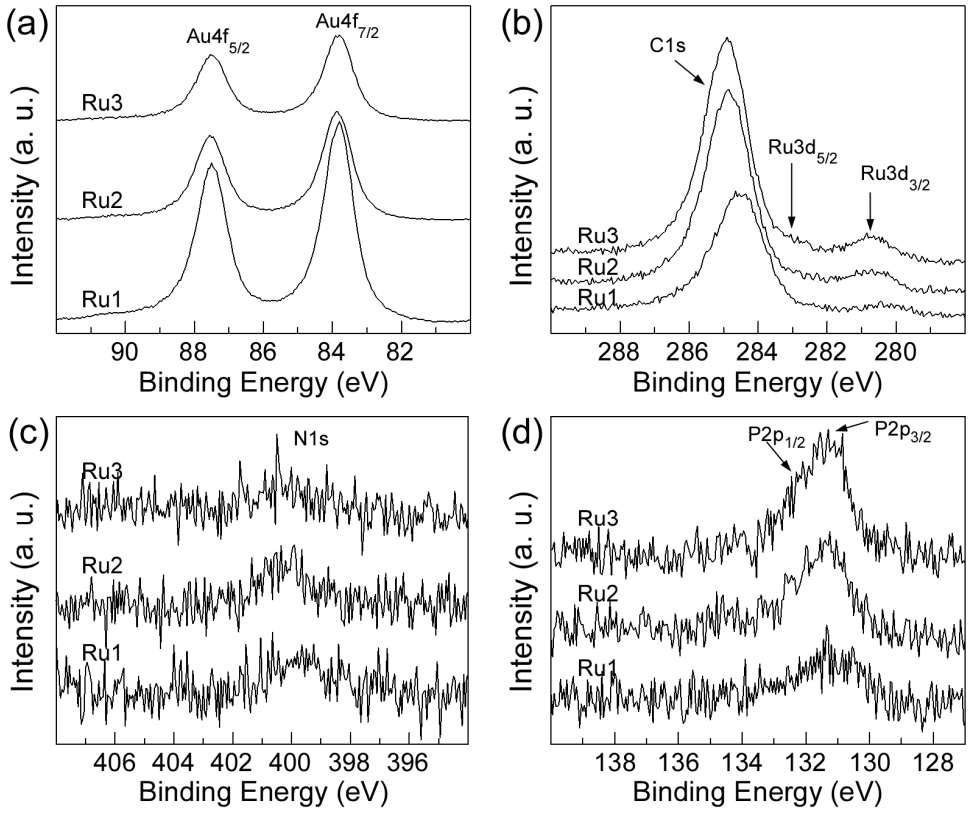

Figure 8.2. High-resolution XPS spectra of Au 4f (a), C 1s and Ru 3d (b), N 1s (c), and P 2p (d) regions for SAMs of **Ru1**, **Ru2**, and **Ru3**.

RAIRS spectra are shown in Figure 8.3. The peak intensities are normalized to the C≡C stretching peak intensity. The isocyanide peak positions are compiled in Table 8.2. The wavenumber of bound isocyanide is ~50 cm^{-1} higher than that of the unbound species, and the relative intensity of the N≡C stretching peak to the C≡C stretching peak decreases with molecular length, as expected. In addition, RAIRS spectra reveal two important facts. First, the intensities of bound and unbound isocyanide are approximately the same. This is a critical indication of the lack of physisorbed multilayers on the SAMs. Second, the C≡C vibrational stretching appears at low frequency (2052 cm^{-1}). When compared to cases where back bonding is weak or absent (2100 − 2200 cm^{-1}),[21,26] this observation indicates a strong back bonding between ruthenium and the carbon-rich ligands.

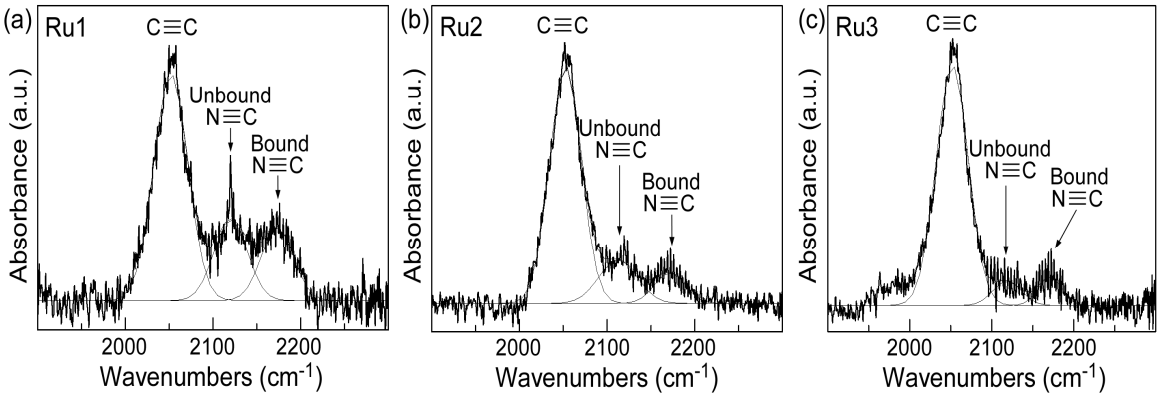

Figure 8.3. RAIRS spectra of SAMs of ruthenium complexes in the region of 1900-2300 cm^{-1}: **Ru1** (a), **Ru2** (b), and **Ru3** (c). The intensities are normalized to the C≡C stretching peak intensity.

Table 8.2. Vibrational frequencies of isocyanide (N≡C) and acetylene (C≡C) bond. (unit: cm^{-1})

Compound	N≡C		C≡C
	Unbound	Bound	
Ru1	2120	2173	2052
Ru2	2112	2172	2052
Ru3	2119	2171	2052

Cyclic voltammograms of **Ru1**-**Ru3** are displayed in Figure 8.4. The potentials of oxidation states within the range of 0.0 to 0.9 V vs. Ag/AgCl are compiled in Table 8.3. All oxidation peaks were reversible within the range, and no reduction was detected within the solvent voltage window for all the complexes. The number of oxidation states corresponds to the number of ruthenium metal centers, and the first oxidation peak shifts to lower oxidation potential as the number of ruthenium centers increases. Along with RAIRS data, this observation suggests a strong electronic communication between the ruthenium centers, and is consistent with previous results indicating that electrons are delocalized across the entire length of the molecule.[27-31]

From the cyclic voltammetry data, the surface coverage was estimated to be 1-2 × 10^{13} molecules/cm^2 for each of the ruthenium complexes. The comparable surface coverage across the molecular series, **Ru1**-**Ru3**, indicates that the number of molecules contacted by the electrodes in junction experiments is essentially invariant, and thus differences in the magnitude of measured current cannot be explained by surface coverage arguments in the analysis of data obtained from CP-AFM. Moreover, assuming a close-packed monoclinic lattice (1.4 nm × 1.6 nm × molecular length), the maximum theoretical coverage was estimated to be 4 × 10^{13} molecules/cm^2. The discrepancy between the experimentally determined surface coverage and the estimated maximum coverage can likely be explained through a tilt of the molecular backbone with respect to the surface normal as well as by the presence of bulky ligands. The idea that the molecular backbones are tilted is supported by structural characterization data of other

isocyanide monolayers on Au reported in the literature,[16,24] all of which possess some degree of tilt. This is further consistent with the analysis of XPS and ellipsometry data for these molecules, mentioned above, which indicated that the molecules must be slightly tilted to account for the measured SAM thicknesses.

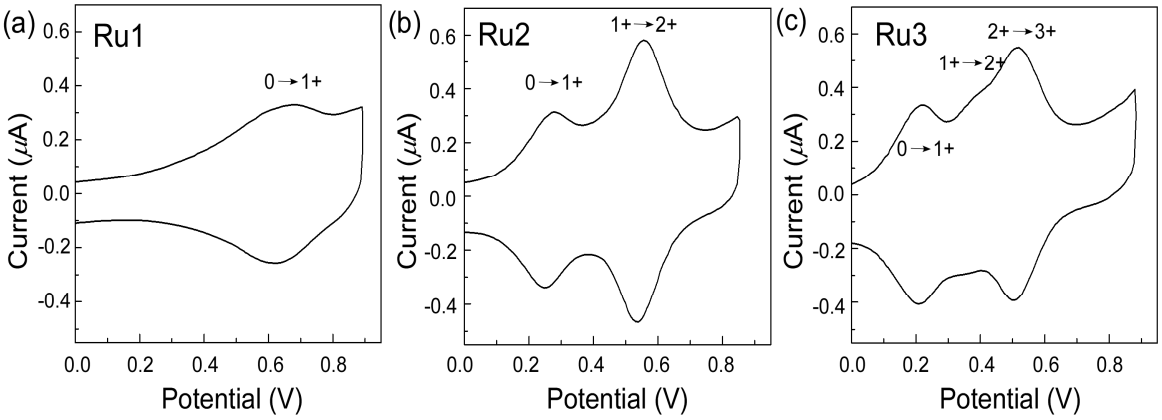

Figure 8.4. Cyclic voltammograms of a SAM of **Ru1** (a), **Ru2** (b), and **Ru3** (c) in CH_2Cl_2 (0.2 M Bu_4NPF_6). The reference and counter electrode were Ag/AgCl and a Pt gauze, respectively. The scan rate was 50 mV/s.

Table 8.3. Oxidation potentials of ruthenium complexes vs. Ag/AgCl

	E^o_1 [V]	E^o_2 [V]	E^o_3 [V]
Ru1	0.64	-	-
Ru2	0.26	0.54	-
Ru3	0.22	0.38	0.51

Room temperature *I-V* characteristics. When measured in both the CP-AFM and the X-wire geometry at room temperature, each of the molecules exhibited a sigmoidal dependence of current on applied bias. Figure 8.5 displays average *I-V* curves (10 traces) obtained from CP-AFM and X-wire junctions. The current scale was normalized to the maximum current at 1.0 V for direct comparison of *I-V* curve shapes. These two test platforms exhibited very similar *I-V* curves.

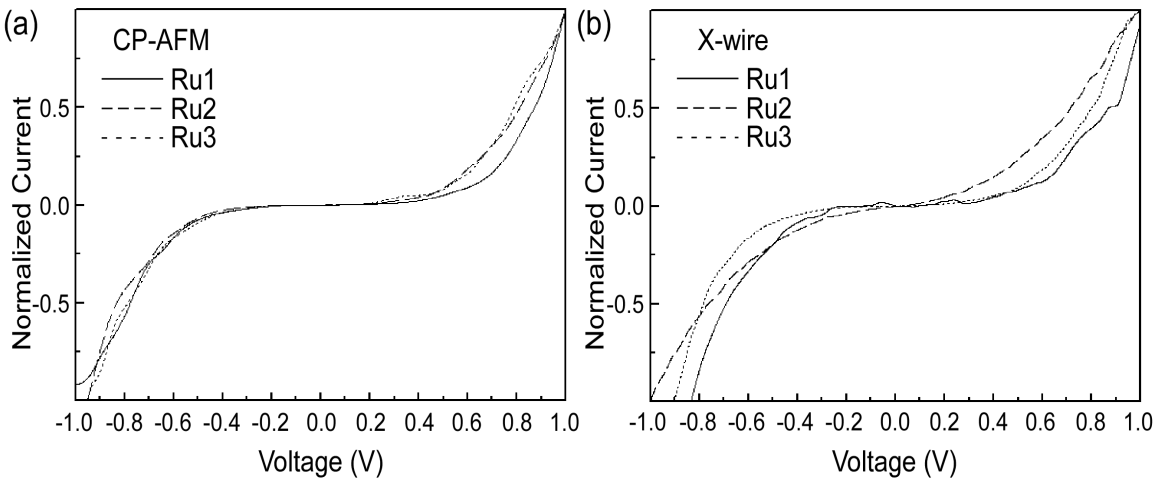

Figure 8.5. *I-V* characteristics of **Ru1**, **Ru2**, and **Ru3** SAMs obtained in CP-AFM (a) and X-wire junctions (b) at room temperature. Current has been normalized to the maximum current at 1.0 V for direct comparison of *I-V* curve shapes**.**

Molecular length dependence was investigated in the CP-AFM junctions. Figure 8.6 shows a semilog plot of resistance versus molecular length for junctions of the ruthenium complexes. Data are shown for 5 trials (5 different tips). Each resistance value represents the average of ten *I-V* traces within ±0.1 V. In each trial, a single Au-coated AFM tip was used on each of the three ruthenium complexes to maintain a constant contact area. The through bond molecular lengths are 2.4 nm, 3.6 nm, and 4.9 nm for **Ru1**, **Ru2**, and **Ru3**, respectively. These values were estimated by the addition of the Au-isocyanide bond length (2 × 0.19 nm) to the unbound molecular length determined through a molecular mechanics energy minimization.[16] The key result of the room temperature CP-AFM studies is that resistance is nearly independent of molecular length. From a conventional semilog plot of resistance versus molecular length, the overall slope of **Ru1** through **Ru3** is 0.9 nm^{-1}, a remarkably low value (In general, conjugated organic molecular wires yield 2-7 nm^{-1}).[15-18] This exceptionally low length dependence suggests that the Au Fermi level (E_{Fermi}) lies close to the energy levels of the frontier orbitals in **Ru1**, **Ru2**, and **Ru3**. Small energy offsets between E_{Fermi} and the frontier orbital levels will enhance the efficiency of tunneling but also can facilitate direct charge injection into

the molecular wires. In fact, charge injection into **Ru3** is supported by low temperature measurements (see below). The very weak length dependence is also in accordance with cyclic voltammetry and RAIRS data, which indicated a high degree of electronic communication between ruthenium centers across the aryldiethynyl bridging ligand. We note that the resistance of **Ru3** (~10^{11} Ω/molecule!) is actually low when it is compared to that of aliphatic or aromatic molecules of comparable length that have been examined thus far. The exception is carotenoid polyenes which give ~10^{10} Ω/molecule for molecules 4.3 nm in length.[15-18]

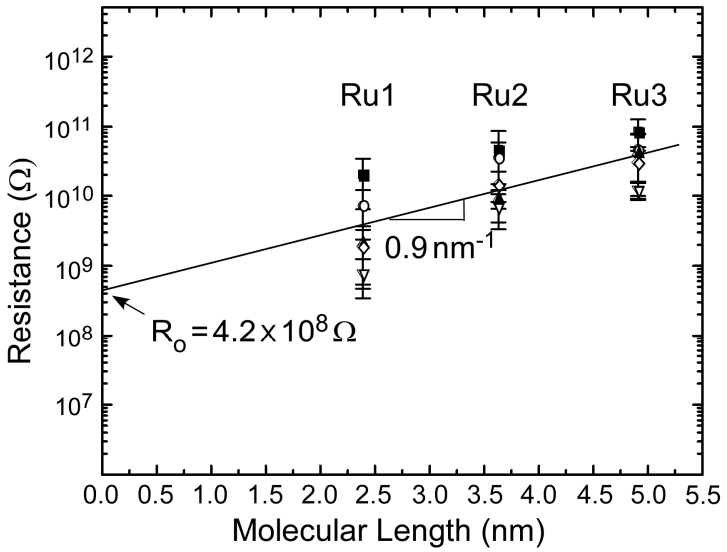

Figure 8.6. Semilog plot of resistance versus molecular length for Au/SAM/Au CP-AFM junctions. Data are shown for 5 trials with 5 different tips. Different symbols represent different tips. Each data point is the average of ten *I-V* traces within ±0.1 V. In each trial, a single Au-coated AFM tip was used to measure the current-voltage response of each of the three ruthenium complexes. The error bars represent one standard deviation from the mean.

Furthermore, the overall resistance of **Ru3** likely has a large contact resistance contribution. From Figure 8.6, we extract a contact resistance for the junction of R_0 = 4.2 × 10^8 Ω or 10^8~10^9 Ω/molecule. This large value indicates that contact effects are significant. The high contact resistance is especially interesting given that, in general, a

low contact resistance is expected from the small energy offsets.[16] For clear resolution on the origin of high contact resistance, more detailed experimental and computational studies will be required. Nevertheless, we note that the high contact resistance value should be an important factor in facilitating charge localization on the molecule **Ru3** at low temperature (see below).

Low temperature *I-V* characteristics. When measured in liquid helium with the X-wire geometry, average current-voltage traces of **Ru1** and **Ru2** are nearly indistinguishable from those measured at room temperature, as shown in the insets in Figure 8.7(a). However, Coulomb blockade-like behavior is observed in the junction incorporating the very long **Ru3** at low temperature. Figure 8.7 shows 20 *I-V* and conductance-voltage (*dI/dV-V*) traces of the **Ru3** junction at 5 K. In Figure 8.7(a), there is an abrupt increase in current at ~0.25 V, leading to a current plateau between 0.25 and 0.35 V. Such a current step is characteristic of Coulomb blockade behavior[32] and suggests that charge has been injected into the **Ru3** SAM. The current step corresponds to a conductance peak visible in Figure 8.7(b) near 0.25 V. Two additional conductance peaks are also evident between 0.5 and 0.9 V. Importantly, the conductance peak shapes and the peak positions on the right-hand side of Figure 8.7(b) are strikingly similar to the results of cyclic voltammetry measurements on **Ru3**, as shown in Figure 8.4(c), although the peak positions are naturally not at the same potential due to the very different experimental conditions (*e.g.*, the presence of liquid electrolyte in the cyclic voltammetry experiment).[33] The observed correlation between the shape of the *dI/dV-V* spectrum and the shape of the electrochemical oxidation waves strongly suggests that the three observed peaks in the conductance spectrum correspond to discrete electronic (redox) states. This is supported by recent results demonstrating conductance switching mediated by molecular redox states.[2,12,19,34-37] Based on the conductance peaks, we describe the transport process in **Ru3** as Coulomb blockade-like, but in fact the observed behavior in Figure 8.7 differs from the classical Coulomb staircase in which the conductance peaks are evenly separated. This is because the voltage required to inject charge into the **Ru3**

SAM depends substantially on the molecular energy level spectrum in addition to the Coulomb interaction. Nevertheless, our view is that charge is injected into the SAM and that the *dI/dV-V* spectrum reveals that multiple charge states are accessible in **Ru3** molecular junctions. The asymmetry in the *I-V* and *dI/dV-V* curves likely reflects some inherent structural asymmetry in the X-wire junction related to the junction formation process (*i.e.*, molecules are adsorbed to one wire, and then the second wire is brought into contact).

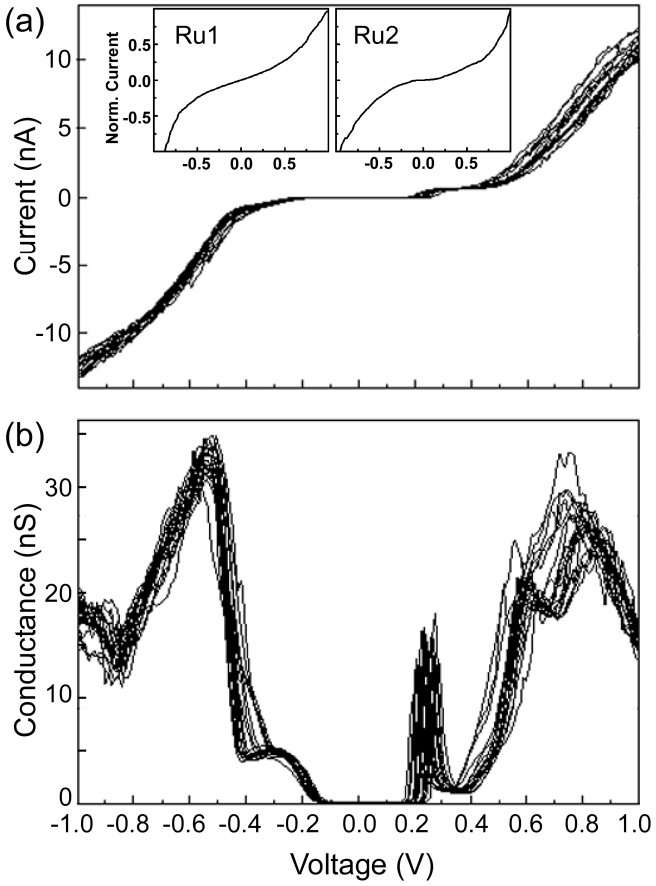

Figure 8.7. *I-V* characteristics (a) and conductance (*dI/dV-V*) traces (b) of the Au/**Ru3**/Au X-wire junction at 5 K. Each figure shows 20 traces. Typical current (normalized)-voltage behaviors of **Ru1** and **Ru2** X-wire junctions at 5 K are displayed in insets (a).

Figure 8.8 illustrates the principal charge transport mechanisms at low temperature. Structurally-related phenyldiacetylene derivatives examined by others have been shown to follow a direct tunneling mechanism for wire lengths shorter than 4.4 nm.[21,38,39] Both **Ru1** (2.4 nm) and **Ru2** (3.6 nm) fall within the length range where direct tunneling is expected to be the principal charge transport mechanism, Figure 8.8(a). However, it is likely that if the molecular length is appreciably longer than 4.4 nm as in **Ru3** (4.9 nm), direct tunneling diminishes substantially, and thus charge injection into the molecule can be observed when the Au Fermi level of one contact comes into resonance with molecular levels, Figure 8.8(b).[32] The conductance peak at 0.25 V indicates that the $E_{Fermi} - E_{HOMO}$ offset is small (≤ 0.25 eV) which also facilitates direct charge injection from the Au electrodes into **Ru3** at low voltages.

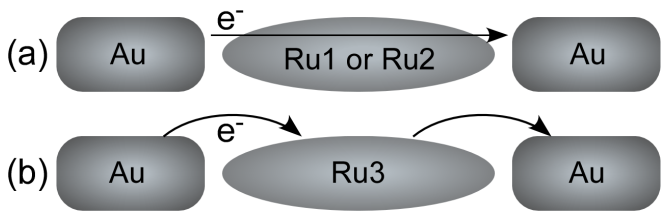

Figure 8.8. Illustration of charge transport mechanisms at 5 K: (a) direct tunneling in junctions of **Ru1** and **Ru2**, (b) sequential tunneling with Coulomb blockade in the **Ru3** junction. Arrows show the electron flow.

8.5 Conclusion

We have examined a series of organometallic wires in CP-AFM and X-wire junctions. Room temperature CP-AFM measurements revealed minimal length dependence illustrating that charge transport through the ruthenium σ-arylacetylide bridges is extremely efficient. Low temperature X-wire measurements are consistent with direct tunneling in both **Ru1** and **Ru2**, and charge injection in **Ru3**. By coupling the current-voltage results with data from standard electrochemistry experiments, we conclude that the observed peaks in the conductance spectrum of the **Ru3** junction arise

from discrete electronic states. Further experiments to build longer organometallic wires and to examine their transport properties as a function of electrochemically controlled oxidation state are underway.

8.6 Acknowledgment

We thank NSF (CHE-0616427) for financial support, and the French collaborators thank the MENESR for a Ph.D. grant to C.O., and the CNRS and the Universite de Rennes 1 for additional support.

8.7 References

(1) Chae, D. H.; Berry, J. F.; Jung, S.; Cotton, F. A.; Murillo, C. A.; Yao, Z. *Nano Lett.* **2006**, *6*, 165.

(2) Kubatkin, S.; Danilov, A.; Hjort, M.; Cornil, J.; Bredas, J. L.; Stuhr-Hansen, N.; Hedegard, P.; Bjornholm, T. *Nature* **2003**, *425*, 698.

(3) Park, H.; Park, J.; Lim, A. K. L.; Anderson, E. H.; Alivisatos, A. P.; McEuen, P. L. *Nature* **2000**, *407*, 57.

(4) Park, J.; Pasupathy, A. N.; Goldsmith, J. I.; Chang, C.; Yaish, Y.; Petta, J. R.; Rinkoski, M.; Sethna, J. P.; Abruna, H. D.; McEuen, P. L.; Ralph, D. C. *Nature* **2002**, *417*, 722.

(5) Yu, L. H.; Natelson, D. *Nano Lett.* **2004**, *4*, 79.

(6) Yu, L. H.; Keane, Z. K.; Ciszek, J. W.; Cheng, L.; Stewart, M. P.; Tour, J. M.; Natelson, D. *Phys. Rev. Lett.* **2004**, *93*, 266802.

(7) Liang, W. J.; Shores, M. P.; Bockrath, M.; Long, J. R.; Park, H. *Nature* **2002**, *417*, 725.

(8) Metzger, R. M. *Chem. Rev.* **2003**, *103*, 3803.

(9) McCreery, R.; Dieringer, J.; Solak, A. O.; Snyder, B.; Nowak, A. M.; McGovern, W. R.; DuVall, S. *J. Am. Chem. Soc.* **2003**, *125*, 10748.

(10) Cai, L.; Cabassi, M. A.; Yoon, H.; Cabarcos, O. M.; McGuiness, C. L.; Flatt, A. K.; Allara, D. L.; Tour, J. M.; Mayer, T. S. *Nano Lett.* **2005,** *5*, 2365.

(11) Blum, A. S.; Kushmerick, J. G.; Long, D. P.; Patterson, C. H.; Yang, J. C.; Henderson, J. C.; Yao, Y. X.; Tour, J. M.; Shashidhar, R.; Ratna, B. R. *Nat. Mater*. **2005**, *4*, 167.

(12) Chen, J.; Reed, M. A.; Rawlett, A. M.; Tour, J. M. *Science* **1999**, *286*, 1550.

(13) Rawlett, A. M.; Hopson, T. J.; Nagahara, L. A.; Tsui, R. K.; Ramachandran, G. K.; Lindsay, S. M. *Appl. Phys. Lett.* **2002**, *81*, 3043.

(14) Fan, F. R. F.; Yao, Y. X.; Cai, L. T.; Cheng, L.; Tour, J. M.; Bard, A. J. *J. Am. Chem. Soc.* **2004**, *126*, 4035.

(15) He, J.; Chen, F.; Li, J.; Sankey, O. F.; Terazono, Y.; Herrero, C.; Gust, D.; Moore, T. A.; Moore, A. L.; Lindsay, S. M. *J. Am. Chem. Soc.* **2005**, *127*, 1384.

(16) Kim, B.-S.; Beebe, J. M.; Jun, Y.; Zhu, X.-Y.; Frisbie, C. D. *J. Am. Chem. Soc.* **2006**, *128*, 4970.

(17) Moth-Poulsen, K.; Patrone, L.; Stuhr-Hansen, N.; Christensen, J. B.; Bourgoin, J.-P.; Bjornholm, T. *Nano Lett.* **2005**, *5*, 783.

(18) Seferos, D. S.; Blum, A. S.; Kushmerick, J. G.; Bazan, G. C. *J. Am. Chem. Soc.* **2006**, *128*, 11260.

(19) Fan, F.-R. F.; Yang, J.; Cai, L.; Price, D. W.; Dirk, S. M.; Kosynkin, D. V.; Yao, Y.; Rawlett, A. M.; Tour, J. M.; Bard, A. J. *J. Am. Chem. Soc.* **2002**, *124*, 5550.

(20) Blum, A. S.; Ren, T.; Parish, D. A.; Trammell, S. A.; Moore, M. H.; Kushmerick, J. G.; Xu, G. L.; Deschamps, J. R.; Pollack, S. K.; Shashidhar, R. *J. Am. Chem. Soc.* **2005**, *127*, 10010.

(21) Schull, T. L.; Kushmerick, J. G.; Patterson, C. H.; George, C.; Moore, M. H.; Pollack, S. K.; Shashidhar, R. *J. Am. Chem. Soc.* **2003**, *125*, 3202.

(22) Beebe, J. M.; Kim, B.-S.; Gadzuk, J. W.; Frisbie, C. D.; Kushmerick, J. G. *Phys. Rev. Lett.* **2006**, *97*, 026801.

(23) Huc, V.; Bourgoin, J. P.; Bureau, C.; Valin, F.; Zalczer, G.; Palacin, S. *J. Phys. Chem. B* **1999**, *103*, 10489.

(24) Stapleton, J. J.; Daniel, T. A.; Uppili, S.; Cabarcos, O. M.; Naciri, J.; Shashidhar, R.; Allara, D. L. *Langmuir* **2005**, *21*, 11061.

(25) Engelkes, V. B.; Beebe, J. M.; Frisbie, C. D. *J. Phys. Chem. B* **2005**, *109*, 16801.

(26) Stapleton, J. J.; Harder, P.; Daniel, T. A.; Reinard, M. D.; Yao, Y. X.; Price, D. W.; Tour, J. M.; Allara, D. L. *Langmuir* **2003**, *19*, 8245.

(27) Rigaut, S.; Costuas, K.; Touchard, D.; Saillard, J. Y.; Golhen, S.; Dixneuf, P. H. *J. Am. Chem. Soc.* **2004**, *126*, 4072.

(28) Rigaut, S.; Perruchon, J.; Guesmi, S.; Fave, C.; Touchard, D.; Dixneuf, P. H. *Eur. J. Inorg. Chem.* **2005**, 447.

(29) Rigaut, S.; Olivier, C.; Costuas, K.; Choua, S.; Fadhel, O.; Massue, J.; Turek, P.; Saillard, J. Y.; Dixneuf, P. H.; Touchard, D. *J. Am. Chem. Soc.* **2006**, *128*, 5859.

(30) Powell, C. E.; Cifuentes, M. P.; Morrall, J. P.; Stranger, R.; Humphrey, M. G.; Samoc, M.; Luther-Davies, B.; Heath, G. A. *J. Am. Chem. Soc.* **2003**, *125*, 602.

(31) McGrady, J. E.; Lovell, T.; Stranger, R.; Humphrey, M. G. *Organometallics* **1997**, *16*, 4004.

(32) Grabert, H.; Devoret, M. H. *Single Charge Tunneling: Coulomb Blockade Phenomena in Nanostructures*, **1992**, Plenum, New York.

(33) Barriere, F.; Geiger, W. E. *J. Am. Chem. Soc.* **2006**, *128*, 3980.

(34) He, J.; Fu, Q.; Lindsay, S.; Ciszek, J. W.; Tour, J. M. *J. Am. Chem. Soc.* **2006**, *128*, 14828.

(35) Tao, N. J. *Phys. Rev. Lett.* **1996**, *76*, 4066.

(36) Fan, F. R. F.; Lai, R. Y.; Cornil, J.; Karzazi, Y.; Bredas, J. L.; Cai, L. T.; Cheng, L.; Yao, Y. X.; Price, D. W.; Dirk, S. M.; Tour, J. M.; Bard, A. J. *J. Am. Chem. Soc.* **2004**, *126*, 2568.

(37) Tran, E.; Grave, C.; Whitesides, G. M.; Rampi, M. A. *Electrochimica Acta* **2005**, *50*, 4850.

(38) Creager, S.; Yu, C. J.; Bamdad, C.; O'Connor, S.; MacLean, T.; Lam, E.; Chong, Y.; Olsen, G. T.; Luo, J. Y.; Gozin, M.; Kayyem, J. F. *J. Am. Chem. Soc.* **1999**, *121*, 1059.

(39) Getty, S. A.; Engtrakul, C.; Wang, L.; Liu, R.; Ke, S. H.; Baranger, H. U.; Yang, W.; Fuhrer, M. S.; Sita, L. R. *Phys. Rev. B* **2005**, *71*, 241401.

9 Bibliography

Chapter 1. Measuring Electrical Resistance of Molecular Wires

(1) Heath, J. R.; Ratner, M. A. *Physics Today* **2003**, *56*, 43.

(2) Kubatkin, S.; Danilov, A.; Hjort, M.; Cornil, J.; Bredas, J. L.; Stuhr-Hansen, N.; Hedegard, P.; Bjornholm, T. *Nature* **2003**, *425*, 698.

(3) Park, H.; Park, J.; Lim, A. K. L.; Anderson, E. H.; Alivisatos, A. P.; McEuen, P. L. *Nature* **2000**, *407*, 57.

(4) Park, J.; Pasupathy, A. N.; Goldsmith, J. I.; Chang, C.; Yaish, Y.; Petta, J. R.; Rinkoski, M.; Sethna, J. P.; Abruna, H. D.; McEuen, P. L.; Ralph, D. C. *Nature* **2002**, *417*, 722.

(5) Metzger, R. M. *Chem. Rev.* **2003**, *103*, 3803.

(6) Blum, A. S.; Kushmerick, J. G.; Long, D. P.; Patterson, C. H.; Yang, J. C.; Henderson, J. C.; Yao, Y. X.; Tour, J. M.; Shashidhar, R.; Ratna, B. R. *Nat. Mater.* **2005**, *4*, 167.

(7) Chen, J.; Reed, M. A.; Rawlett, A. M.; Tour, J. M. *Science* **1999**, *286*, 1550.

(8) Rawlett, A. M.; Hopson, T. J.; Nagahara, L. A.; Tsui, R. K.; Ramachandran, G. K.; Lindsay, S. M. *Appl. Phys. Lett.* **2002**, *81*, 3043.

Chapter 2. Molecular Self-Assembly

(1) Nuzzo, R.G.; Allara, D. L. *J. Am. Chem. Soc.* **1983**, *105*, 4481.

(2) Ulman, A. *Chem. Rev.* **1996**, *96*, 1533.

(3) Andres, R. P.; Bielefeld, J. D.; Henderson, J. I.; Janes, D. B.; Kolagunta, V. R.; Kubiak, C. P.; Mohoney, W. J. Osifchin, R. G. *Science* **1996**, *273*, 1690.

(4) Castner, D. G.; Hinds, K.; Grainager, D. W. *Langmuir* **1996**, *12*, 5083.

(5) Nelles, G.; Schonherr, H.; Jaschke, M.; Wolf, H.; Schaub, M.; Kuther, J.; Tremel, W.; Bamberg, E.; Ringsdorf, H.; Butt, H.-J. *Langmuir* **1998**, *14*, 808.

(6) Lii, J.-H.; Allinger, N. L. *J. Am. Chem. Soc.* **1989**, *111*, 8576.

(7) Porter, M. D.; Bright, T. B.; Allara, D. L.; Chidsey, D. E. D. *J. Am. Chem. Soc.* **1987**, *109*, 3559.

(8) Blackstock, J. J.; Li, Z.; Freeman, M. R.; Stewart, D. R. Surface *Science* **2003**, *546*, 87.

(9) Wagner, P.; Hegner, M.; Guntherodt, H.-J., Semenza, G. *Langmuir* **1995**, *11*, 3867.

(10) Wasserman, S. R.; Whitesides, G. M.; Tidswell, I. M.; Ocko, B. M.; Pershan, P. S.; Axe, J. D. *J. Am. Chem. Soc.* **1989**, *111*, 5852.

(11) Bain, C.D.; Troughton, E. B.; Tao, Y.-T.; Evall, J.; Whitesides, G. M.; Nuzzo, R. G. *J. Am. Chem. Soc.* **1989**, *111*, 321.

(12) Engelkes, V. B.; Beebe, J. M.; Frisbie, C. D. *J. Am. Chem. Soc.* **2004,** *126*, 14287.

(13) Ulman, A. *An introduction to ultrathin organic films: from Langmuir-Blodgett to self-assembly*, First ed, (Academic Press, San Diego, **1991**).

(14) Tolstoy, V. P.; Chernyshova, I.V.; Skryshevsky, V. *A Handbook of infrared spectroscopy of ultrathin films* (John Wiley & Sons, Inc., New Jersey, **2003**).

(15) Arnold, R.; Terfort, A.; Woll, C. *Langmuir* **2001**, *17*, 4980.

(16) Jun, Y.; Zhu, X.-Y. *J. Am. Chem. Soc.* **2004**, *126*, 13224.

(17) Sikes, H. D.; Smalley, J. F.; Dudek, S. P.; Cook, A. R.; Newton, M. D.; Chidsey, C. E. D.; Feldberg, S. W. *Science* **2001**, *291*, 1519.

(18) Nuzzo, R. G.; Fusco, F. A.; Allara, D. L. *J. Am. Chem. Soc.* **1987**, *109*, 2358.

(19) Bain, C. D.; Evall, J.; Whitesides, G. M. *J. Am. Chem. Soc.* **1989**, *111*, 7155.

(20) Liu, D.; Szulczewski, G. J.; Kispert, L. D.; Primak, A.; Moore, T. A.; Moore, A. L.; Gust, D. *J. Phys. Chem. B.* **2002**; *106*, 2933.

(21) Fuxen, C.; Azzam, W.; Arnold, R.; Witte, G.; Terfort, A.; Woll, C. *Langmuir* **2001**, *17*, 3689-3695.

(22) Strong, L.; Whitesides, G. M. *Langmuir* **1988**, *4*, 546.

(23) Chidsey, C. E. D.; Liu, G.-Y.; Rowntree, Y. P.; Scoles, G. *J. Chem. Phys.* **1989**, *91*, 4421.

(24) Alves, C. A.; Smith, E. L.; Porter, M. D. *J. Am. Chem. Soc.* **1992**, *114*, 1222.

(25) Poirier, G. E.; Tarlov, M. J.; Rushneier, H. E. *Langmuir* **1994**, *10*, 3383.

(26) Poirier, G. E. *Chem. Rev.* **1997,** *97*, 1117.

(27) Poirier, G. E.; Tarlov, M. J. *Langmuir* **1994**, *10*, 2853.

(28) Sabatani, E.; Cohne-Boulakia, J.; Bruening, M.; Rubinstein, I. *Langmuir* **1993,** *9*, 2914.

(29) Leung, T.; Schwartz, P.; Scoles, G.; Schreiber, F.; Ulman, A. *Surf. Sci.* **2000**, *458*, 34.

(30) Ishida, T.; Mizutani, W.; Akiba, U.; Umemura, K.; Inoue, A.; Choi, N.; Rujihira, M.; Tokumoto, H. *J. Phys. Chem. B* **1999**, *103*, 1686.

(31) Poirier, G. E. *Langmuir* **1999,** *15*, 1167.

(32) Schneider, T. W.; Butty, D. A. *J. Am. Chem. Soc.* **1993**, *115*, 12391.

(33) Ishida, T.; Mizutani, W.; Azehara, H.; Sato, F.; Choi, N.; Akiba, U.; Fujihira, M.; Tokumoto, H. *Langmuir* **2001**, *17*, 7459.

(34) Dannenberger, O.; Buck, M.; Grunze, M. *J. Phys. Chem. B* **1999**, *103*, 2202.

(35) Yamada, R.; Wano, H.; Uosaki, K. *Langmuir* **2000,** *16*, 5523.

Chapter 3. Molecular Electronics

(1) Aviram, A.; Ratner, M.A. *Chem. Phys. Lett.* **1974**, *29*, 277.

(2) Fendler, J. H. *Chem. Mater.* **2001**, *13*, 3196.

(3) Simmons, J. G. *J. Appl. Phys.* **1963**, *34*, 1793.

(4) Engelkes, V. B.; Beebe, J. M.; Frisbie, C. D. *J. Am. Chem. Soc.* **2004,** *126*, 14287.

(5) Wold, D. J.; Haag, R.; Rampi, M. A.; Frisbie, C. D. *J. Phys. Chem. B* **2002**, *106*, 2813.

(6) Dorneles, L. S.; Schaefer, D. M.; Carara, M.; Schelp, L. F. *Appl. Phys. Lett.* **2003**, *82*, 2832.

(7) Landauer, R. *Phys. Lett. A.* **1981**, *85*, 91.

(8) Nitzan, A. *Annu. Rev. Phys. Chem.* **2001**, *52*, 681.

(9) Samanta, M. P.; Tian, W.; Datta. S.; Henderson, J. I.; Kubiak, C. P. *Phys. Rev. B.* **1996**, *79*, 7626.

(10) Datta. S.; Tian, W.; Hong, S.; Reifenberger, R.; Henderson, J. I.; Kubiak, C. P. *Phys. Rev. Lett.* **1997**, *79*, 2530.

(11) Yaliraki, S. N.; Kemp, M.; Ratner, M. A. *J. Am. Chem. Soc.* **1999**, *121*, 3428.

(12) Zhu, X.-Y. *J. Phys. Chem. B* **2004**, *108*, 8778.

(13) Burin, A. L.; Berlin, Y. A.; Ratner, M. A. *J. Phys. Chem. A.* **2001**, *105*, 2652.

(14) Nitzan, A.; Jortner, J.; Wilkie, J.; Burin, A. L.; Ratner, M. A. *J. Phys. Chem. B* **2000**, *104*, 5661.

(15) Ness, H.; Shevlin, S. A.; Fisher, A. J. *Phys. Rev. B* **2001**, *63*, 125422.

(16) Nitzan, A.; Ratner, M. A. *Science* **2003**, *300*, 1384.

(17) Skourtis, S. S.; Waldeck, D. H.; Beratan, D. N. *J. Phys. Chem. B.* **2004**, *108*, 15511.

(18) Kummel, A. C. *Science* **2003**, *302*, 69.

(19) Bumm, L. A.; Arnold, J. J.; Dunbar, T. D.; Allara, D. L.; Weiss, P. S. *J. Phys. Chem. B* **1999**, *103*, 8122.

(20) Xu, B.; Tao, N. J. *Science* **2003**, *301*, 1221.

(21) Reed, M. A.; Zhou, C.; Muller, C. J.; Burgin, T. P.; Tour, J. M. *Science* **1997**, *278*, 252.

(22) Reichert, J.; Ochs, R.; D. Beckmann, D.; Weber, H. B.; Mayor, M.; Löhneysen H. V. *Phys. Rev. Lett.* **2002**, *88*, 176804.

(23) Muller, C. J.; Krans J. M.; Todorov, T. N.; Reed, M. A. *Phys. Rev. B* **1996**, *53*, 1022.

(24) Muller, C. J.; Vleeming, B. J.; Reed, M. A.; Lamba, J. J. S.; Hara, R.; Jones II, L.; Tour, J. M. *Nanotechnology* **1996**, *7*, 409.

(25) Holmlin, R.; Haag, R.; Chabinyc, M. L.; Ismagilov, R. F.; Cohen, A. E.; Terfort, A.; Rampi, M. A.; Whitesides, G. M. *J. Am. Chem. Soc.* **2001**, *123*, 5075.

(26) Slowinski, K.; Majda, M.; *J. Electroanal. Chem.* **2000**, *491*, 139.

(27) Slowinski, K.; Fong, H. K. Y.; Majda, M. *J. Am. Chem. Soc.* **1999**, *121*, 7257.

(28) Kushmerick, J. G.; Holt, D. B.; Pollack, S. K.; Ratner, M. A.; Yang, J. C.;

Schull, T. L.; Naciri, J.; Moore, M. H.; Shashidhar, R. *J. Am. Chem. Soc.* **2002**, *124*, 10654.

(29) Chen, J.; Reed, M. A.; Rawlett, A. M.; Tour, J. M. *Science* **1999**, *286*, 1550.

(30) Chen, J.; Calvet, L. C.; Reed, M. A.; Carr, D. W.; Grubisha, D. S.; Bennett, D. W. *Chem. Phys. Lett.* **1999**, *313*, 741.

(31) Beebe, J. M.; Engelkes, V. B.; Miller, L. L.; Frisbie, C. D. *J. Am. Chem. Soc.* **2002**, *124*, 11268.

(32) Wold, D. J.; Haag, R.; Rampi, M. A.; Frisbie, C. D. *J. Phys. Chem. B* **2002**, *106*, 2813.

(33) Wold, D. J.; Frisbie, C. D. *J. Am. Chem. Soc.* **2001**, *123*, 5549.

(34) Wold, D. J.; Frisbie, C. D. *J. Am. Chem. Soc.* **2000**, *122*, 2970.

(35) Cui, X.D.; Zarate, X.; Tomfohr, J.; Sankey, O.F.; Primak, A.; Moore, A.L.; Moore, T.A.; Gust, D.; Harris, G.; Lindsay, S.M. *Nanotechnology* **2002,** *13*, 5.

(36) Cui, X.D.; Primak, A.; Zarate, X.; Tomfohr, J.; Sankey, O.F.; Moore, A.L.; Moore, T.A.; Gust, D.; Harris, G.; Lindsay, S.M. *Science* **2001,** *294*, 571.

Chapter 4. Correlation between HOMO Alignment and Contact Resistance in Molecular Junctions: Aromatic Thiols versus Isocyanides

(1) (a) Kushmerick, J. G. *Materials Today* **2005**, *8*, 26. (b) Nitzan, A.; Ratner, M. A. *Science* **2003**, *300*, 1384. (c) Heath, J. R.; Ratner, M. A. *Physics Today* **2003**, *56*, 43.

(2) (a) Patrone, L.; Palacin, S.; Charlier, J.; Armand, F.; Bourgoin, J. P.; Tang, H.; Gauthier, S. *Phys. Rev. Lett.* **2003**, *91*, 096802. (b) Yaliraki, S. N.; Kemp, M.; Ratner, M. A. *J. Am. Chem. Soc.* **1999**, *121*, 3428.

(3) (a) Engelkes, V. B.; Beebe, J. M.; Frisbie, C. D. *J. Am. Chem. Soc.* **2004**, *126*, 14287. (b) Engelkes, V. B.; Beebe, J. M.; Frisbie, C. D. *J. Phys. Chem. B* **2005**, *109*, 16801.

(4) (a) Beebe, J. M.; Engelkes, V. B.; Miller, L. L.; Frisbie, C. D. *J. Am. Chem. Soc.* **2002**, *124*, 11268. (b) Salomon, A.; Cahen, D.; Lindsay, S.; Tomfohr, J.; Engelkes, V. B.; Frisbie, C. D. *Adv. Mater*. **2003**, *15*, 1881.

(5) (a) Magoga, M.; Joachim, C. *Phys. Rev. B* **1997**, *56*, 4722. (b) Kaun, C. C.; Larade, B.; Guo, H. *Phys. Rev. B* **2003**, *67*, 121411. (c) Wold, D. J.; Haag, R.; Rampi, M. A.; Frisbie, C. D. *J. Phys. Chem. B* **2002**, *106*, 2813. (d) McCreery, R. *Electrochem. Soc. Interface* **2004**, 46.

(6) (a) Yaliraki, S. N.; Roitberg, A. E.; Gonzalez, C.; Mujica, V.; Ratner, M. A. *J. Chem. Phys.* **1999**, *111*, 6997. (b) Taylor, J.; Brandbyge, M.; Stokbro, K. *Phys. Rev. Lett.* **2002**, *89*, 138301. (c) Tomfohr, J. K.; Sankey, O. F. *Phys. Rev. B* **2002**, *65*, 245105

(7) Davis, W. B.; Svec, W. A.; Ratner, M. A.; Wasielewski, M. R. *Nature* **1998**, *396*, 60.

(8) He, J.; Chen, F.; Li, J.; Sankey, O. F.; Terazono, Y.; Herrero, C.; Gust, D.; Moore, T. A.; Moore, A. L.; Lindsay, S. M. *J. Am. Chem. Soc.* **2005**, *127*, 1384.

(9) (a) Sikes, H. D.; Smalley, J. F.; Dudek, S. P.; Cook, A. R.; Newton, M. D.; Chidsey, C. E. D.; Feldberg, S. W. *Science* **2001**, *291*, 1519. (b) Creager, S.; Yu, C. J.; Bamdad, C.; O'Connor, S.; MacLean, T.; Lam, E.; Chong, Y.; Olsen, G. T.; Luo, J. Y.; Gozin, M.; Kayyem, J. F. *J. Am. Chem. Soc.* **1999**, *121*, 1059. (c) Sachs, S. B.; Dudek, S. P.; Hsung, R. P.; Sita, L. R.; Smalley, J. F.; Newton, M. D.; Feldberg, S. W.; Chidsey, C. E. D. *J. Am. Chem. Soc.* **1997**, *119*, 10563. (d) Helms, A.; Heiler, D.; McLendon, G. *J. Am. Chem. Soc.* **1991**, *113*, 4325.

(10) (a) Xue, Y.; Ratner, M. A. *Phys. Rev. B* **2003**, *68*, 115406. (b) Xue, Y.; Datta, S.; Ratner, M. A. *J. Chem. Phys.* **2001**, *115*, 4292.

(11) Tada, T.; Nozaki, D.; Kondo, M.; Hamayama, S.; Yoshizawa, K. *J. Am. Chem. Soc.* **2004**, *126*, 14182.

(12) Weber, W. P.; Gokel, G. W.; Ugi, I. K. *Angew. Chem. Int. Ed.* **1972**, *11*, 530.

(13) Beebe, J. M.; Engelkes, V. B.; Liu, J. Q.; Gooding, J.; Eggers, P. K.; Jun, Y.; Zhu, X.-Y.; Paddon-Row, M. N.; Frisbie, C. D. *J. Phys. Chem. B* **2005**, *109*, 5207.

(14) Fuxen, C.; Azzam, W.; Arnold, R.; Witte, G.; Terfort, A.; Woll, C. *Langmuir* **2001**, *17*, 3689.

(15) Jun, Y. S.; Zhu, X.-Y. *J. Am. Chem. Soc.* **2004**, *126*, 13224.

(16) Bain, C. D.; Whitesides, G. M. *J. Phys. Chem.* **1989**, *93*, 1670.

(17) Laibinis, P. E.; Bain, C. D.; Whitesides, G. M. *J. Phys. Chem.* **1991**, *95*, 7017.

(18) Tour, J. M.; Jones, L.; Pearson, D. L.; Lamba, J. J. S.; Burgin, T. P.; Whitesides, G. M.; Allara, D. L.; Parikh, A. N.; Atre, S. V. *J. Am. Chem. Soc.* **1995**, *117*, 9529.

(19) Huc, V.; Bourgoin, J. P.; Bureau, C.; Valin, F.; Zalczer, G.; Palacin, S. *J. Phys. Chem. B* **1999**, *103*, 10489.

(20) Robertson, M. J.; Angelici, R. J. *Langmuir* **1994**, *10*, 1488.

(21) Shih, K. C.; Angelici, R. J. *Langmuir* **1995**, *11*, 2539.

(22) Swanson, S. A.; McClain, R.; Lovejoy, K. S.; Alamdari, N. B.; Hamilton, J. S.; Scott, J. C. *Langmuir* **2005**, *21*, 5034.

(23) Murphy, K. L.; Tysoe, W. T.; Bennett, D. W. *Langmuir* **2004**, *20*, 1732.

(24) Henderson, J. I.; Feng, S.; Bein, T.; Kubiak, C. P. *Langmuir* **2000**, *16*, 6183.

(25) Kim, B.-S.; Heimel, G.; da Silva Filho, D. A.; Bredas, J.-L.; Zhu, X.-Y.; Frisbie, C. D., unpublished results.

(26) Stapleton, J. J.; Daniel, T. A.; Uppili, S.; Cabarcos, O. M.; Naciri, J.; Shashidhar, R.; Allara, D. L. *Langmuir* **2005**, *21*, 11061.

(27) Hickman, J. J.; Laibinis, P. E.; Auerbach, D. I.; Zou, C.; Gardner, T. J.; Whitesides, G. M.; Wrighton, M. S. *Langmuir* **1992**, *8*, 357.

(28) Walker, B. R.; Wassel, R. A.; Stefanescu, D. M.; Gorman, C. B. *J. Am. Chem. Soc.* **2004**, *126*, 16330.

(29) Tao, Y. T.; Wu, C. C.; Eu, J. Y.; Lin, W. L.; Wu, K. C.; Chen, C. H. *Langmuir* **1997**, *13*, 4018.

Chapter 5. Length-Dependent Transport in Molecular Junctions Based on SAMs of Aromatic Thiols and Dithiols: Effect of Contact Type and Metal Work Function

(1) Hamadani, B. H.; Corley, D. A.; Ciszek, J. W.; Tour, J. M.; Natelson, D. *Nano Lett.* **2006**, *6*, 1303.

(2) Campbell, I. H.; Rubin, S.; Zawodzinski, T. A.; Kress, J. D.; Martin, R. L.; Smith, D. L.; Barashkov, N. N.; Ferraris, J. P. *Phys Rev B* **1996**, *54*, 14321.

(3) Heimel, G.; Romaner, L.; Zojer, E.; Bredas, J. L. *Nano Lett.* **2007**, *7*, 932.

(4) Paniagua, S. A.; Hotchkiss, P. J.; Jones, S. C.; Marder, S. R.; Mudalige, A.; Marrikar, F. S.; Pemberton, J. E.; Armstrong, N. R. *J. Phys. Chem. C* **2008**, *112*, 7809.

(5) Alloway, D. M.; Hofmann, M.; Smith, D. L.; Gruhn, N. E.; Graham, A. L.; Colorado, R.; Wysocki, V. H.; Lee, T. R.; Lee, P. A.; Armstrong, N. R. *J. Phys. Chem. B* **2003**, *107*, 11690.

(6) Simmons, J. G. *J. Appl. Phys.* **1963**, *34*, 1973.

(7) Nitzan, A. *Annu. Rev. Phys. Chem.* **2001**, *52*, 681.

(8) Nitzan, A.; Ratner, M. A. *Science* **2003**, *300*, 1384.

(9) Kim, B.-S.; Beebe, J. M.; Jun, Y.; Zhu, X.-Y.; Frisbie, C. D. *J. Am. Chem. Soc.* **2006**, *128*, 4970.

(10) Zangmeister, C. D.; Beebe, J. M.; Naciri, J.; Kushinerick, J. G.; van Zee, R. D. *Small* **2008**, *4*, 1143.

(11) Zangmeister, C. D.; Picraux, L. B.; van Zee, R. D.; Yao, Y. X.; Tour, J. M. *Chem. Phys. Lett.* **2007**, *442*, 390.

(12) Zangmeister, C. D.; Robey, S. W.; van Zee, R. D.; Kushmerick, J. G.; Naciri, J.; Yao, Y.; Tour, J. M.; Varughese, B.; Xu, B.; Reutt-Robey, J. E. *J. Phys. Chem. B* **2006**, *110*, 17138.

(13) Zangmeister, C. D.; Robey, S. W.; vanZee, R. D.; Yao, Y.; Tour, J. M. *J. Am. Chem. Soc.* **2004**, *126*, 3420.

(14) Xue, Y. Q.; Datta, S.; Ratner, M. A. *J Chem Phys* **2001**, *115*, 4292.

(15) Venkataraman, L.; Park, Y. S.; Whalley, A. C.; Nuckolls, C.; Hybertsen, M. S.; Steigerwald, M. L. *Nano Lett.* **2007**, *7*, 502.

(16) Quinn, J. R.; Foss, F. W.; Venkataraman, L.; Breslow, R. *J. Am. Chem. Soc.* **2007**, *129*, 12376.
(17) Heimel, G.; Romaner, L.; Bredas, J. L.; Zojer, E. *Phys. Rev. Lett.* **2006**, *96*, 196806.
(18) Watkins, N. J.; Zangmeister, C. D.; Chan, C. K.; Zhao, W.; Ciszek, J. W.; Tour, J. M.; Kahn, A.; van Zee, R. D. *Chem. Phys. Lett.* **2007**, *446*, 359.
(19) Beebe, J. M.; Engelkes, V. B.; Miller, L. L.; Frisbie, C. D. *J. Am. Chem. Soc.* **2002**, *124*, 11268.
(20) Beebe, J. M.; Kim, B.-S.; Frisbie, C. D.; Kushmerick, J. G. *Acs Nano* **2008**, *2*, 827.
(21) Beebe, J. M.; Kim, B.-S.; Gadzuk, J. W.; Frisbie, C. D.; Kushmerick, J. G. *Phys. Rev. Lett.* **2006**, *97*, 026801.
(22) Engelkes, V. B.; Beebe, J. M.; Frisbie, C. D. *J. Am. Chem. Soc.* **2004**, *126*, 14287.
(23) Chen, F.; Li, X.; Hihath, J.; Huang, Z.; Tao, N. *J. Am. Chem. Soc.* **2006**, *128*, 15874.
(24) Fujii, S.; Akiba, U.; Fujihira, M. *Chem Lett* **2008**, *37*, 408.
(25) Park, Y. S.; Whalley, A. C.; Kamenetska, M.; Steigerwald, M. L.; Hybertsen, M. S.; Nuckolls, C.; Venkataraman, L. *J. Am. Chem. Soc.* **2007**, *129*, 15768.
(26) Tivanski, A. V.; He, Y. F.; Borguet, E.; Liu, H. Y.; Walker, G. C.; Waldeck, D. H. *J. Phys. Chem. B* **2005**, *109*, 5398.
(27) Kiguchi, M.; Miura, S.; Hara, K.; Sawamura, M.; Murakoshi, K. *Appl. Phys. Lett.* **2007**, *91*, 053110.
(28) Armarego, W. L. F.; Chai, C. L. L. *Purification of Laboratory Chemicals* **2003**, *5th edition*, Butterworth Heinemann.
(29) Lloyd, J. B. F.; Ongley, P. A. *Tetrahedron* **1965**, *21*, 245.
(30) Ulman, A. *Chem Rev* **1996**, *96*, 1533.
(31) Li, Z. Y.; Chang, S. C.; Williams, R. S. *Langmuir* **2003**, *19*, 6744.
(32) Salomon, A.; Cahen, D.; Lindsay, S.; Tomfohr, J.; Engelkes, V. B.; Frisbie, C. D. *Adv. Mater.* **2003**, *15*, 1881.
(33) Moulder, J. F.; Bomben, K. D.; Sobol, P. E.; Stickle, W. F. *Handbook of X-ray Photoelectron Spectroscopy* **1995**, Physical Electronics, Inc.
(34) Shaporenko, A.; Elbing, M.; Baszczyk, A.; von Hanisch, C.; Mayor, M.; Zharnikov, M. *J. Phys. Chem. B* **2006**, *110*, 4307.

(35) We found a peak from adventitious surface contaminants around 288.0 eV even in the C 1s spectra of alkanethiols on metal surfaces as others did (Himmelhaus, M. *et al. J. Electron Spectrosc. Relat. Phenom.* **1998**, *92*, 139-149, and Petrovykh, D. Y. *et al. Langmuir* **2006**, *22*, 2578-2587).

(36) Weckenmann, U.; Mittler, S.; Naumann, K.; Fischer, R. A. *Langmuir* **2002**, *18*, 5479.

(37) Laibinis, P. E.; Bain, C. D.; Whitesides, G. M. *J. Phys. Chem.* **1991**, *95*, 7017; the attenuation length is also confirmed by our experiment.

(38) Beebe, J. M.; Engelkes, V. B.; Liu, J. Q.; Gooding, J.; Eggers, P. K.; Jun, Y.; Zhu, X. Y.; Paddon-Row, M. N.; Frisbie, C. D. *J. Phys. Chem. B* **2005**, *109*, 5207.

(39) Diao, L.; Frisbie, C. D.; Schroepfer, D. D.; Ruden, P. P. *J. Appl. Phys.* **2007**, *101*, 014510.

(40) Amy, F.; Chan, C.; Kahn, A. *Org. Electron.* **2005**, *6*, 85.

(41) Crispin, X.; Geskin, V.; Crispin, A.; Cornil, J.; Lazzaroni, R.; Salaneck, W. R.; Bredas, J. L. *J. Am. Chem. Soc.* **2002**, *124*, 8131.

(42) De Renzi, V.; Rousseau, R.; Marchetto, D.; Biagi, R.; Scandolo, S.; del Pennino, U. *Phys. Rev. Lett.* **2005**, *95*, 046804.

(43) Beebe, J. M.; Kushmerick, J. G. *Appl. Phys. Lett.* **2007**, *90*, 083117.

(44) Terabe, K.; Hasegawa, T.; Nakayama, T.; Aono, M. *Nature* **2005**, *433*, 47.

(45) Liu, K.; Li, G. R.; Wang, X. H.; Wang, F. S. *J. Phys. Chem. C* **2008**, *112*, 4342.

(46) Yamada, R.; Kumazawa, H.; Noutoshi, T.; Tanaka, S.; Tada, H. *Nano Lett.* **2008**, *8*, 1237.

(47) Tada, T.; Nozaki, D.; Kondo, M.; Hamayama, S.; Yoshizawa, K. *J. Am. Chem. Soc.* **2004**, *126*, 14182.

(48) Quinn, J. R.; Foss, F. W.; Venkataraman, L.; Hybertsen, M. S.; Breslow, R. *J. Am. Chem. Soc.* **2007**, *129*, 6714.

(49) Duwez, A. S.; Pfister-Guillouzo, G.; Delhalle, J.; Riga, J. *J. Phys. Chem. B* **2000**, *104*, 9029.

(50) Gundlach, K. H.; Kadlec, J. *J. Appl. Phys.* **1975**, *46*, 5286.

(51) Landauer, R. *Phys. Lett. A* **1981**, *85*, 91-93.

Chapter 6. Transition from Direct Tunneling to Field Emission in Metal-Molecule-Metal Junctions

(1) Chen, J.; Reed, M. A.; Rawlett, A. M; Tour, J. M. *Science* **1999**, *286*, 1550.

(2) Gorman, C. B.; Carroll, R. L.; Fuierer, R. R. *Langmuir* **2001**, *17*, 6923.

(3) Reed, M. A.; Chen, J.; Rawlett, A. M.; Price, D.W.; Tour, J. M. *Appl. Phys. Lett.* **2001**, *78*, 3735.

(4) Blum, A. S.; Kushmerick, J. G.; Long, D. P.; Patterson, C. H.; Yang, J. C.; Henderson, J. C.; Yao, Y.; Tour, J. M.; Shashidhar, R.; Ratna, B. R. *Nat. Mater.* **2005**, *4*,167.

(5) Cai, L.; Cabassi, M. A.; Yoon, H.; Cabarcos, O. M.; McGuiness, C. L.; Flatt, A. K.; Allara, D. L.; Tour, J. M.; Mayer, T. S. *Nano Lett.* **2005**, *5*, 2365.

(6) Nitzan, A.; Ratner, M. A. *Science* **2003**, 300, 1384.

(7) Wang, W.; Lee, T.; Reed, M. A. *Phys. Rev. B* **2003**, *68*, 035416.

(8) Wold, D. J.; Frisbie, C. D. *J. Am. Chem. Soc.* **2001**, *123*, 5549.

(9) Holmlin, R. E.; Haag, R.; Chabinyc, M. L.; Ismagilov, R. F.; Cohen, A. E.; Terfort, A.; Rampi, M. A.; Whitesides, G. M. *J. Am. Chem. Soc.* **2001**, *123*, 5075.

(10) Selzer, Y.; Cai, L.; Cabassi, M. A.; Yao, Y.; Tour, J. M.; Mayer, T. S.; Allara, D. L. *Nano Lett.* **2005**, *5*, 61.

(11) Young, R.; Ward, J.; Scire, F. *Phys. Rev. Lett.* **1971**, *27*, 922.

(12) Simmons, J. G. *J. Appl. Phys.* **1963**, *34*,1793.

(13) Gadzuk, J.W.; Plummer, E.W. *Rev. Mod. Phys.* **1973**, *45*, 487.

(14) Leatherman, G.; Durantini, E. N.; Gust, D.; Moore, T. A.; Moore, A. L.; Stone, S.; Zhou, Z.; Rez, P.; Liu, Y. Z.; Lindsay, S. M. *J. Phys. Chem. B* **1999**, *103*, 4006.

(15) Engelkes, V. B.; Beebe, J. M.; Frisbie, C. D. *J. Phys. Chem. B* **2005**, *109*, 16801.

(16) Wold, D. J.; Frisbie, C. D. *J. Am. Chem. Soc*. **2000**, *122*, 2970.

(17) Kushmerick, J. G.; Holt, D. B.; Yang, J. C.; Naciri, J.; Moore, M. H.; Shashidhar, R. *Phys. Rev. Lett.* **2002**, *89*, 086802.

(18) Kushmerick, J. G. ; Holt, D. B.; Pollack, S. K.; Ratner, M. A.; Yang, J. C.;

Schull, T. L.; Naciri, J.; Moore, M. H.; Shashidhar, R. *J. Am. Chem. Soc.* **2002**, *124*, 10654.

(19) Walker, A.V.; Tighe, T. B.; Haynie, B. C.; Uppili, S.; Winograd, N.; Allara, D. L. *J. Phys. Chem. B* **2005**, *109*, 11263.

(20) Richter, C. A.; Hacker, C. A.; Richter, L. J. *J. Phys.Chem. B* **2005**, 109, 21836.

(21) Kim, B.-S.; Beebe, J. M.; Jun, Y.; Zhu, X.Y.; Frisbie, C. D. *J. Am. Chem. Soc.* **2006**, 128, 4970.

(22) Xue, Y. Q.; Ratner, M. A. *Phys. Rev. B* **2003**, *68*, 115406.

(23) Kushmerick, J. G. *Mater. Today* **2005**, *8*, 26.

(24) Engelkes, V. B.; Beebe, J. M.; Frisbie, C. D. *J. Am. Chem. Soc.* **2004**, *126*, 14287.

(25) Beebe, J. M.; Engelkes, V. B.; Miller, L. L.; Frisbie, C. D. *J. Am. Chem. Soc.* **2002**, 124, 11268.

Chapter 7. Measuring Relative Barrier Heights in Molecular Electronic Junctions with Transition Voltage Spectroscopy

(1) Donhauser, Z. J.; Mantooth, B. A.; Kelly, K. F.; Bumm, L. A.; Monnell, J. D.; Stapleton, J. J., Jr.; Rawlett, A. M.; Allara, D. L.; Tour, J. M. *Science* **2001**, *292*, 2303.

(2) Reed, M. A.; Chen, J.; Rawlett, A. M.; Price, D. W.; Tour, J. M. *Appl. Phys. Lett.* **2001**, *78*, 3735.

(3) Szuchmacher Blum, A.; Kushmerick, J. G.; Long, D. P.; Patterson, C. H.; Yang, J. C.; Henderson, J. C.; Yao, Y.; Tour, J. M.; Shashidhar, R.; Ratna, B. R. *Nat. Mater.* **2005**, *4*, 167.

(4) Lortscher, E.; Ciszek, J. W.; Tour, J.; Riel, H. *Small* **2006**, *2*, 973.

(5) Kubatkin, S.; Danilov, A.; Hjort, M.; Cornil, J.; Bredas, J. L.; Stuhr-Hansen, N.; Hedegard, P.; Bjornholm, T. *Nature* **2003**, *425*, 698.

(6) Park, J.; Pasupathy, A. N.; Goldsmith, J. I.; Chang, C.; Yaish, Y.; Petta, J. R.; Rinkoski, M.; Sethna, J. P.; Abruna, H. D.; McEuen, P. L. *Nature* **2002**, *417*, 722–725.

(7) Yu, L. H.; Zangmeister, C. D.; Kushmerick, J. G. *Nano Letters* **2006**, *6*, 2515.

(8) Beebe, J. M.; Kim, B.-S.; Gadzuk, J. W.; Frisbie, C. D.; Kushmerick, J. G. *Phys. Rev. Lett.* **2006**, *97*, 026801.

(9) Salomon, A.; Cahen, D.; Lindsay, S. M.; Tomfohr, J.; Engelkes, V. B.; Frisbie, C. D. *Adv. Mater.* **2003**, *15*, 1881.

(10) Muntwiler, M.; Lindstrom, C. D.; Zhu, X. Y. *J. Chem. Phys.* **2006**, *124*, 081104.

(11) Zangmeister, C. D.; Robey, S. W.; van Zee, R. D.; Yao, Y. X.; Tour, J. M. *J. Am. Chem. Soc.* **2004**, *126*, 3420.

(12) Wang, W.; Lee, T.; Reed, M. A. *Phys. Rev. B* **2003**, *68*, 035416.

(13) Engelkes, V. B.; Beebe, J. M.; Frisbie, C. D. *J. Am. Chem. Soc.* **2004**, *126*, 14287.

(14) Beebe, J. M.; Engelkes, V. B.; Miller, L. L.; Frisbie, C. D. *J. Am. Chem. Soc.* **2002**, *124*, 11268.

(15) Mujica, V.; Roitberg, A. E.; Ratner, M. A. *J. Chem. Phys.* **2000**, *112*, 6834.

(16) Liang, G. C.; Ghosh, A. W.; Paulsson, M.; Datta, S. *Phys. Rev. B* **2004**, *69*, 115302.

(17) Andres, R. P.; Bein, T.; Dorogi, M.; Feng, S.; Henderson, J. I.; Kubiak, C. P.; Mahoney, W.; Osifchin, R. G.; Reifenberger, R. *Science* **1996**, *272*, 1323.

(18) Datta, S.; Tian, W.; Hong, S.; Reifenberger, R.; Henderson, J.; Kubiak, C. P. *Phys. Rev. Lett.* **1997**, *79*, 2530.

(19) Cui, X. D.; Zarate, X.; Tomfohr, J.; Sankey, O. F.; Primak, A.; Moore, A. L.; Moore, T. A.; Gust, D.; Harris, G.; Lindsay, S. M. *Nanotechnology* **2002**, *13*, 5.

(20) Wold, D. J.; Frisbie, C. D. *J. Am. Chem. Soc.* **2000**, *122*, 2970.

(21) Kushmerick, J. G.; Holt, D. B.; Pollack, S. K.; Ratner, M. A.; Yang, J. C.; Schull, T. L.; Naciri, J.; Moore, M. H.; Shashidhar, R. *J. Am. Chem. Soc.* **2002**, *124*, 10654.

(22) Kushmerick, J. G.; Holt, D. B.; Yang, J. C.; Naciri, J.; Moore, M. H.; Shashidhar, R. *Phys. Rev. Lett.* **2002**, *89*, 086802.

(23) Walker, A. V.; Tighe, T. B.; Stapleton, J. J.; Haynie, B. C.; Upilli, S.; Allara, D. L.; Winograd, N. *Appl. Phys. Lett.* **2004**, *84*, 4008.

(24) Yu, L. H.; Zangmeister, C. D.; Kushmerick, J. G. *Phys. Rev. Lett.* **2007**, *98*, 206803.

(25) Alloway, D. M.; Hofmann, M.; Smith, D. L.; Gruhn, N. E.; Graham, A. L.; Colorado, R, Jr.; Wysocki, V. H.; Lee, R.; Lee, P. A.; Armstrong, N. *J. Phys. Chem. B* **2003**, *107*, 11690.

(26) Duwez, A. S.; Pfister-Guillouzo, G.; Delhalle, J.; Riga, J. *J. Phys. Chem. B* **2000**, *104*, 9029.

(27) O'Neill, L.; Byrne, H. J. *J. Phys. Chem. B* **2005**, *109*, 12685.

(28) Szuchmacher Blum, A.; Kushmerick, J. G.; Pollack, S. K.; Yang, J. C.; Moore, M. H.; Naciri, J.; Shashidhar, R.; Ratna, B. *J. Phys. Chem. B* **2004**, *108*, 18124.

(29) Szuchmacher Blum, A.; Yang, J. C.; Shashidhar, R.; Ratna, B. *Appl. Phys. Lett.* **2003**, *82*, 3322.

(30) Holmlin, R. E.; Ismagilov, R. F.; Haag, R.; Mujica, V.; Ratner, M. A.; Rampi, M. A.; Whitesides, G. M. *Angew. Chem., Int. Ed.* **2001**, *40*, 2316.

(31) Kushmerick, J. G.; Whitaker, C. M.; Pollack, S. K.; Schull, T. L.; Shashidhar, R. *Nanotechnology* **2004**, *15*, S489.

(32) Kim, B.-S.; Beebe, J. M.; Jun, Y.; Zhu, X.-Y.; Frisbie, C. D. *J. Am. Chem. Soc.* **2006**, *128*, 4970.

(33) Xue, Y.; Datta, S.; Ratner, M. A. *J. Chem. Phys.* **2001**, *115*, 4292.

(34) Michaelson, H. B. *J. Appl. Phys.* **1977**, *48*, 4729.

(35) Reddy, P.; Jang, S.-Y.; Segalman, R. A.; Majumdar, A. *Science* **2007**, *315*, 1568.

(36) Salaneck, W. R.; Seki, K.; Kahn, A.; Pireaux, J.-J. *Conjugated Polymer and Molecular Interfaces: Science and Technology for Photonic and Optoelectronic Applications*; Marcel Dekker: New York, **2001**.

(37) Zangmeister, C. D.; Robey, S. W.; van Zee, R. D.; Kushmerick, J. G.; Naciri, J.; Yao, Y.; Tour, J. M.; Varughese, B.; Xu, B.; Reutt-Robey, J. E. *J. Phys. Chem. B* **2006**, *110*, 17138.

(38) Zangmeister, C. D.; Picraux, L. B.; van Zee, R. D.; Yao, Y.; Tour, J. M. *Chem. Phys. Lett.* **2007**, *442*, 390.

(39) Seminario, J. M.; De La Cruz, C. E.; Derosa, P. A. *J. Am. Chem. Soc.* **2001**, *123*, 5616.

(40) Stapleton, J. J.; Daniel, T. A.; Upilli, S.; Cabarcos, O. M.; Naciri, J.; Shashidhar, R.; Allara, D. L. *Langmuir* **2005**, *21*, 11601.

(41) Stapleton, J. J.; Harder, P.; Daniel, T. A.; Reinard, M. D.; Yao, Y.; Price, D. W.; Tour, J. M.; Allara, D. L. *Langmuir* **2003**, *19*, 8245.

(42) Frisch, M. J.; Trucks, G. W.; Schlegel, H. B.; Scuseria, G. E.; Robb, M. A.; heeseman, J. R.; Montgomery, J., J. A.; Vreven, T.; Kudin, K. N.; Burant, J. C. *et al. Gaussian 03, Revision C.02*, Gaussian, Inc.: Wallingford CT, **2004**.

Chapter 8. Temperature and Length Dependence of Charge Transport in Redox-Active Molecular Wires Incorporating Ruthenium (II) Bis(σ-arylacetylide) Complexes

(1) Chae, D. H.; Berry, J. F.; Jung, S.; Cotton, F. A.; Murillo, C. A.; Yao, Z. *Nano Lett.* **2006**, *6*, 165.

(2) Kubatkin, S.; Danilov, A.; Hjort, M.; Cornil, J.; Bredas, J. L.; Stuhr-Hansen, N.; Hedegard, P.; Bjornholm, T. *Nature* **2003**, *425*, 698.

(3) Park, H.; Park, J.; Lim, A. K. L.; Anderson, E. H.; Alivisatos, A. P.; McEuen, P. L. *Nature* **2000**, *407*, 57.

(4) Park, J.; Pasupathy, A. N.; Goldsmith, J. I.; Chang, C.; Yaish, Y.; Petta, J. R.; Rinkoski, M.; Sethna, J. P.; Abruna, H. D.; McEuen, P. L.; Ralph, D. C. *Nature* **2002**, *417*, 722.

(5) Yu, L. H.; Natelson, D. *Nano Lett.* **2004**, *4*, 79.

(6) Yu, L. H.; Keane, Z. K.; Ciszek, J. W.; Cheng, L.; Stewart, M. P.; Tour, J. M.; Natelson, D. *Phys. Rev. Lett.* **2004**, *93*, 266802.

(7) Liang, W. J.; Shores, M. P.; Bockrath, M.; Long, J. R.; Park, H. *Nature* **2002**, *417*, 725.

(8) Metzger, R. M. *Chem. Rev.* **2003**, *103*, 3803.

(9) McCreery, R.; Dieringer, J.; Solak, A. O.; Snyder, B.; Nowak, A. M.;

McGovern, W. R.; DuVall, S. *J. Am. Chem. Soc.* **2003**, *125*, 10748.

(10) Cai, L.; Cabassi, M. A.; Yoon, H.; Cabarcos, O. M.; McGuiness, C. L.; Flatt, A. K.; Allara, D. L.; Tour, J. M.; Mayer, T. S. *Nano Lett.* **2005,** *5*, 2365.

(11) Blum, A. S.; Kushmerick, J. G.; Long, D. P.; Patterson, C. H.; Yang, J. C.; Henderson, J. C.; Yao, Y. X.; Tour, J. M.; Shashidhar, R.; Ratna, B. R. *Nat. Mater.* **2005**, *4*, 167.

(12) Chen, J.; Reed, M. A.; Rawlett, A. M.; Tour, J. M. *Science* **1999**, *286*, 1550.

(13) Rawlett, A. M.; Hopson, T. J.; Nagahara, L. A.; Tsui, R. K.; Ramachandran, G. K.; Lindsay, S. M. *Appl. Phys. Lett.* **2002**, *81*, 3043.

(14) Fan, F. R. F.; Yao, Y. X.; Cai, L. T.; Cheng, L.; Tour, J. M.; Bard, A. J. *J. Am. Chem. Soc.* **2004**, *126*, 4035.

(15) He, J.; Chen, F.; Li, J.; Sankey, O. F.; Terazono, Y.; Herrero, C.; Gust, D.; Moore, T. A.; Moore, A. L.; Lindsay, S. M. *J. Am. Chem. Soc.* **2005**, *127*, 1384.

(16) Kim, B.-S.; Beebe, J. M.; Jun, Y.; Zhu, X.-Y.; Frisbie, C. D. *J. Am. Chem. Soc.* **2006**, *128*, 4970.

(17) Moth-Poulsen, K.; Patrone, L.; Stuhr-Hansen, N.; Christensen, J. B.; Bourgoin, J.-P.; Bjornholm, T. *Nano Lett.* **2005**, *5*, 783.

(18) Seferos, D. S.; Blum, A. S.; Kushmerick, J. G.; Bazan, G. C. *J. Am. Chem. Soc.* **2006**, *128*, 11260.

(19) Fan, F.-R. F.; Yang, J.; Cai, L.; Price, D. W.; Dirk, S. M.; Kosynkin, D. V.; Yao, Y.; Rawlett, A. M.; Tour, J. M.; Bard, A. J. *J. Am. Chem. Soc.* **2002**, *124*, 5550.

(20) Blum, A. S.; Ren, T.; Parish, D. A.; Trammell, S. A.; Moore, M. H.; Kushmerick, J. G.; Xu, G. L.; Deschamps, J. R.; Pollack, S. K.; Shashidhar, R. *J. Am. Chem. Soc.* **2005**, *127*, 10010.

(21) Schull, T. L.; Kushmerick, J. G.; Patterson, C. H.; George, C.; Moore, M. H.; Pollack, S. K.; Shashidhar, R. *J. Am. Chem. Soc.* **2003**, *125*, 3202.

(22) Beebe, J. M.; Kim, B.-S.; Gadzuk, J. W.; Frisbie, C. D.; Kushmerick, J. G. *Phys. Rev. Lett.* **2006**, *97*, 026801.

(23) Huc, V.; Bourgoin, J. P.; Bureau, C.; Valin, F.; Zalczer, G.; Palacin, S. *J. Phys. Chem. B* **1999**, *103*, 10489.

(24) Stapleton, J. J.; Daniel, T. A.; Uppili, S.; Cabarcos, O. M.; Naciri, J.; Shashidhar, R.; Allara, D. L. *Langmuir* **2005**, *21*, 11061.

(25) Engelkes, V. B.; Beebe, J. M.; Frisbie, C. D. *J. Phys. Chem. B* **2005**, *109*, 16801.

(26) Stapleton, J. J.; Harder, P.; Daniel, T. A.; Reinard, M. D.; Yao, Y. X.; Price, D. W.; Tour, J. M.; Allara, D. L. *Langmuir* **2003**, *19*, 8245.

(27) Rigaut, S.; Costuas, K.; Touchard, D.; Saillard, J. Y.; Golhen, S.; Dixneuf, P. H. *J. Am. Chem. Soc.* **2004**, *126*, 4072.

(28) Rigaut, S.; Perruchon, J.; Guesmi, S.; Fave, C.; Touchard, D.; Dixneuf, P. H. *Eur. J. Inorg. Chem.* **2005**, 447.

(29) Rigaut, S.; Olivier, C.; Costuas, K.; Choua, S.; Fadhel, O.; Massue, J.; Turek, P.; Saillard, J. Y.; Dixneuf, P. H.; Touchard, D. *J. Am. Chem. Soc.* **2006**, *128*, 5859.

(30) Powell, C. E.; Cifuentes, M. P.; Morrall, J. P.; Stranger, R.; Humphrey, M. G.; Samoc, M.; Luther-Davies, B.; Heath, G. A. *J. Am. Chem. Soc.* **2003**, *125*, 602.

(31) McGrady, J. E.; Lovell, T.; Stranger, R.; Humphrey, M. G. *Organometallics* **1997**, *16*, 4004.

(32) Grabert, H.; Devoret, M. H. *Single Charge Tunneling: Coulomb Blockade Phenomena in Nanostructures*, **1992**, Plenum, New York.

(33) Barriere, F.; Geiger, W. E. *J. Am. Chem. Soc.* **2006**, *128*, 3980.

(34) He, J.; Fu, Q.; Lindsay, S.; Ciszek, J. W.; Tour, J. M. *J. Am. Chem. Soc.* **2006**, *128*, 14828.

(35) Tao, N. J. *Phys. Rev. Lett.* **1996**, *76*, 4066.

(36) Fan, F. R. F.; Lai, R. Y.; Cornil, J.; Karzazi, Y.; Bredas, J. L.; Cai, L. T.; Cheng, L.; Yao, Y. X.; Price, D. W.; Dirk, S. M.; Tour, J. M.; Bard, A. J. *J. Am. Chem. Soc.* **2004**, *126*, 2568.

(37) Tran, E.; Grave, C.; Whitesides, G. M.; Rampi, M. A. *Electrochimica Acta* **2005**, *50*, 4850.

(38) Creager, S.; Yu, C. J.; Bamdad, C.; O'Connor, S.; MacLean, T.; Lam, E.; Chong, Y.; Olsen, G. T.; Luo, J. Y.; Gozin, M.; Kayyem, J. F. *J. Am. Chem. Soc.* **1999**, *121*, 1059.
(39) Getty, S. A.; Engtrakul, C.; Wang, L.; Liu, R.; Ke, S. H.; Baranger, H. U.; Yang, W.; Fuhrer, M. S.; Sita, L. R. *Phys. Rev. B* **2005**, *71*, 241401.

Curriculum Vitae

BongSoo Kim

August 16, 1974 **Born in Kyeong-sang-buk-do, Republic of Korea**

Education

Ph.D. Candidate in Materials Chemistry, October 2008

University of Minnesota, Minneapolis, MN

Thesis: Charge Transport and Contact Effects in Nanoscopic Conjugated Molecular Junctions Characterized by Conducting Probe Atomic Force Microscopy

Advisor: Professor C. Daniel Frisbie

M.S. Organic/Polymer Chemistry, February 2002

Korea University, Seoul, Republic of Korea

Thesis: Synthesis and Characterization of New Light-emitting Small Conjugated Molecules and Poly(*p*-phenylenevinylene) Derivatives

Advisor: Professor Jung-Il Jin

B.S. Chemistry, February 2000

Korea University, Seoul, Republic of Korea

List of Publications

• *"Length-Dependent Transport in Molecular Junctions based on SAMs of Aromatic Monothiols and Aromatic Dithiols: Effect of Contact Type and Metal Work Function."* Kim, B.-S.; Choi, S. H.; Kang, M. S.; Zhu, X.-Y.; Frisbie, C. D.
In preparation for ***J. Am. Chem. Soc***.

• *"Printable Ion Gel Gate Dielectrics for High Performance Polymer Thin Film Transistors."* Cho, J. H.; Lee, J.; Kim, B.-S.; He, Y.; Lodge, T. P.; Frisbie, C. D.
Nat. Mater. **2008**, in press.

• *"Electrical Resistance of Long Conjugated Molecular Wires."* Choi, S. H.; Kim, B.-S.; Frisbie, C. D. ***Science*** **2008**, *320*, 1482.

• *"Measuring Relative Barrier Heights in Molecular Electronic Junctions with Transition Voltage Spectroscopy."* Beebe, J. M.; Kim, B.-S.; Frisbie, C. D.; Kushmerick, J. G.
ACS nano **2008**, *2*, 827.

• *"Redox-active Molecular Wires Incorporating Ruthenium (II) σ-Arylacetylide Complexes for Molecular Electronics."* Olivier, C.; Kim, B.-S.; Touchard, D.; Rigaut, S.
Organometallics **2008**, *27*, 509.(*a Most-Accessed Article for the first-quarter of 2008*)

• *"High Capacitance Ion Gel Gate Dielectrics with Faster Polarization Response Times for Organic Thin Film Transistors."* Cho, J. H.; Lee, J.; He, Y.; Kim, B.-S.; Lodge, T. P.; Frisbie, C. D. ***Adv. Mater.*** **2008**, 20, 686.

• *"Temperature and Length Dependence of Charge Transport in Redox-Active Molecular Wires Incorporating Ruthenium (II) Bis(σ-arylacetylide) Complexes."* Kim, B.-S.; Beebe, J. M.; Olivier, C.; Rigaut, S.; Touchard, D.; Kushmerick, J. G.; Zhu, X.-Y.; Frisbie, C. D. ***J. Phys. Chem. C*** **2007**, *111*, 7521.

• *"Transition from Direct Tunneling to Field Emission in Metal-Molecule-Metal Junctions."* Beebe, J. M.; Kim, B.-S.; Gadzuk, J. W.; Frisbie, C. D.; Kushmerick, J. G.
Phys. Rev. Lett. **2006**, *97*, 026801.

• *"Correlation between HOMO Alignment and Contact Resistance in Molecular Junctions: Aromatic Thiols versus Aromatic Isocyanides."* Kim, B.-S.; Beebe, J. M.; Jun, Y.; Zhu, X.-Y.; Frisbie, C. D. ***J. Am. Chem. Soc.*** **2006,** *128*, 4970**.**

Science
AAAS

Permissions Letter

Ref # 08-28027

DATE: Friday, October 24, 2008

TO: BongSoo Kim
University of Minnesota
Department of Chemistry 207 Pleasant St. SE
Minneapolis, MN 55455
United States

FROM: Elizabeth Sandler, Rights and Permissions
RE: Your request for permission dated 10/22/08 (submission id 37755)

Regarding your request, we are pleased to grant you non-exclusive, non-transferable permission to use the AAAS material identified below in your dissertation or thesis identified below, but limited to the formats identified below, and provided that you meet the conditions / requirements below. Such permission is for one time use and therefore does not include permission for future editions, revisions, additional printings, updates, ancillaries, other formats, translations, or promotional pieces, unless otherwise permitted below. This permission does not apply to figures / artwork that are credited to non-AAAS sources. This permission does not include the right to modify AAAS material.

The following credit line must be printed along with the AAAS material: "From [Insert Full Reference Citation]. Reprinted with permission from AAAS."

This permission covers the use of the AAAS material identified herein in the following format versions of your dissertation/thesis:
[x] print
[x] microform
[x] Digitized / electronic versions , provided the reprinted AAAS material remains in situ and is not made digitally available separated from your dissertation/thesis

AAAS agrees that ProQuest/UMI may supply copies of the dissertation/thesis on demand.

If the requested material is sourced to or references non-AAAS sources, you must obtain authorization from that source as well.

Permission fees are waived in this instance. AAAS reserves the right to charge for reproduction of AAAS controlled material in the future.

AAAS must publish the full paper prior to use of any text.

AAAS does not supply photos or artwork. AAAS material must not be used in a derogatory manner. Use of the AAAS material must not imply any endorsement by the American Association for the Advancement of Science. This permission is not valid for the use of the AAAS and/or SCIENCE logos.

Permission is valid for use of the following AAAS material only:
Fig 2 and Figure 4(c) from M. A. Reed et al., SCIENCE 278:252-254 (10 October 1997)
In the following work only:
Chapter 3. Molecular Electronics, CHARGE TRANSPORT AND CONTACT EFFECTS IN NANOSCOPIC CONJUGATED MOLECULAR JUNCTION . . . published by University of Minnesota in 10/24/2008
Thank you for writing. If you have any questions please call me at (202) 326-7074 or write to me via fax at (202) 682-0816. For international calls, +1 is the country code for the United States.

Headquarters:
1200 New York Avenue, NW, Washington, D.C. 20005 USA

Science
AAAS

Permissions Letter

Ref # 08-28028

DATE: Friday, October 24, 2008

TO: BongSoo Kim
University of Minnesota
Department of Chemistry, 207 Pleasant St. SE.
Minneapolis, MN 55455
United States

FROM: Elizabeth Sandler, Rights and Permissions
RE: Your request for permission dated 10/22/08 (SUBMISSION ID 37756)

Regarding your request, we are pleased to grant you non-exclusive, non-transferable permission to use the AAAS material identified below in your dissertation or thesis identified below, but limited to the formats identified below, and provided that you meet the conditions / requirements below. Such permission is for one time use and therefore does not include permission for future editions, revisions, additional printings, updates, ancillaries, other formats, translations, or promotional pieces, unless otherwise permitted below. This permission does not apply to figures / artwork that are credited to non-AAAS sources. This permission does not include the right to modify AAAS material.

The following credit line must be printed along with the AAAS material: "From [Insert Full Reference Citation]. Reprinted with permission from AAAS."

This permission covers the use of the AAAS material identified herein in the following format versions of your dissertation/thesis:
[x] print
[x] microform
[x] Digitized / electronic versions , provided the reprinted AAAS material remains in situ and is not made digitally available separated from your dissertation/thesis

AAAS agrees that ProQuest/UMI may supply copies of the dissertation/thesis on demand.

If the requested material is sourced to or references non-AAAS sources, you must obtain authorization from that source as well.

Permission fees are waived in this instance. AAAS reserves the right to charge for reproduction of AAAS controlled material in the future.

AAAS must publish the full paper prior to use of any text.

AAAS does not supply photos or artwork. AAAS material must not be used in a derogatory manner. Use of the AAAS material must not imply any endorsement by the American Association for the Advancement of Science. This permission is not valid for the use of the AAAS and/or SCIENCE logos.

Permission is valid for use of the following AAAS material only:
Fig 1 from J. Chen et al., SCIENCE 286:1550-1552 (19 November 1999)
In the following work only:
Chapter 3. Molecular Electronics, CHARGE TRANSPORT AND CONTACT EFFECTS IN NANOSCOPIC CONJUGATED MOLECULAR JUNCTION published by University of Minnesota in 10/24/2008
Thank you for writing. If you have any questions please call me at (202) 326-7074 or write to me via fax at (202) 682-0816. For international calls, +1 is the country code for the United States.

Headquarters:
1200 New York Avenue, NW, Washington, D.C. 20005 USA

10/23/2008 13:27 FAX 2027768112 001/001

RECEIVED

OCT 22 2008

ACS COPYRIGHT OFFICE

PERMISSION REQUEST FORM

Date: October 21, 2008

I need permission ASAP Because My graduation will be Oct.31,2008 (or by Oct. 24, 2008)

~~To:~~ From: Copyright Office
Publications Division
American Chemical Society
1155 Sixteenth Street, N.W.
Washington, DC 20036

FAX: 202-776-8112

~~From:~~ To:
BongSoo Kim
Department of Chemistry
University of Minnesota
207 Pleasant Street SE
Minneapolis, MN 55455-0431

Your Phone No. 612-270-8756
Your Fax No. 612-626-7246

I am preparing a paper entitled: _____

to appear in a **(circle one)** book, magazine, journal, proceedings, other **(My Thesis)**
entitled: Charge Transport and Contact Effects in Nanoscopic Conjugated Molecular Junctions Characterized by Conducting Probe Atomic Force Microscopy
to be published by: University of Minnesota

I would appreciate your permission to use the following ACS material in print and other formats with the understanding that the required ACS copyright credit line will appear with each item and that this permission is for only the requested work listed above:

From ACS journals or magazines (for ACS magazines, also include issue no.):

ACS Publication Title	Issue Date	Vol.	No.	Page(s)	Material to be used*
J. Am. Chem. Soc.	Aug.11, 1999	121	31	p.7258	Figure 1.
J. Am. Chem. Soc.	May 30, 2001	123	21	p.5076	Figure 1.
J. Am. Chem. Soc.	Sept.11, 2002	124	36	p.10654	Figure 1.
J. Am. Chem. Soc.	June 10, 1987	109	12	p.3560	Figure 1.
Langmuir	Sept. , 1994	10	9	p.2854	Figure 2.
Langmuir	June 12, 2001	17	12	p.3694	Figure 7.

From ACS books: include ACS book title, series name and number, year, page(s), book editor's name(s), chapter author's name(s), and material to be used, such as Figs. 2 & 3, full text, etc.*

If you use more than three figures/tables on will also be required.
Questions? Please call Arleen Courtney at (2

This space is reserved for ACS Copyright Office Use

PERMISSION TO REPRINT IS GRANTED BY THE AMERICAN CHEMICAL SOCIETY

ACS CREDIT LINE REQUIRED. Please follow this sample: Reprinted with permission from (reference citation). Copyright (year) American Chemical Society.

APPROVED BY: C. Arleen Courtney 10/22/08
ACS Copyright Office

☐ **If box is checked, author permission is also required. See original article for address.**